UNIVERSITY OF CALIFORNIA, SAN DIEGO

The effects of electronic delocalization in highly coupled mixed valence systems

A dissertation submitted in partial satisfaction of the requirements for the degree of Doctor of Philosophy

in

Chemistry

by

Benjamin James Lear

Committee in charge:

Professor Clifford P. Kubiak, Chair
Professor Seth M. Cohen
Professor Michael J. Sailor
Professor Jan B. Talbot
Professor Wei Wang

2007

The dissertation of Benjamin James Lear is approved, and it is acceptable in quality and form for publication on microfilm.

Chair

University of California, San Diego

2007

to Shana for all her love and patience

to my parents for their unwavering support

to my brother for good advice based on experience

to my friends and family for making life fun

TABLE OF CONTENTS

Signature Page iii

Table of Contents v

List of Figures vii

List of Schemes x

List of Tables xi

Acknowledgements xii

Vita xv

Abstract xvi

Chapter 1: A brief introduction to the science of electron transfer 1
- 1.1 Introduction 1
- 1.2 Electron transfer reactions 1
- 1.3 The Marcus and Marcus-Hush theory of electron transfer 3
- 1.4 Mixed valency and the Robin-Day classification scheme 12
- 1.5 The emergence of class II-III mixed valency 14
- 1.6 Conclusions 22

Chapter 2: A thermodynamic estimation of H_{AB} for asymmetric class II-III mixed valence systems 23
- 2.1 Introduction 23
- 2.2 Spectroscopic observation of mixed valence isomers 28
- 2.3 Calculation of electronic coupling 30
- 2.4 Implications of the values of the thermodynamically obtained H_{AB} 33
- 2.5 Conclusions 36

Chapter 3: Determination of ΔH and ΔS for asymmetric class II-III mixed valence systems 38
- 3.1 Introduction 38
- 3.2 Experimental 38
- 3.3 Results and discussion 39
- 3.4 Conclusions 46

Chapter 4: Dynamical solvent control of the electron transfer rates for a class II-III mixed valence system 47
- 4.1 Introduction 47
- 4.2 Solvent effects on electron transfer rates 49
- 4.3 Electron transfer rate dependence on the time-independent solvent parameters 53
- 4.4 Electron transfer rate dependence on time-dependent solvent parameters 56
- 4.5 Conclusions 62
- 4.6 Experimental 63

Chapter 5: Electron transfer rates in class II-III mixed valence systems in solid media: Decoupling of the solvent and electronic motions 64
- 5.1 Introduction 64
- 5.2 Decoupling of solvent modes from rate of electron transfer 65
- 5.3 Conclusions 70

Chapter 6: Changes in electronic coupling in class II-III systems as a driving force for chemical interactions 71
6.1 Introduction 71
6.2 Electronic effects of the binding of clalix[6]arene to $[Ru_3O(OAc)_6(CO)(ppy)]_2$-$\mu_2$-pz 73
6.3 Cooperative binding of calyx[6]arene to $[Ru_3O(OAc)_6(CO)(ppy)]_2$-μ-pz – direct thermodynamic effects 78
6.4 Cooperative binding of calyx[6]arene to $[Ru_3O(OAc)_6(CO)(ppy)]_2$-μ-pz – effect of changes to electronic delocalization 83
6.5 Conclusions 85
6.6 Experimental methods 86

Chapter 7: Electronic delocalization as a driving force for chemical interactions 88
7.1 Introduction 88
7.2 Changes in conductance as a driving force for chemical interactions 90
7.3 Conclusions 96

Chapter 8: Charge transfer and charge re-organization in a dendritic assembly of trinuclear ruthenium clusters 98
8.1 Introduction 98
8.2 Synthesis 99
8.3 Electrochemistry 99
8.4 Infrared spectroelectrochemistry 100
8.5 Discussion 104
8.6 Conclusions 106

Chapter 9: Intermolecular electron transfer to and from highly coupled mixed valence complexes 108
9.1 Introduction 108
9.2 Experimental methods 113
9.3 Electron transfer from the excited state porphyrin to ruthenium complexes 113
9.4 Conclusions 122

Chapter 10: Future experiments for trinuclear ruthenium based class II-III mixed valence complexes 124
10.1 Introduction 124
10.2 Speaking the language of mixed valency – studying the intervalence charge transfer (IVCT) band 125
10.3 The confirmation of the electron transfer rate for ruthenium dimers of trimers 126
10.4 Braking the ruthenium cluisters out of the electron transfer box and using them to make metal-organic boxes 134
10.5 Conclusions 137

References 138

LIST OF FIGURES

Figure 1.1 Diabatic potential energy curves for the reactants (solid line) and products (dashed line) of an electron transfer reaction. The reaction coordinate is a measure of the nuclear configuration of the system undergoing the electron transfer reaction 4

Figure 1.2 Diabatic (dashed lines) and adiabatic (solid lines) potential energy curves for a system undergoing electron transfer 9

Figure 1.3 A schematic respresentation of how the potential energy surfaces change with increasing electronic coupling. Drawn on the surfaces are the vertical transitions that are associated with the photo-induced electron transfer event. 12

Figure 1.4 Depiction of the potential energy surfaces associated with the three classes of the Robin-Day classification scheme for mixed valence systems 14

Figure 1.5 (a) Structure of ruthenium cluster based mixed valence complex. (b) IR spectrum of ν(CO) for the neutral complex. (c) IR spectrum of ν(CO) for the singly reduced, mixed valence ion. (d) IR spectrum of ν(CO) for the doubly reduced ion (both clusters reduced) 19

Figure 1.6 (a) A ruthenium dimer and the IR spectra in the neutral, -1 (mixed valence), and -2 states. (b) Structures of the ruthenium and osmium dimers studied by Shreve and co-workers 19

Figure 2.1 Structures of the asymmetric complexes 1-5 used in order to obtain thermodynamic estimates of H_{AB} 27

Figure 2.2 Diabatic and Adiabatic potential energy surfaces associated with mixed valence systems in the Marcus-Hush model of electron transfer. ΔG_0^0 is the difference between the diabatic potential energy surfaces and ΔG_1^0 is the energy difference between the wells in the lower adiabatic potential energy surface 27

Figure 2.3 Structure of a representative asymmetric dimmer with the spectra associated with the neutral, minus 1, and minus 2 states 29

Figure 3.1 (a) The asymmetric dimer, 1. (b) The diabatic (Blue and pink) and adiabatic (green and red) potential energy surfaces associated with 1. (c) The IR spectra for 1^{-1} 40

Figure 3.2 Carbonyl stretching region for 1^{-1} taken at +10° C, 0° C, -40° C, and -90° C. The assessment of the peak positions are the same as outlined in Figure 3.. The changes in relative intensities for the major and minor isomers are a result of changes in the relative Boltzmann populations of these species 42

Figure 3.3 Experimental and simulated ν(CO) spectra for 1^{-1} at 0° C 43

Figure 3.4 Van't Hoff plot for 1^{-1}. The red line is a linear fit of the data giving ΔH = 0.64 kJ/mol (53 cm^{-1}/mol) and a $\Delta S = 1.5 \times 10^{-3}$ kJ/mol (0.12 cm^{-1}/mol) 45

Figure 4.1 Stuctures of $[Ru_3O(OAc)_6(CO)L]_2$-μ-pz where pz=pyrazine with ancillary ligands 1 = 4-dimethylaminopyridine, 2 = pyridine, 3 = 3-cyanopyridine, and 4 = 4-cyanopyridine 50

Figure 4.2 IR bandshapes for the ν(CO) band of 2^- in CH_3CN, CH_2Cl_2, and THF. The estimated electron transfer rate (k_{et}) is given below the spectra. More coalesced spectra are associated with faster electron transfer rates 50

Figure 4.3 Plot ($1/\varepsilon_{op} - 1/\varepsilon_s$) -- the variable portion of the outersphere reorganization energy, λ_{out} -- versus the lifetime for electron transfer, k_{et}^{-1}, for complexes 1(■), 2(●), 3(▲), and 4(▼). The average of the R^2 values for this plot is 0.191 55

Figure 4.4 Plot of the micoscopic polarity of the solvent, E_T, versus the lifetime for electron transfer, k_{et}^{-1}, for complexes 1(■), 2(●), 3(▲), and 4(▼). The average of the R^2 values for this plot is 0.169 55

Figure 4.5 Plot of solvent viscosity, η, versus the lifetime for electron transfer, k_{et}^{-1}, for complexes 1(■), 2(●), 3(▲), and 4(▼). The average of the R^2 values for this plot is 0.334 58

Figure 4.6 Plot of the moment of inertia along the solvent's *x*-axis, I_x, versus the lifetime for electron transfer, k_{et}^{-1}, for complexes 1(■), 2(●), 3(▲), and 4(▼). The average of the R^2 values for this plot is 0.825 58

Figure 4.7 Plot of the characteristic solvent relaxation time, t_{1e}, versus the lifetime for electron transfer, k_{et}^{-1}, for complexes 1(■), 2(●), 3(▲), and 4(▼). The average of the R^2 values for this plot is 0.860 61

Figure 5.1 IR bandshape for ν(CO) of mixed valence 4 in CH_2Cl_2 as a function of temperature. The bandshape shows increasing coalescence as the freezing point of the solution is approached (ca. -95° C). To the right of each spectrum are listed the electron transfer rates obtained from simulation of that spectrum 67

Figure 5.2 IR bandshape for ν(CO) of mixed valence 4 in CH_3CN as a function of temperature. The bandshape shows increasing coalescence as the freezing point of the solution is approached (ca. -44° C). To the right of each spectrum are listed the electron transfer rates obtained from simulation of that spectrum 67

Figure 6.1 (left) Structure of $[Ru_3O(OAc)_6(CO)(ppy)]_2$-μ-pz (1) and (right) structure of calyx[6]arene 72

Figure 6.2 Forward (top) and reverse (bottom) DPV of 2 mM 1 with 0 eq of calix[6]arene (solid lines) and 6 eq of calix[6]arene (dashed lines) 74

Figure 6.3 Square scheme for the binding of calix[6]arene to 1 and the reduction of the bound and unbound dimer. The scheme presented is only for the first binding event, though the results are generally applicable for the binding of the second calixarene 76

Figure 6.4 Plot of $\Delta E_{1/2}$ vs equivalents of calix[6]arene 79

Figure 7.1 Conductance histograms of (a) TMPDI and (b) the TMPDI/TCNE CT complex. The conductance of the TPMDI in the CT complex is 50 times that of the TMPDI alone 90

Figure 7.2 A schematic diagram of the break-junction conductance experiment. A TMPDI molecule is attached to a gold surface (rectangle). A STM tip (triangle) is then repeatedly brought into contact with the surface and pulled away. Current is passed through the system and monitored throughout this process 92

Figure 7.3 Square scheme depicting the various sequences possible for the formation of the CT complex and the passing of current 92

Figure 8.1 Spectroelectrochemical response of (a) LCD at -30 C and -0.95 V, (b) LCD at room temperature and -1.05 V, (c) 2,4,6-tri-(4-pyridyl)-s-triazine at room temperature and -1.20 V, (d) LCD at room temperature and -1.05 V, (e) LCD at room temperature and -1.05 V, and (f) a comparison of spectra at the LCD at both -30 C and room and temperature 101

Figure 8.2 (a) ν(CO) band of LCD at -30 C. (b) ν(CO) band of LCD at room temperature. (c-e) Simulated ν(CO) band assuming an electron transfer rate of $3x10^{11}$ s^{-1}, $1.1x10^{11}$ s^{-1}, and $5x10^{11}$ s^{-1}, respectively 103

Figure 9.1 Complexes 1-12 used for this study grouped by type of dimer and type of monomer 112

Figure 9.2 Decay curves for ^{3}ZnTPP in the presence of various concentrations of 2. The ^{3}ZnTPP was generated by excitation at 555 nm and the decay monitored at 470 nm 116

Figure 9.3 Stern-Volner plot of k_{obs} versus the concentration of 2. The intrinsic rate of the electron transfer process (k_{et}) from ^{3}ZnTPP to 2 is given by the slope of a linear fit to the data. In this case $k_{et} = 1.54 \times 10^9$ s^{-1} 116

Figure 9.4 Graphical representation of the forward electron transfer rates from ^{3}ZnTPP to Complexes 1-12 117

Figure 9.5 Cyclic voltammogram of 3 120

Figure 9.6 The driving forces associated with electron transfer from ^{3}ZnTPP to the pyridyl monomers, the pyrazine monomers, the dabco bridged dimers, the adiabatic wavefunctions of the pyrazine bridged dimers, and the diabatic wavefunctions of the pyrazine bridged dimers 121

Figure 10.1 Diagram of a simple 2D NOESY NMR experiment showing the magnetization of two nuclei (I and S) 128

Figure 10.2 (a) The pulse sequence used in a typical 2D IR experiment. (b) Diagram of how chemical or electronic exchange can lead to the exchange the frequencies of vibrational modes. (c) Diagram of a 2D IR graph 130

Figure 10.3 Diagram showing the magnetization of a nucleus during a typical T_1 relaxation experiment 132

Figure 10.4 Synthetic route for the formation of supramolecular assemblies of ruthenium clusters 136

Figure 10.5 Proposed structure formed upon the reaction of ruthenium chloride hydrate with oxylic acid. In this structure the geometry of the chelating oxylates prevent the formation of the trinuclear clusters of type $Ru_3(O)(L_3)$ 136

LIST OF SCHEMES

Scheme 6.1 In stage A, the dimer, $[Ru_3O(OAc)_6(CO)(ppy)]_2$-μ-pz, is in its symmetric uncomplexed form. In stage B, a single calix[6]arene has bound to the dimer 82

Scheme8.1 The LCD initially undergoes a three-electron reduction (step 1)..... 106

LIST OF TABLES

Table 2.1 $\Delta\Delta E_{1/2}$, ΔG_0, K_{eq}, and ΔG_1 for complexes 1-4 29

Table 2.2 λ_{asymm} and H_{AB} for 1-4, calculated using several methods 33

Table 3.1 Equilibrium constants (K_{eq}) for 1^{-1} at +10° C, 0° C, -40° C, and -90° C. The K_{eq} were obtained through simulation of the spectra in Figure 3.2 43

Table 4.1 k_{et}^{-1} for complexes 1-4 and selected solvent thermodynamic parameters 51

Table 4.2 k_{et}^{-1} for complexes 1-4 and selected solvent dynamic parameters 52

Table 5.1 k_{et}^{a} for complexes 1,2 and 4 in CH_2Cl_2 68

Table 5.2 k_{et}^{a} for complexes 2 and 4 in CH_3CN 68

Table 6.1 Values for $E_{1/2}(1)$, $E_{1/2}(2)$ and $\Delta E_{1/2}$ for complex **1** as a function of the equivalents of calix[6]arene present 74

Table 9.1 Extinction coefficients for one of the maximums in the UV-vis spectra for complexes **1-12** 114

Table 9.2 Potentials for the reduction of the clusters from $Ru^{III}Ru^{III}Ru^{II}$ to $Ru^{III}Ru^{II}Ru^{II}$ for complexes **1-12** 114

Table 9.3 k_{et} for the forward electron transfer from ^{3}ZnTPP to complexes 1-12 as well as driving force associated with this reaction 120

ACKNOWLEDGEMENTS

It is not often that one has the opportunity to overtly thank those around him. Or rather, the opportunity arises almost daily, but it is rarely taken. So, let me seize this chance to say what needs to be said about those people that have surrounded me throughout my graduate years.

Most obvious is my advisor, Cliff. I am truly fortunate to have worked for him. Cliff has functioned as almost the definitive advisor (as opposed to a boss) letting a biochemist discover for himself (with a bit of advice from time to time) the world of physical and inorganic chemistry. I am extremely grateful for the patience Cliff has showed and the leeway he has given me in my years under his direction. I am certain that I have learned more – both about chemistry and scholarship in general – than I would have should he have held a tighter grip on the reigns.

Just as obvious a contribution has been from my labmates. Uniquely amongst those I have interacted closely with in my graduate career, they have contributed support both intellectually as well as emotionally. They have been present for discussions on science as well as discussions on life and it would be no exaggeration to say that I have learned orders of magnitude more from them than they have from me. It seems unlikely that I will ever find myself in a work environment as wonderful as the one I have spent the last five years of my life. But beyond this they are all wonderful people. Even during weeks that my chemistry was working terribly I looked forward to going to work if only to have the opportunity to interact with these people. Truly, they are an amazing bunch and I cannot but hope the best for the lot of them.

Moving to the perhaps less obvious (but in all likely-hood more important) we have my wife. There is an old saying, “If the wife ain’t happy, ain’t nobody happy.” And, to a great extent, this rings true. In a marriage, your enjoyment of life depends heavily on how much your spouse is determined to let you (or encourage you) to enjoy it. I must say that on this front I have been very blessed. Throughout the past five years my wife, Shana, has been understanding of weekends lost to work, weeks lost to conferences, dinner conversations lost to the obscure corners of science, and her aspirations put on hold while I tried to improve myself. I truly hope that I am able to repay her over the many years ahead of us.

Progressing to those even more removed from my academic career, we find my friends. Those who have supported me through the (admittedly rare) tough times of graduate school, have reminded me that there is much more to do in life than add pyridine to ruthenium and then shine light on it, and have provided me with a home for my craziest of ideas. If friends are the spice of life, I have been given an Indian buffet.

Most removed from my academic career, but in some ways most integral, is my family. My father, mother, and brother are people that I have always been able to depend on. Any venture (such as undergrad, graduate school, and my career beyond) is made less intimidating – inviting even – knowing that there is always unconditional support for me. To them I owe a debt of gratitude that I fear I can never repay.

And with that ends the acknowledgements section of my thesis. It is woefully inadequate that out of a work spanning over a hundred pages I have devoted not even two full pages to those people that have encouraged and enabled me to complete it. I only hope that I have contributed similarly to their endeavors in life.

"Perhaps, if I am very lucky, the feeble efforts of my lifetime will someday be noticed, and maybe, in some small way, they will be acknowledged as the greatest works of genius ever created by Man."

~ Jack Handy

SPECIFIC CHAPTER ACKNOWLEDGMENTS

Chapter 6: Much of the material in this chapter comes directly from a manuscript entitled, "Charge Gating and Electronic Delocalization over a Dendrimeric Assembly of Trinuclear Ruthenium Clusters," by Benjamin J. Lear and Clifford P. Kubiak, which has been published in Inorganic Chemistry (2006), 45(18), 7041-7043.

Chapter 8: Much of the material in this chapter comes directly from a manuscript entitled "Origins of cooperative noncovalent host-guest chemistry in mixed valence complexes," by Benjmain J. Lear and Clifford P. Kubiak, which has been published in Journal of Physical Chemistry B (2007), 111(24), 6766-6771.

VITA

2002	Bachelor of Science, University of California, Davis
2004	Master of Science, University of California, San Diego
2007	Doctor of Philosophy, University of California, San Deigo

PUBLICATIONS

Lear, B. J., Glover, S. G., Londergan, C. H., Salsman, J. C., Kubiak, C. P. *Solvent dynamical control of ultra fast ground state electron transfer: Implications for class II-III mixed valency.* Journal of the American Chemical Society (2007), *submitted*

Glover, S. D., Lear, B. J., Salsman, J. C., Londergan, C.H. Kubiak, C. P. *Electron transfer at the class II/III borderline of mixed valency. Dependence of rates on solvent dynamics and observation of a localized – to delocalized – transition in freezing solvents.* Philosophic Transaction of the Royal Society, A (2007) *Submitted*

Lear, Benjamin J.; Kubiak, Clifford P. *Origins of cooperative noncovalent host-guest chemistry in mixed valence complexes.* Journal of Physical Chemistry B (2007), 111(24), 6766-6771

Lear, Benjamin J.; Kubiak, Clifford P. *Charge Gating and Electronic Delocalization over a Dendrimeric Assembly of Trinuclear Ruthenium Clusters.* Inorganic Chemistry (2006), 45(18), 7041-7043.

Londergan, Casey H.; Salsman, J. Catherine; Lear, Benjamin J.; Kubiak, Clifford P. *Observation and dynamics of "mixed-valence isomers" and a thermodynamic estimate of electronic coupling parameters.* Chemical Physics (2006), 324(1), 57-62.

ABSTRACT OF THE DISSERTATION

The effects of electronic delocalization in highly coupled mixed valence systems

by

Benjamin James Lear

Doctor of Philosophy in Chemistry

University of California, San Diego, 2007

Professor Clifford P. Kubiak, Chair

The trinuclear ruthenium cluster $RuO(OAc)_6L_3$ (where L is an ancillary ligand) is used to make a variety of mixed valence compounds in which two or more clusters are joined together by an organic bridging ligand. The magnitude of electronic coupling in the mixed valance state of these compounds is quite large and the complexes reside on the Robin-Day class II/class III borderline. The large degree of coupling in these complexes gives rise to ultrafast electron transfer whose effects are observable in the infrared (IR) spectra of these complexes. Utilizing the IR properties of the complexes we are able to arrive at thermodynamic estimates of the electronic coupling parameter (H_{AB}) for asymmetric mixed valence compounds. These asymmetric compounds give rise to mixed valence isomers and the temperature dependence of the isomer populations is used to determine ΔH and ΔS for the electron transfer event in these complexes.

The large coupling in these complexes reduces the barrier to electron transfer significantly (enabling ultrafast electron transfer). This places the rate of electron transfer under the control of the nuclear dynamics of the complex and the surrounding environment. The result is that the rate of electron transfer in these mixed valence complexes shows a strong dependence on kinetic parameters of the solvent (those that describe the movement of the nuclei of the system), but not on thermodynamic parameters of the

solvent (that describe more static energetic contributions of the environment). This, in turn, leads to an unexpected temperature dependence of the electron transfer rate. It is found that the electron transfer rate dramatically increases when the solvent is frozen. This results form a decoupling of the relatively slow solvent motions from the electron transfer event allowing for the faster internal vibrational motions of the mixed valence complex to control the rate of electron transfer.

The effects of the large electronic coupling in these complexes also gives rise to other suprising behaviors. The extent of the electronic coupling in the mixed valence systems is known to depend on the electron donor strength of the attached ancillary ligands. It is shown that, through supramoleuclar interactions at the ancillary ligands of these mixed valence systems, the electronic coupling may be modulated. There is a significant decrease in the resonance stabilization associated with breaking of symmetry in a mixed valence system and that this energy (together with the energy gained by restoration of symmetry) can provide substantial driving force for chemical interactions. This effect is explained in terms of both the direct stabilization of the compound through electronic coupling and in terms of resonance stabilization of the unpaired electron in the mixed valence compound. This result is then extended to molecular electronics where it is shown that changes in current effected by a chemical interaction can provide a driving force for said chemical interaction.

The large magnitude of electronic coupling in these mixed valence systems is also shown to be sufficient to stabilize as the ground state what would be thought of as low-lying excited states. It is shown that an electron may transfer from a cluster to the bridging ligand and that this electron transfer gives rise to an increase in electronic coupling throughout the mixed valence state. This increase in electronic coupling is found to be sufficient to stabilize the radical state of the organic bridge.

The large energy difference between uncoupled (diabatic) and coupled (adiabatic) mixed valence compounds is also exploited in order to determine whether an electron entering into the mixed valence molecule enters into a diabatic or adiabatic wavefunction. The electron transfer rate from photo-generated triplet zinc tetraphenylphorpyrin to the mixed valence compounds was observed. Comparisons of the observed electron transfer rate to the diabatic and adiabatic driving force for electron transfer are made. It

is concluded that the electron enters into a diabatic wavefunciton of the mixed valence compound after which the compound evolves into the adiabatic wavefunciton.

The major theme throughout this thesis is the exploitation of the huge value of electronic coupling (H_{AB}) in order to give rise to and explain some very unique and unexpected behaviors of these mixed valence complexes.

Chapter 1: A brief introduction to the science of electron transfer

1.1 Introduction

You cannot do chemistry without electrons. The chemist often spends time determining what the electron count of a complex is and where the electrons in a complex are likely to go. "Pushing electrons" is standard practice in rationalizing chemical mechanisms. Indeed, while the identity of the elements is given by their protons their chemical reactivity is given by the number of electrons. This holds true for all of chemistry. In order to understand the behavior of molecules, one needs to understand their electronics. Throughout most of chemical history it seems that the understanding of chemical behavior is paramount to the understanding of chemical reactions, which, in most reductionist view, are just the movement of electrons between chemical species. In these reactions, electrons are given to, taken from, or shared between two chemical species or parts of a single chemical. As such, the transfer of a single electron may be viewed as the simplest of chemical reactions. Thus, if we are to understand the very heart of chemistry (when do electrons move, why do they move, how do they move, what makes them move, and how quickly can they move) then it would seem the first step is to understand the transfer of a single electron. Indeed, over the last 50 years much has been accomplished in understanding this most simple of chemical reactions.

1.2 Electron transfer reactions

While the vast majority of chemical reactions can be understood to involve electron transfer, most of these reactions are unfit for the study of electron transfer because most chemical reactions are too complex to allow the easy study of the parameters which govern the comparatively simple movement of an electron from one site to another. Ideally, the study of electron transfer would involve little change in the chemical makeup of the involved species (other than the transfer of the electron). Thus, classic organic reactions are unsuitable because they are accompanied by the formation of drastically different chemical species (as in the esterification of an acid with an alcohol). In order to study electron transfer, early

experimentalists turned to inorganic complexes, which had the advantage of tunable driving forces for the reaction, stable coordination spheres (so that the movement of electrons can be unaccompanied by other chemical changes), the ability to transfer a single electron, and the ability to incorporate spectroscopic markers for product detection. To this day, electron transfer remains largely in the realm of physical and inorganic chemistry.

The majority of early research centered on the bimolecular electron transfer between chemical species in solution. Such a reaction can be written as;

$$A^- + B \rightarrow A + B^- \quad (1)$$

In the event that A and B are the same chemical species, differing only by the electron count on each, the overall reaction is termed "self-exchange." There are two basic mechanisms by which these electron transfer reactions can proceed. The first, termed "outer-sphere" is a simple bimolecular reaction in which the two chemical species act as hard spheres. That is, the two chemical species contact each other, the electron is transferred, and the products diffuse away. Alternatively, this reaction can proceed through an "inner-sphere" mechanism in which the two chemical species encounter one another and form an intermediate complex in which the two are connected by some chemical bridge. The electron is then transferred between the two sites within this intermediate complex after which they separate and the products diffuse away. This inner sphere mechanism can be represented by equation 2.

$$A^- + B \rightarrow A^-\text{—}B \rightarrow A\text{—}B^- \rightarrow A + B^- \quad (2)$$

In general, the outer-sphere electron transfer presents a larger enthalpic barrier to electron transfer (the electron must travel farther and through space) while the inner-sphere electron transfer presents a larger entropic barrier to electron transfer (the intermediate complex must be formed prior to electron transfer).[1]

Electron transfer had been extensively studied and the difference in the inner-and outer-sphere mechanisms established early on in the last century, however, no definitive theory of electron transfer

emerged until, following a 1952 meeting on electron transfer[2], Rudy Marcus developed and presented his theory on electron transfer.[3]

1.3 The Marcus and Marcus-Hush theories of electron transfer

The Marcus theory of electron transfer (for which Marcus won the Nobel Prize in 1992) can be understood through the use of a few simple diagrams, the first of which is displayed in Figure 1.1. First, one constructs a potential energy curve for the reactants (the electron donor and the electron acceptor) which takes into consideration all of the energetic contributions from the various bond length changes in the molecule as well as the energetic contributions from the surrounding environment (solvent dipole orientation, counter ions, etc.). Generally, the potential energy curves are generated using a simple harmonic oscillator approximation so that the resulting curves are parabolas. This is drawn on a graph in which the y axis is taken to be energy and the x axis is the reaction coordinate, X. The reaction coordinate is a variable that keeps track of the nuclear coordinates of the electron transfer system and varies between 0 (the most stable reactant nuclear configuration) and 1 (the most stable product nuclear configuration). The reactant potential energy curve is then centered at X=0. Thus, when the electron resides in the bottom of this curve it is said to exist on the electron donor (the electron is on the reagent's potential energy curve) and, additionally, the electron donor, electron acceptor, and surrounding medium are in the most stable nuclear configuration for the electron existing on the donor. Next a potential energy curve is generated for the products (taking into consideration all bond length changes for the donor and acceptor as well as the environmental effects) and is centered at X=1. Thus, an electron residing at the bottom of this curve exists on the electron acceptor (this *is* the product curve!) and the donor, acceptor, and environment all are at their lowest energy nuclear configurations for the electron existing on the acceptor. Besides the offset along the reaction coordinate, the two curves are also displaced from one another along the energy coordinate (the y axis). This difference represents any change in free energy that results from the electron transfer. Thus, the entire electron transfer system is represented by these two intersecting parabolas.

There are three points of interest in this diagram, the minimum of the reactant curve, the minimum of the product curve, and the point at which the two curves meet. The difference in energy between the two

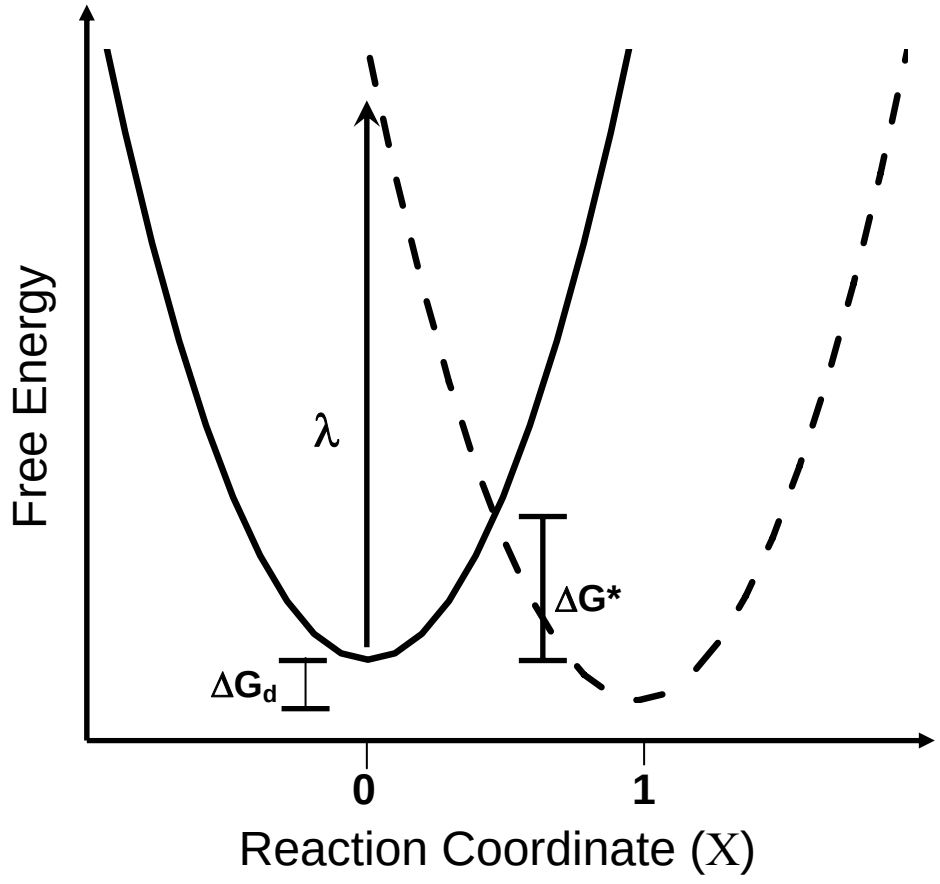

Figure 1.1. Diabatic potential energy curves for the reactants (solid line) and products (dashed line) of an electron transfer reaction. The reaction coordinate is a measure of the nuclear configuration of the system undergoing the electron transfer reaction. At X=0, the system is in the most stable nuclear configuration assuming the electron is on the electron donor. At X=1 the system is in the most stable nuclear configuration assuming that the electron has been transferred to the acceptor. ΔG_d is the free energy change associated with the electron transfer between these two diabatic curves. ΔG^* is the barrier to thermal electron transfer (activation energy) and λ (called the reorganization energy) is the energy required to optically excite the electron from the donor to the acceptor.

minima (ΔG_d) is the driving force for electron transfer associated with the diabatic wavefunctions. Since conservation of energy requires that the products and the reactants be isoenergetic at the point at which radiationless (thermally activated) electron transfer occurs, the point at which the two diabatic potential energy curves cross is the point at which thermal electron transfer occurs. Thus, the electron may proceed along the potential energy curve of the products to the point at which the reactant and product potential curves meet. At this point, the electron may hop from the reactant curve to the product curve. This curve hopping does not always take place and the frequency with which this occurs is given by the transmission coefficient, κ (which varies between 0 and 1). If the electron does not transfer to the product curve (no electron transfer event) the electron continues along the reactant potential energy curve. For a thermal electron transfer event the rate of the electron transfer is exponentially dependent on the energetic barrier (activation energy) to electron transfer. This barrier (ΔG^*) controls the electron transfer rate (k_{et}) in the normal Arrhenius manner. Specifically, k_{et} is given by[4];

$$k_{et} = \kappa \nu_N \exp[-(\Delta G^*)/RT] \tag{3}$$

In which ν_N is the collision frequency, κ is the transmission coefficient, ΔG^* is the activation energy (given by equation 5), R is the gas constant, and T is the temperature of the system.

Besides the thermally activated process there is one other means by which electron transfer may be acheived. Specifically, the electron may be optically excited from the donor to the acceptor. Consider an electron which is located in the bottom of the potential curve for the reactants. Some distance above it displaced along the y coordinate is the product's potential energy curve. If light of sufficient energy is shined on the system, then the electron may be promoted from the donor to the acceptor (the electron moves from the reactant's to the product's potential energy curve). The Frank-Condon approximation states that the electronic motion can be assumed to occur instantaneously with respect to the nuclear motion and the system does not evolve along the reaction coordinate during this electron transfer event. Thus, we are left with an electron which resides on the acceptor (the electron is on the product potential energy curve), but in a system that is in the equilibrium geometry of the reactants. That is, the nuclear coordinates

of the donor, the nuclear coordinates of the acceptor, and the nuclear coordinates (and dipole moments) of the solvent and the counter ions are as if the electron was on the donor and not the acceptor. Again, this is a result of the Frank-Condon approximation. The energy required for this transition is termed the reorganization energy, λ. The total value of λ is a sum of both inner-sphere (changes to bond lengths, etc.) as well as outer-sphere (solvent dipole reorientation) barriers to electron transfer. Because the process involves the movement of an electron between redox sites (exchanging valencies) then the absorption feature associated with this process is called the intervalence charge transfer (IVCT) band. Typically, the solvent is treated as a dielectric continuum and the contribution from the outer sphere portion, λ_o, is given by[5];

$$\lambda_o = \frac{(\Delta e)^2}{8\pi}\left(\frac{1}{\varepsilon_{op}} - \frac{1}{\varepsilon_s}\right)\int (D_A - D_B)^2 \, d\tau \tag{4}$$

Here, Δe is the amount of charge being transferred, ε_{op} is the optical dielectric constant of the solvent, ε_s is the static dielectric constant of the solvent, and the integral accounts for the distance the electron travels. Because the potential curves are generated using the harmonic oscillator model, then there exists a simple relationship between the thermal activation energy, ΔG*, and the reorganization energy for optically induced electron transfer, λ. This relationship is one of the great triumphs of Marcus theory and is given by[4];

$$\Delta G^* = \frac{1}{4}\lambda\left(1 + \frac{\Delta G_d}{\lambda}\right)^2 \tag{5}$$

The above discussion of thermal and optically induced electron transfer assumed that the electron donor and electron acceptor did not interact appreciably (outer-sphere electron transfer). However, in the case of inner-sphere electron transfer, this assumption may no longer be valid. The formation of a chemical bridge between the donor and acceptor can allow the two chemical sites to couple electronically. That is,

the electronic properties (the wavefunctions) of these two species may be mixed. In physical terms, the potential energy surfaces can no longer be treated diabatically and must instead be treated adiabtically. In this case, the non-crossing rule applies and the two wavefunctions are mixed. The mixing is quantified by a quantum mechanical operator, H_{AB} (termed the electronic coupling matrix), which functions to mix the donor and acceptor wavefunctions to produce two new wavefunctions – a symmetric and antisymmetric combination – each with their own associated potential energy curve. Figure 1.2 presents the original diabatic and the newly created adiabatic curves. There are four important effects of H_{AB} upon the electron transfer system. First, the barrier to thermal electron transfer is decreased. The new value for ΔG* is given by the following equation[4].

$$\Delta G^* = \frac{\lambda}{4} + \frac{\Delta G_d}{2} + \frac{\Delta G_d^2}{4(\lambda - 2H_{AB})} - H_{AB} + \frac{H_{AB}^2}{(\lambda + \Delta G_d)} \tag{6}$$

The second effect that H_{AB} has on the potential energy surface is that the minima of the reactants and products are moved toward each other along the reaction coordinate and are no longer located at X=0 and X=1. The positions of the minima are given by the following equations (7a is the minima for the reactant curve and equation 7b is the minima for the product curve);[4]

$$\mathrm{X}_{\min} = \frac{H_{AB}^2}{(\lambda + \Delta G_d)^2} \tag{7a}$$

$$\mathrm{X}_{\min} = 1 - \frac{H_{AB}^2}{(\lambda - \Delta G_d)^2} \tag{7b}$$

This movement is a result of the mixing of the two wave functions in which the ground state of the reactants incorporate properties of the products and the ground state of the products begin to incorporate the properties of the reactants. Third, any difference in energy between the reactants and the products is decreased[4, 6] – again a direct result of the mixing of the two states. And fourth, the overall energy of the

ground state (symmetric) wavefunction is stabilized and the overall energy of the excited state (anitsymmetric) wavefunction is destabilized. The overall effect is that the symmetric and antisymmetric wavefunctions move apart from each other along the y axis – each by an amount equal to H_{AB}. Thus, at the crossing point the distance between the two curves will equal $2H_{AB}$. This effect may be thought of as a type of resonance similar to what is found during the formation of the hydrogen molecule in which the two wavefunctions of the hydrogen atoms couple to give stabilized (bonding, symmetric) and destabilized (antibonding, antisymmetric) combinations, where the stabilization energy arises from electron exchange in the form of the "resonance" integral, $H_{12} = \int \Psi(1) H \Psi(2) d\tau$.

It is worth addressing the specific effects of H_{AB} upon electron transfer in more detail. As mentioned above, the activation energy, ΔG^*, is decreased as a direct result of the action of H_{AB}. The natural and logical consequence is that the thermal electron transfer rate will proceed more quickly in complexes that are more electronically coupled to one another. Remembering that the reorganization energy for optical electron transfer is related to the thermal activation energy, it is natural to wonder how λ might be affected by H_{AB}. As it so happens, the value of λ in symmetric systems ($\Delta G = 0$) is unaffected by the action of H_{AB}.[7] Qualitatively, the movement of the minima along the ground state wavefunction along X (which functions to decrease λ) is exactly cancelled out by the movement of the ground state and excited state wavefunction apart from one another along y (increasing the value of λ). Thus the value of λ is not sensitive to the value of H_{AB}. In asymmetric systems the value of λ *is* sensitive to H_{AB} and the value of λ that depends on H_{AB}, λ', is given by;

$$\lambda' = \lambda - \frac{4H_{AB}^2}{\lambda} \tag{8}$$

The effects of H_{AB} upon the potential energy surfaces draws attention to this operator. Specifically we can see that there are three possible shapes for the potential energy curves and that these shapes are dependent on the value of H_{AB}. First, when $H_{AB} = 0$, then the two diabatic curves remain as drawn in Figure 1.1. Second, as soon as H_{AB} deviates from zero, then the curves become adiabatic and as a result $\kappa = 1$ (the

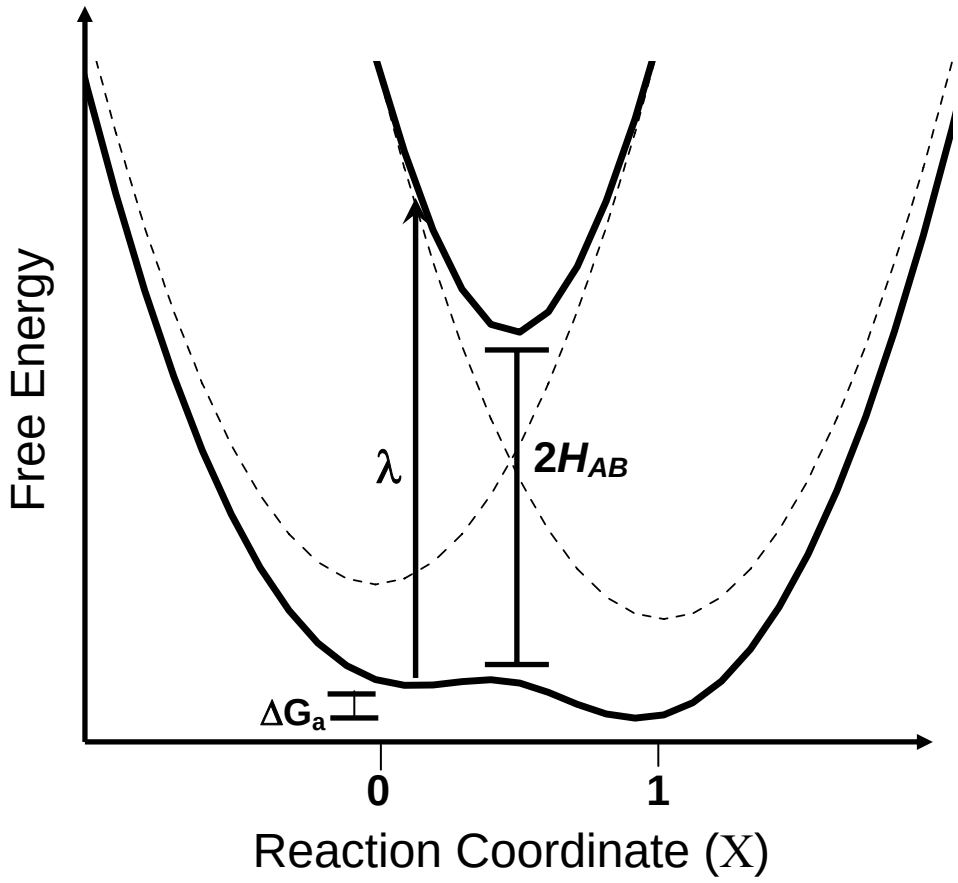

Figure 1.2. Diabatic (dashed lines) and adiabatic (solid lines) potential energy curves for a system undergoing electron transfer. The diabatic curves are generated assuming no electronic interaction between the redox sites among which the electron is transferred. The adiabatic curves are generated from the diabatic curves assuming there is significant electronic coupling between the redox sites. This coupling functions to mix the two diabatic curves to generate the adiabatic curves. The lower (groundstate) adiabatic curve is the result of symmetric combination of the two diabatic curves and the upper (excited state) adiabatic curves is the result of the antisymmetric combination of the two diabatic curves. The magnitude of coupling is given by H_{AB}. ΔG_a is the free energy change for the electron transfer process and λ is the energy required for optical excitation from the ground state wavefunction to the excited state wavefunction.

bottom curve is continuous along X and an electron traveling along it has no choice but to move from reactants to products). In this case the lower potential energy curve contains two minima, a condition that remains until $H_{AB} = \lambda/2$. At this point the third shape is obtained. In this case the lower potential energy surface contains a single minimum and the electron neither resides exclusively on the donor or the acceptor, but on both equally and simultaneously. The implication of this will be thoroughly addressed when the classification of mixed valence complexes is discussed later in this chapter. For now it is sufficient to realize that to understand the behavior of an electron transfer system it is useful to know the value of both λ and H_{AB}. The value of λ may be read from near IR or UV-vis spectra of the system but no immediately obvious experimental method presents itself for determining the value of H_{AB}.

In 1967 Noel Hush demonstrated that the placement, intensity, and shape of the absorption band can be used to determine the value of H_{AB}.[8] The placement of this band (ν_{max}) in the electromagnetic spectrum is assigned to the peak of the absorption profile and is related to λ by $\nu_{max}=\lambda+\Delta G_a$. The energetics of electron transfer are such that this band is usually found in the near IR or UV-vis spectrum of these complexes. The intensity is given by the extinction coefficient (ε) of ν_{max}. The extinction coefficient for the IVCT band is found to increase with H_{AB} for transition metal complexes. This is because for such metal complexes the electron is being transferred between two d orbitals and, as such, is symmetry forbidden. However, as H_{AB} mixes together the donor and acceptor wavefunctions the optical transition gains increasing π to π^* character, which is symmetry allowed. Finally, the shape of the IVCT band is given by the full width at half maximum ($\Delta\nu_{1/2}$) for the band, which is found to decrease with increasing H_{AB}.[7] The band is not dynamically broadened as in IR bandshapes, where coupled solvent modes can broaden the bands.[9, 10] This is because the timescale for near IR and UV-vis processes are too short for solvent modes to have an effect. Additionally, the transition is an electronic one and occurs much faster than the timescale of nuclear motions of the molecule or the surrounding medium. Rather, the shape of the band may largely be understood by consideration of the topography of the potential energy curves associated with the transition. In uncoupled cases, one can see that there should be a Gaussian distribution of energies for the transition based upon a Boltzmann distribution of states in the ground state wave function. As the coupling between sites increases, then the low energy side of the transition will be

increasingly cut off. In the extreme case, there will be no transitions that have an energy less than λ itself and the IVCT band will be truncated at ν_{max}.[7] Thus, H_{AB} functions to both sharpen the IVCT band as well as to add asymmetry. This is illustrated in Figure 1.3. If this were the only physical contribution then, in the fully delocalized case, one would expect a sharp cutoff at ν_{max}. However, this is never observed. The reason for this is three-fold. First, the uncertainty principle does not allow for infinitely sharp energy cutoffs and so the low energy limit of the IVCT band will be broadened from the predicted vertical line. Second, the energy of NIR and UV-vis transitions are such that the uncertainty principle must contribute noticeably to the bandshape. Third, the electronic transition can be coupled to vibronic transitions. That is the electronic transition can be accompanied by transitions in the vibrational quantum number. This also functions to broaden the observed IVCT band. Despite these complications, it is clear that the intensity and shape of the IVCT is dependent on H_{AB}. Thus, Hush was able to derive the following equation that relates these properties;

$$H_{AB} = \frac{\left(2.06\times10^{-2}\right)\left(\upsilon_{\max}\varepsilon_{\max}\Delta\upsilon_{1/2}\right)}{r_{AB}} \tag{9}$$

Where ν_{max}, ε_{max}, and $\Delta\nu_{1/2}$ have the meanings defined above, r_{AB} is the distance over which the electron is transferred, and 2.06 x 10^{-2} is an empirically determined factor.

For systems in which H_{AB} is rather small (much less that λ/2) the Hush equation gives very reasonable estimates for H_{AB}. However, for cases in which H_{AB} approaches λ/2, then the Hush equation gives increasingly poor estimates of H_{AB}. The reason for this two-fold. First, as H_{AB} increases the electron transfer distance decreases and values of r_{AB} determined from x-ray crystallography become increasing inaccurate.[11-14] Secondly, as the system becomes more delocalized, vibrational coupling to the electronic transition becomes more important, rendering the $\Delta\nu_{1/2}$ value less accurate.[15, 16] Despite these deficiencies, the electron transfer theories of Marcus and Hush (which have been heavily reviewed)[4, 5, 7, 11, 17-24] have guided research into electron transfer for almost six decades and still provide the common language spoken within this area of chemical research.

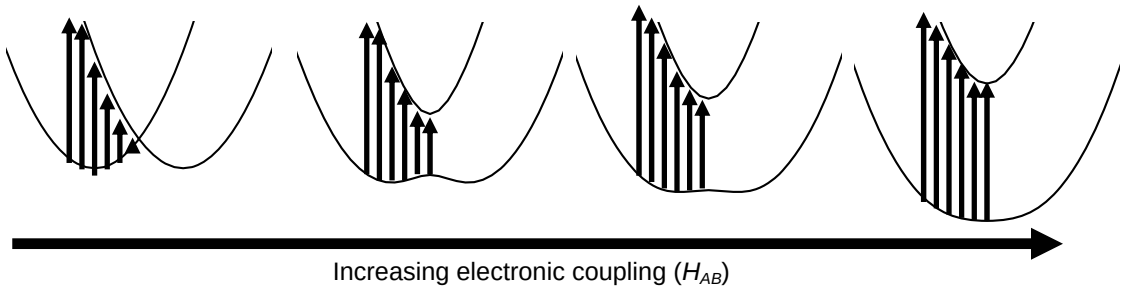

Figure 1.3. A schematic respresentation of how the potential energy surfaces change with increasing electronic coupling. Drawn on the surfaces are the vertical transitions that are associated with the photo-induced electron transfer event. Of note is that as the coupling increases to the point that the lower energy curve has only a single minima, the lowest energy transition (from the middle of the potential energy surface) increases in energy. The result is that as electronic coupling increases in mixed valence complexes the lower energy side of the IVCT band will be increasingly cut off.

1.4 Mixed valency and the Robin-Day classification scheme

In the early days of electron transfer research the emphasis was placed on intermolecular electron transfer reactions – reactions in which the electron is transferred between two distinct chemical species. This reaction could proceed through outer-sphere or inner-sphere mechanisms. The fact that the inner-sphere mechanism proceeds through a bridged intermediate raised interesting questions. Could permanently joined chemical species be made that would undergo electron transfer? In its simplest form such *intra*molecular electron transfers could involve the same metal centers with the same coordination sphere, but in which the two metal centers would have differing oxidation states. The metal centers could then exchange electrons (and by way of this, oxidation states) between them. Such complexes are termed mixed valence complexes, reflecting the fact that within a mixed valence complex there exists the same type of redox site in different valences. Examples of mixed valence complexes had been known for quite some time, the most famous of these perhaps being Prussian Blue (an inorganic dye whose intense blue coloration arising from an IVCT absorption). However, until the 1969 all known mixed valence compounds were naturally occurring, and today even more are being identified (mixed valency is liberally employed by living organisms to form the active centers of proteins and enzymes). In 1969 the first synthetic mixed valence compound was made by Carol Cruetz and Henry Taube[25]. This so-called Cruetz-

Taube ion, $[(Ru(NH_3)_5]\text{-}\mu_2\text{-}pz^{+4,\,+5,\,+6}$, when in the mixed valence (+5) state contains a ruthenium (II) and a ruthenium (III) between which an electron is exchanged.

One of the key features of mixed valence compounds is that the bridge is able to mediate electronic coupling between the redox sites within the molecule. Thus, the magnitude of the coupling is dependent on the nature of the bridge. Considerations for the effect of the bridge upon the value of H_{AB} consist of the energetic overlap between the sites and bridge, the distance between the sites (determined by the length of the bridge), and the geometric overlap between the orbitals of the site and the bridge. The result is that mixed valence species can display a large spread in the degree of electronic coupling and that the degree of electronic coupling can be synthetically tuned. Robin and Day recognized that there existed this large variation in the magnitude of the electronic coupling (H_{AB}) and devised a classification system that relies upon its value.[26]

The system of classification created by Robin and Day breaks mixed valence compounds into three classes based on the electronic structure of the mixed valence system in question. In the first class (class I) there is no electronic coupling between the two oxidation sites. In such a compound, where $H_{AB} = 0$, the potential energy curves associated with this reaction remain diabatic (Figure 1.4a), and the compound is valence trapped (the odd electron exists definitively on either of the two oxidation sites). In the second class (class II) the electronic coupling is non-zero, resulting in two adiabatic potential energy curves. However, for class II ($0 < H_{AB} < \lambda/2$) compounds the ground state potential energy curve retains two minima (associated with the reactants and products) and the system is valence trapped (Figure 1.4b). In the final class (class III) $H_{AB} \geq \lambda/2$. The result is that the ground state wavefunction contains but a single minima and the system is valence averaged (Figure 1.4c). In this case, the odd electron does not exist on either of the two oxidation centers, but rather on both of them at once and each of the centers is ascribed a electron occupancy of ½. Thus, the Robin-Day scheme is seen to separate out compounds biased upon the extent of electronic delocalization (the shape of the lower potential energy surface) and, because the shape of the lower potential energy curve can be shown to depend on H_{AB}, H_{AB} becomes an important metric for the classification of mixed valence systems.

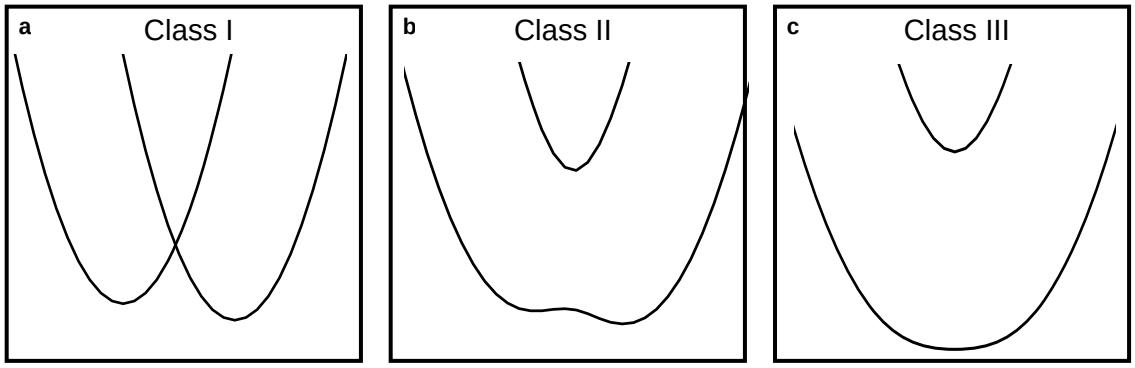

Figure 1.4. Depiction of the potential energy surfaces associated with the three classes of the Robin-Day classification scheme for mixed valence systems. (a) In class I systems (H_{AB}=0), there is no coupling between the two redox sites and the reactant and product curves remain diabatic. (b) In class II systems ($0<H_{AB}<\lambda/2$), there is electronic coupling between the two redox sites and adiabatic curves are generated from the diabatic curves. However, the adiabatic surface retains two minima in its surface and the electron is considered to be valence trapped. (c) In class III systems ($H_{AB}\geq\lambda/2$) the electronic coupling is large enough that the ground state (lower) adiabatic potential energy curve contains only a single minimum. In this case the electron is not valence trapped, but instead is delocalized between the two coupled redox sites.

1.5 The emergence of class II-III mixed valency

The nature of the Robin-Day scheme naturally begs a question; if the difference between class II and class III is a localized versus delocalized electron, then how does one decide when an electron is delocalized? Marcus-Hush theory appears to provide an easy metric – full delocalization occurs when $H_{AB} = \lambda/2$. However, while λ can be easily obtained form NIR or UV-vis spectra, H_{AB} (in the limit that its value approaches $\lambda/2$) is a much more difficult quantity to accurately determine. This, in a large part is due the failure of the Hush equation when electronic coupling is large.[11] Other means of estimating H_{AB}, through determination of ΔG^* or ionization energies are likewise fraught with difficulty and it remains problematic to obtain reliable values of H_{AB} for strongly coupled systems. Thus, while it is easy to determine when a system is definitively valence trapped or obviously valence averaged, it can be troublesome to classify those compounds that reside near the localized to delocalized transition. Instead of relying upon the values

of λ and H_{AB}, one must instead examine other properties of mixed valence systems in order to place them into class II or class III.

As discussed above, the bandshape of the IVCT band is heavily dependent on the underlying shape of the ground state wavefunction. Thus, by examination of the bandshape one can make tentative assignments to class II or class III. However, while in theory bandshape analysis can provide a means for discriminating between class II and class III, the criteria are somewhat nebulous mostly owing to the fact that quantitative discussions of the shape of the ICVT band are clouded by vibronic coupling[15, 16, 27-30] and the so-called interconfigurational (IC) bands that can occur within the d-orbital manifold of transition metal mixed valence compounds.[17, 31, 32] A much better method for determination of the class using the IVCT band is to study its solvent dependence. Because the IVCT band is associated with the optically induced electron transfer, then it must involve a change in the dipole moment of the compound. If, as is usual, one assumes the solvent to be a dielectric continuum, then some of the energy required for the electron transfer stems from the energy required to effect a dipole change in this dielectric medium. Since different solvents will necessarily have differing dielectric constants, one may assume that the contribution to λ from the solvent will vary with changes in the identity of the solvent. Therefore, what is predicted (and usually observed) is that for valence trapped systems the energy of the IVCT band is found to change with solvent and this dependence correlates well with the dielectric constant of the solvent.[11, 17] For fully delocalized (class III) systems, however, no such dependency is observed. In class III complexes the electron is averaged between the two sites and the IVCT band is no longer the optical excitation of the electron from one site to another. Instead, the IVCT is an electronic transition within the orbital manifold of the complex and is quite analogous to a π to π* transition. As such, there is no change in the dipole moment of the molecule upon excitation of the IVCT band and, as as result, the IVCT band shows no solvent dependence. Thus, if one is able obtain the IVCT band for a mixed valence compound in a variety of solvents then one could easily be able to classify the complex at class II or class III.

There is one problem that arises, however, with this treatment. It stems from the inherent timescales involved in the thermal electron transfer and the nuclear motions of the solvent. It can be shown that the dielectric response of a solvent becomes averaged when the applied electric field (the dipole)

oscillates at a frequency faster than 10 ps.[33] Thus, if the electron is exchanging with a frequency faster than this, then the dielectric response of the solvent may not keep tempo with the changing electronic field and the IVCT band would not be expected to show any solvent dependence. On the other hand, the timescale for nuclear motions (vibrations) of the molecule can be as fast as 0.1 ps. Thus, it is possible (for electron transfer lifetimes between 10 ps and 0.1 ps) that the IVCT band could be solvent independent (which would lead to an assignment of class III), while with respect to the nuclear motions of the mixed valence complex the electron would be localized (in which case the compound would be class II). Clearly, if the electron is localized on the timescale of the vibrations of the complex, then it cannot be fully delocalized and the solvent independence of the IVCT band would lead to incorrect classification.

It seems likely that the most important experimental consideration when deciding between localized versus delocalized electrons is the timescale of the electron transfer relative to the timescale of the molecular vibrations. If the timescale of the electron transfer is faster than the timescale of nuclear motions of the complex, then the electron may be considered delocalized. If, however, the timescale of the electron transfer is slower than the timescale of the nuclear motions then the electron may be considered localized. What is needed is a way to determine the relative rates of the electron transfer and the vibrational modes of the molecule. The lifetime of the vibrational modes may be determined from their position in the IR using the relationship, $\tau=\lambda/c$ (where τ is the lifetime, λ is the wavelength of IR light, and c is the speed of light in a vacuum). Determination of the timescale of electron transfer may be accomplished through many means, such as NMR, EPR, dynamic IR. etc. Once the timescales of electron transfer and vibrational motions are known it is a simple matter to compare the two and determine if the complex is localized. However, in the regime that k_{et} approaches the rate of molecular vibrations it may be difficult to determine k_{et}. Instead, the relative rates of k_{et} and the molecular vibrations may be determined by IR bandshape analysis.[34-36] Such analysis has two requirements. First, one must have a vibrational mode whose frequency is sensitive to its electronic environment. That is, the band associated with the vibration should shift in the IR depending on where the electron is on the mixed valence complex. Second, the positions of these bands should not overlap with any other bands in the IR. If these two conditions are met, then one can use the resulting bandshape of the mixed valence complex to determine the rate of electron transfer. The procedure for this

is similar to that for NMR and can be best illustrated by example. Consider the complex shown in Figure 1.5a. Each of the ruthenium clusters in this molecule may undergo a single electron reduction. The two clusters in the complex are electronically coupled to one another through the pyrazine bridge. Thus, it is possible to isolate the complex in its neutral, -1 (singly reduced), and -2 (doubly reduced forms). The carbonyl of these clusters undergoes π-backbonding with the ruthenium cluster and, as such, the position of its stretch in the IR is sensitive to the oxidation state of the complex. In the neutral state the ν(CO) band appears at about 1940 cm^{-1} (Figure 1.5b), while in the -2 state (when both clusters are reduced) the ν(CO) band is shifted to lower energy by about 50 cm^{-1} and resides ca 1890 cm^{-1} (Figure 1.5d). In the singly reduced state (when formally one cluster is reduced and the other cluster is not) two ν(CO) bands are not observed. Rather a single band at an intermediate position is observed (Figure 1.5c). This band is the result of the coalescence (or averaging) of the bands for the neutral and reduced clusters. It is a result of electron transfer on the timescale of the ν(CO) stretch and the bandshape observed in the -1 state may be used to estimate the rate of electron transfer. For the complex shown in Figure 1.5a the rate has been estimated to be $9 \pm 3 \times 10^{11}$ s^{-1}.[34, 35] Even in cases where the electron transfer rate may not be determined from the bandshape, the bandshape is still able to provide qualitative information. For instance, if the two bands are not fully coalesced, then the electron transfer rate must be slower than the vibrational timescale whereas if these bands are fully coalesced then the electron transfer rate must be at least as fast as the vibrational timescale (the electron is delocalized with respect to that vibrational mode).[9, 10, 17, 36, 37] Thus, the IR bandshapes can provide a valuable criterion for deciding when an electron is localized versus delocalized.

Besides the use of IR bandshape to discriminate between localized and delocalized electrons, it has been suggested that one may also use the appearance of symmetric stretches in the IR as a means to make this distinction. The appearance of symmetric stretches it taken to be indicative of a dipole present on the timescale of the vibrational mode.[17, 38, 39] The presence of the dipole gives the symmetric stretch a change in dipole and makes it IR allowed. For a dipole to exist on the timescale of the vibration, the electron transfer rate must be slower than the vibration and the appearance of such modes is taken as evidence for electronic localization. This argument was first forwarded by Thomas Meyer in order to

explain the appearance of the totally symmetric ν_{8a} mode of the bridging pyrazines in mixed valence compounds. He claims that the fact that the ν_{8a} disappears in known delocalized complexes as further evidence that the appearance of symmetric modes in the IR indicate charge localization (fully delocalized complexes have average valences and no dipole moment arising from the electron). However, there are at least two examples in the literature that appear to contradict this interpretation. The first example involved complexes of the same form of those shown in Figure 1.5a. In the mixed valence state, it has been shown that the ν_{8a} mode of the pz is IR active (Figure 1.6a) and this activity was ascribed to electronic asymmetry on the timscale of the vibration.[38, 39] In order to further probe the effects of asymmetry, analogous asymmetric complexes were prepared. These complexes have the formula $[Ru_3O(OAc)_6(CO)(L)]$-μ_2-pyrazine-$[Ru_3O(OAc)_6(CO)(L')]$, where L and L' are different pyridyl ligands. These complexes also possess electron transfer rates which are on the same order of magnitude as the vibrational motions of the complex. Additionally, the totally symmetric ν_{8a} mode of the bridging pz was observed in the IR spectra of the mixed valence ions of these complexes. However, in the neutral state no ν_{8a} activity was observed in the IR.[38, 39] Even in the neutral state one would expect these asymmetric dimers to be electronically asymmetric. Thus, if the presence of a dipole on the timescale of the ν_{8a} mode was responsible for its appearance in the IR, then one would expect the IR of the asymmetric complex would also contain this stretch. That it does not is strong evidence against the static dipole explanation of the appearance of ν_{8a}. The second example which appears to contradict Meyer was reported by Andrew Shreve and co-workers. They investigated two pyrazine bridged dimers (one with ruthenium and one with osmium) in the mixed valence state. The structures of these dimers are shown in Figure 1.6b. Based on the solvent dependence of the IVCT bands for these complexes the ruthenium complex had previously been assigned to class II and the osmium complex to the border between class II and class III. They found that the extinction coefficient for the IR band of the ν_{8a} was three times larger for the osmium complex than for the ruthenium complex. The conclusion is that an increase in electronic localization (asymmetry) does not lead to an increase in intensity of the IR band. This again, seems to be in opposition to the mechanism suggested by Meyer and co-workers. If their model is correct, then the exact opposite effect would be expected. Specifically, one

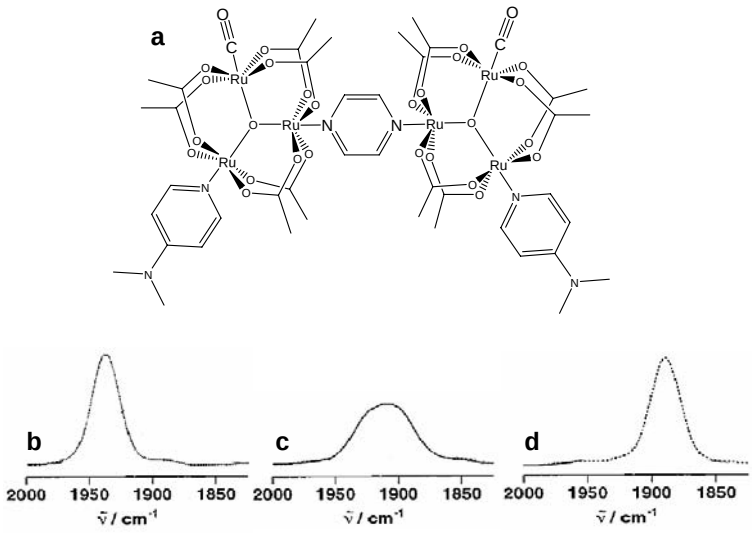

Figure 1.5. (a) Structure of ruthenium cluster based mixed valence complex. The carbonyls in this complex are sensitive to the oxidation state of the ruthenium clusters and are shifted to lower energy upon the reduction of the clusters. (b) IR spectrum of ν(CO) for the neutral complex. (c) IR spectrum of ν(CO) for the singly reduced, mixed valence ion. (d) IR spectrum of ν(CO) for the doubly reduced ion (both clusters reduced). Of particular note in this is that for the singly reduced complex the ν(CO) appears at a position between that for the neutral and doubly reduced complex. This is a result of the fact that in the mixed valence ion the electron transfer rate is on the same timescale as the vibrational motion of the carbonyl and, as such, the ν(CO) bands associated with the reduced and neutral clusters are time averaged.

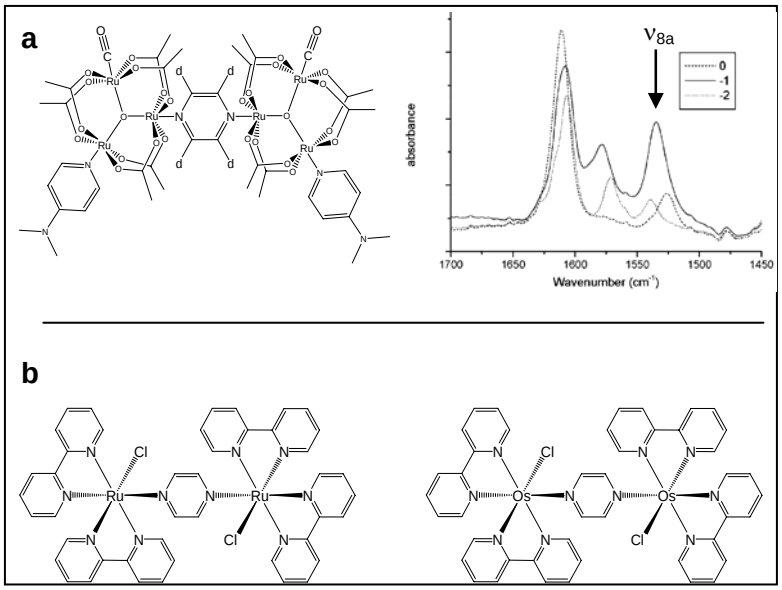

Figure 1.6. (a) A ruthenium dimer and the IR spectra in the neutral, -1 (mixed valence), and -2 states. In the mixed valence state the ν_{8a} mode of pyrazine appears in the IR. (b) Structures of the ruthenium and osmium dimers studied by Shreve and co-workers. In the mixed valence state these dimers also show ν_{8a} activity in the IR. The extinction coefficient for this band is three times larger for the osmium complex than for the ruthenium complex.

would expect that as the compounds became more localized the electric dipole would become more static with respect to the ν_{8a} vibration and the intensity of this band in the IR would increase. Taken together, these two examples cast serious doubt onto the claim that electronic asymmetry is the cause of the appearance of totally symmetric modes in the IR.

Despite these reservations it is almost certain that the appearance of ν_{8a} *is* indicative of electronic localization. However, it seems likely that the mechanism for the appearance of symmetric modes is not the existence of a dipole that is static with respect to the vibration in question. Rather, it seems likely that what is being observed is a resonance phenomenon, where the electron transfer rate approaches the vibrational frequency of the symmetric mode and the dipole changes with a lifetime close to that of the vibration. As a result, the vibrational mode is coupled to an extremely large change in dipole and the formerly IR forbidden stretch becomes IR allowed. This model predicts that the largest enhancement of the symmetric band should occur when the electron transfer rate and the vibrational frequency are the same with the enhancement falling off as the electron transfer rate either decreases or increases. Thus, the appearance of symmetric modes in the IR does not give an upper limit for ET rates, but rather give a window for ET rates – indicating that the ET rate is close to that of the vibrational mode.

It is clear that deciding between fully delocalized and localized electronic structure is quite difficult. Indeed for complexes near this transition it may prove impossible to ever provide a definitive classification for them. The main problem seems to stem from a question of timescales. For the large metallic complexes that are often employed for these studies the timescales of the nuclear vibrations can vary over several orders of magnitude and, in the case of large breathing modes of the complex, can overlap with the timescales required for solvent motion. Thus, it is not unexpected that there might be complexes that possess properties that are associated with both localized and delocalized electrons. Many such complexes were identified in an extensive review by Meyer[17] where he introduced a new mixed valence classification; class II-III, to which such complexes may be assigned. Meyer defined this class as complexes which appear to have averaged solvent environments (thermal electron transfer is much faster than the solvent dielectric response), but that the internal vibrational modes are not fully averaged (the complex is not delocalized with respect to its internal coordinates). The solvent averaging is determined by

studies into the solvent dependence of the IVCT band while localization of the electron with respect to the internal coordinates is verified by either incomplete coalescence of IR bands or the appearance of totally symmetric stretches in the IR. The problems with this approach have been pointed out above, however, the general outline of the properties of this class remain widely accepted by the electron transfer community. While experimentally these criteria are easily accessible, they should be further refined. Specifically, the use of the solvent dependence of the IVCT band provides a lower electron transfer limit that is much too slow. As will be discussed in chapters 4 and 5 in this thesis, it seems more reasonable to use the much faster rotational motions of the solvent, which approach the timescale of molecular vibrations. Use of these motions to decide whether solvent is averaged would significantly narrow the window for class II-III mixed valency. Additionally, as discussed above, it is unclear that the appearance of a symmetric stretch in the IR provides an upper limit for ET rates. Despite these problems with the Meyer definition of class II-III, it is likely that it will continue to be used as it provides simple experimental criteria for the classification of these otherwise difficult to classify complexes.

1.6 Conclusions

This chapter has aimed to provide the reader with a gentle (but physically correct) introduction to the theories that govern discussion of electron transfer. In addition it has been my aim to equip the reader with an appreciation of the problems now facing the study of near-delocalized systems. Specifically, it is my hope that the reader is sufficiently aware of both the thermodynamic considerations of these systems (expressed by the shape of the potential energy curves in Figures 1.1 and 1.2) as well as the kinetic considerations present in these systems (accounted for by the nuclear motions of the solvent and molecular vibrations). Additionally, I have tried to stress the relative importance of the electronic coupling between sites in electron transfer systems as well as how valuable knowledge of the magnitude of this coupling (H_{AB}) can be in discussing the properties of these systems. The relative importance of thermodynamic and kinetic influences on the rate of electron transfer as well as the great importance of determining the value of H_{AB} are recurring themes throughout this thesis. It is found that many unusual behaviors observed in mixed

valence species can be understood in light of these considerations. With this in mind it is now time to move into the thesis proper and discuss the effects of electronic delocalization in highly coupled mixed valence systems.

Chapter 2: A thermodynamic estimation of H_{AB} for asymmetric class II-III mixed valence systems.

2.1 Introduction

The classification of mixed valence systems is important, as it aids in the understanding of the behavior of the electron transfer occurring in the system. Among the many properties addressed by classification are the solvent and temperature dependence of the ET event as well as the NMR, EPR, IR, and UV-vis behavior of the system under consideration. Additionally, correct identification of a system's class can help to explain the thermodynamics of the system and the dynamics of its interaction with its environment. Additionally, use of a simple classification scheme allows for the scientific community to work within a generally accepted conceptual framework, facilitating discussions of the system's mixed valence properties.

Since classification of mixed valence systems is of central importance to the study of electron transfer, it would be good if there were a way to clearly experimentally determine the class of each compound. Marcus[3] and Hush[8] have provided criteria for deciding when a complex obtains delocalization. Specifically, when the magnitude of the electronic coupling matrix is equal to one half the vertical reorganization energy, λ, then the system *must* be delocalized (class III). Likewise, when H_{AB} is close to zero, the complex is assigned to class I. Between these two limits the compound is considered class II.

While in theory it is easy to identify the demarcation between class II and III ($H_{AB} = \lambda/2$), in practice it is quite difficult. Much of this difficulty arises from the fact that there is no way to experimentally determine H_{AB}. While equations exist that relate the shape of the IVCT band to H_{AB} (equation 1)[8], accurate determination of H_{AB} requires that one knows the energy of the transition (ν_{max}), extinction coefficient for the transition (ε_{max}), and the bandwidth of the IVCT ($\Delta\nu_{1/2}$) as well as the distance between the sites undergoing electron exchange (d).

$$H_{AB} = \frac{4x10^4\left(\varepsilon_{max}\Delta\nu_{1/2}\nu_{max}\right)}{d} \quad (1)$$

Determination of the optical properties appears straightforward, however, recent work by Meyer and co-workers has shown that, for transition metal containing systems the shape of the IVCT band can be a composite of many different IVCT and IC transitions that occur between the various d-orbitals of the metals[11, 17, 31]. As a result, it can be difficult to determine ν_{max}, $\nu_{1/2}$, and ε for the IVCT band. Even for systems which do not contain transition metal centers determination of H_{AB} can prove difficult. This is because, in addition to the problems associated with optical data, accurate determination of the distance between electronic sites proves difficult – especially in the case of highly coupled complexes. H_{AB} functions to mix the wavefunctions associated with the sites undergoing electron transfer and has the effect of decreasing the effective charge transfer distance[11]. The result is that distances between sites obtained from crystallography data may not reflect the actual distance that the electron travels within the mixed valence complex. Even when the properties of the vertical reorganization energy, λ, may be obtained unambiguously from near IR or UV-vis spectra of the mixed valence state, accurate values for H_{AB} may remain unobtainable. Without accurate determination of H_{AB}, one cannot easily and unambiguously assign a complex to class II or class III.

While this is a serious problem in mixed valence chemistry, it is encountered relatively rarely. For most complexes, the class II/class III distinction can easily be made from such experimentally determined quantities as the IVCT bandshape[7] (when it is uncomplicated by multiple metal-metal transitions), the solvent dependence of the IVCT band, or the electron transfer rate[17]. However, for compounds which sit close to the class II/class III borderline it is quite difficult to unambiguously determine the class. Indeed, even the archetypal mixed valence system $[Ru(NH_3)_6]_2$-μ_2-pz^{3+} (the so-called Creutz-Taube ion) resisted clear classification until rather recently.[40-43] This has led to the creation of a new mixed valence class, class II-III, proposed by Meyer and co-workers in an extensive review of molecules that reside at the localized to delocalized transition.[17]

From the work of Marcus and Hush, we can see that if H_{AB} could be accurately experimentally determined then the assignment of a class to such systems would be as simple as dividing one experimental quantity by another. Here, we describe how H_{AB} may be accurately determined for asymmetric mixed valence compounds, provided that the isomers of these complexes (so-called "mixed-valence isomers") may be observed. Mixed valence isomers are the two alternate charge distributions of a mixed valence complex (A^-—B and A—B^-). In the normal two-state Marcus-Hush description of a symmetric mixed valence complex,[3, 8] electron exchange is a degenerate process and the "isomers," differing only in the position of the charge, cannot be distinguished. By introducing a slight asymmetry into a mixed valence complex, it is possible, in principle, to introduce a small energy difference between the two sides of the adiabatic Marcus-Hush potential energy surface such that substantial Boltzmann populations of the two mixed valence isomers can exist at equilibrium. Our laboratory recently reported two cases of the direct spectroscopic observation of mixed valence isomers.[44, 45] Previously we had demonstrated that rate constants for electron transfer (ET) in the singly reduced (mixed valence) states of ruthenium cluster dimers can be measured by lineshape analysis of coalesced ν(CO) bands in the IR spectra.[34, 35] The observation of mixed valence isomers by IR spectroscopy requires an asymmetric structure of the mixed valence state to lift the degeneracy of the two mixed valence states and appropriate isotopic substitution to spectroscopically differentiate them.

Complexes **1** - **3** with different pyridyl ligand substitution on each Ru_3 cluster and complexes **4** - **5** with asymmetric bridging ligands (Figure 1) satisfy the criteria for observation of mixed valence isomers. It is known that the reduction potential of the ruthenium clusters is sensitive to the identity of the attached ancillary ligand with the energy of the clusters increasing with the σ donor strength of the attached ligand.[46] Thus, the different pyridyl ligands present in **1**-**3** and the nonequivalent nitrogens of **4** and **5** lead to clusters that have dissimilar energies. That is, the asymmetry in these dimers introduces a driving force for electron transfer in these dimers. Through the use of ruthenium cluster dimers which possessed both asymmetric ligand substitution and regiospecific $^{13}C^{18}O$ labeling, it was possible, in the mixed valence state, to observe IR spectra of both mixed valence isomers in equilibrium population ratios from 1.6 to 3.4 for **1** – **3** [44] and 2.2 for **4**.[45] For complex **5** the minor isomer was present in quantities too small to allow the

equilibrium constant to be obtained. This work established mixed valence isomers as discrete chemical species that exist in equilibrium. Dynamical coalescence of the observed IR lineshapes further indicated that the mixed valence isomers reported exist in *dynamic* equilibrium governed by ETs that occur on the picosecond time scale. The method for calculating H_{AB} presented here relies on thermodynamic data gathered from these mixed valence isomers. The method is built on the relationship between the driving force that exists in the absence of electronic coupling, ΔG_0^0, and the driving force that exists in the presence of electronic coupling, ΔG_1^0 (Figure 2). It has been shown that the direct spectroscopic measurement of the equilibrium population ratio of the two mixed valence isomers, $[A^- - B]/[A - B^-]$ provides the driving force present in the adiabatic potential energy surface (ΔG_1^0).[44] The driving force for ET in the diabatic ($H_{AB} = 0$) limit, (ΔG_0^0), can be obtained from differences in intrinsic reduction potentials of the analogous symmetrically substituted clusters, which depend only on the ligands present. [44] The values of $\Delta\Delta G^0 = \Delta G_0^0 - \Delta G_1^0$ available from this analysis can then be interpreted within the framework of appropriate potential energy surfaces in order to estimate H_{AB}.

Ironically, it seems that if the condition required for the determination of H_{AB} (that both isomers be observable) is met, then the need for accurate determination of H_{AB} for assignment to class II or class III is eliminated. For if both isomers are observable, then the complex is class II, however, if the mixed valence systems is class III, then, by definition, the isomers are unobservable (since the system is delocalized). However, the fact remains that this method promises to provide the most accurate determination of H_{AB} to date for highly coupled systems and (as will be discussed throughout this thesis) accurate information as to the value of H_{AB} is quite useful when discussing the properties of highly coupled systems.

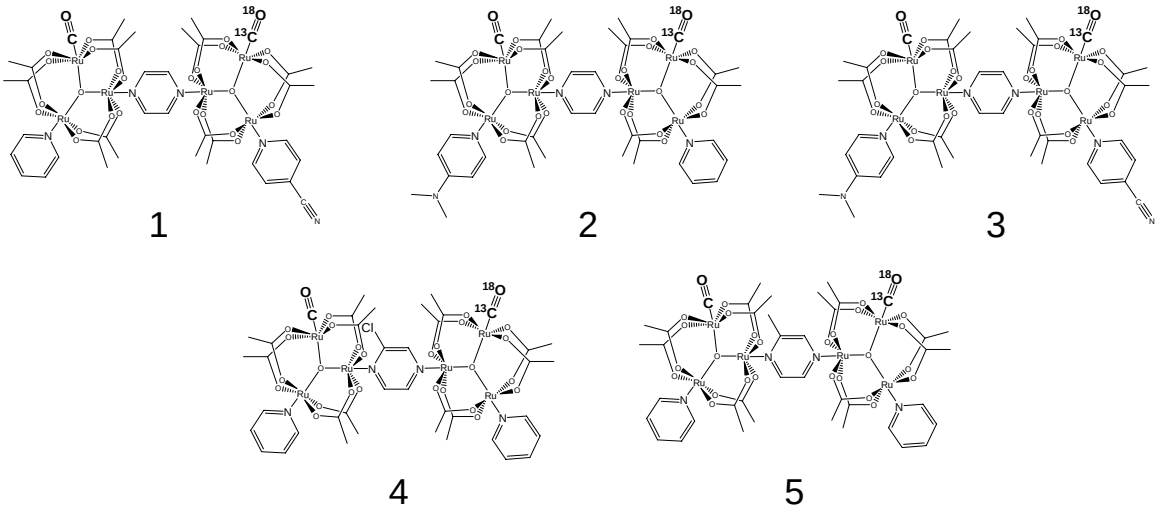

Figure 2.1. Structures of the asymmetric complexes 1-5 used in order to obtain thermodynamic estimates of H_{AB}.

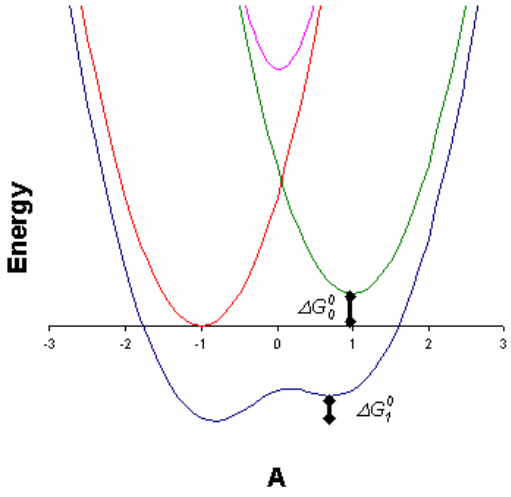

Figure 2.2. Diabatic and Adiabatic potential energy surfaces associated with mixed valence systems in the Marcus-Hush model of electron transfer. ΔG_0^0 is the difference between the diabatic potential energy surfaces and ΔG_1^0 is the energy difference between the wells in the lower adiabatic potential energy surface.

2.2 Spectroscopic observation of mixed valence isomers

Much of the work in our laboratory has focused on the electrochemistry and spectroelectrochemistry of the mixed valence compounds, $[Ru_3O(OAc)_6(CO)(L)]_2$-μ-BL. The introduction of a small asymmetry into these otherwise symmetric mixed valence compounds allows for the formation of distinct mixed valence isomers **1**-**5**. Vibrational spectra for complex **1** in the neutral, -1, and -2 states are presented in Figure 3. In the neutral state two carbonyl bands are observed. The band at lower energy corresponds to $^{13}C^{18}O$,and $^{12}C^{16}O$ is at higher energy. Through π-backbonding, the CO ligands are sensitive to the oxidation state of the clusters to which they are attached. Thus, in the -2 state, both of these bands are observed to shift to lower energy corresponding to the reduction of the ruthenium clusters to which they are attached. The -1 state presents a more complex spectrum in the carbonyl region. In this case, two peaks are observed, each with its own shoulder. The relative intensities of these peaks arise from the relative thermodynamic populations of the species that produce them. The more intense bands are associated with the major (thermodynamically favored) isomer. In this case, the major isomer is the one in which the electron is localized on the cluster containing the 4-cyanopyridine ligand, as it is a weaker base than pyridine and provides greater stabilization to the ruthenium cluster in the reduced state. The shoulders arise from the presence of the minor (thermodynamically unfavored) isomer. This is the mixed valence isomer in which the electron is localized on the cluster to which the pyridine ligand is attached (as py is a stronger base than cpy).

By comparing the intensities of the peaks associated with the major and minor isomers, one can determine the thermodynamic constant (K_{eq}) for the isomerization $[A^-—B] \leftrightarrow [A—B^-]$. K_{eq} values for complexes **1**-**4** are reported in Table 2.1. K_{eq} for complex **5** was unobtainable due the extremely limited presence of the minor isomer. The mixed valence isomerism equilibrium constant can be used to calculate the driving force present in the mixed valence complex (ΔG_1^0, Figure 2) by using the relationship, $\Delta G = -RT\ln K_{eq}$. The spectra presented in Figure 2.3 are representative of those observed for the other asymmetric dimers.

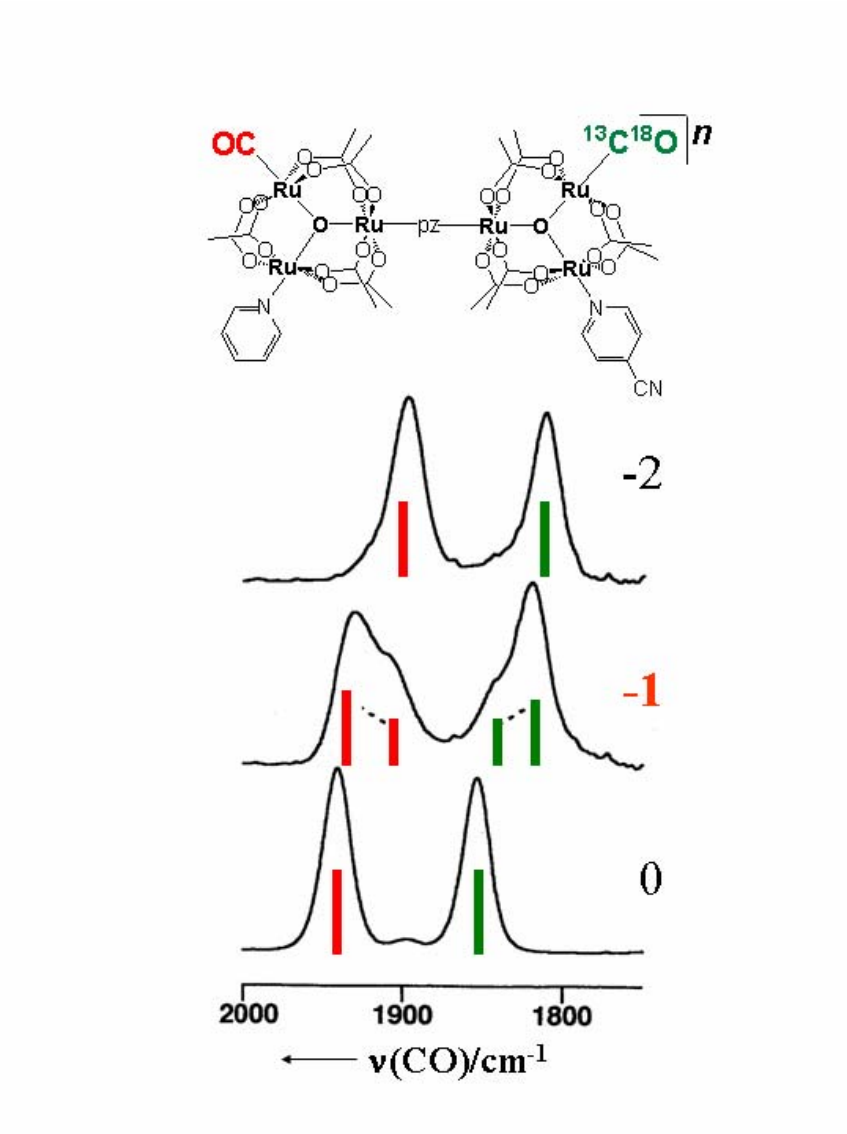

Figure 2.3. Structure of a representative asymmetric dimmer with the spectra associated with the neutral, minus 1, and minus 2 states. The minus 1 state is the mixed valence state and both mixed valence isomers are clearly evident in the spectra. The larger peaks arise from the major isomer (the electron on the cluster bearing the 4-cyanopyridine ligand) and the smaller peaks from the minor isomer (the electron on the cluster bearing the pyridine ligand).

Table 2.1. $\Delta\Delta E_{1/2}$, ΔG_0, K_{eq}, and ΔG_1 for complexes **1-4**

L1-L2	$\Delta\Delta$E1/2 (cm^{-1})	ΔG_0 (cm^{-1})	K_{eq}	ΔG_1 (cm^{-1})
cpy-dmap	230	1850	3.4 ± 0.2	200
cpy-py	130	1050	2.4 ± 0.2	140
py-damp	100	810	1.6 ± 0.2	75
BL=mpz	30	240	2.2 ± 0.2	128

2.3 Calculation of electronic coupling[6]

The effect of electronic coupling (H_{AB}) and driving force (ΔG_0^0) on the rate of CT is usually expressed in terms of a semiclassical model consisting of two interacting potential surfaces.[5] (see Figure 2) The adiabatic surfaces that result when two nonadiabatic surfaces are mixed by means of the electronic coupling matrix, H_{AB}, are typically expressed as a function of a normalized reaction coordinate *X*.

$$E_{\pm} = \lambda \frac{\left(2X^2 - 2X + 1 + \Delta G_0^0\right)}{2} \mp \frac{\left[\left(\lambda(2X-1) - \Delta G_0^0\right)^2 + 4H_{AB}^2\right]^{\frac{1}{2}}}{2} \tag{1}$$

For our purposes it is convenient to express these surfaces in terms of a similar variable, $A = 2X - 1$. The effect of this change of variables is to move the nonadiabatic minima from $X = 0$ and $X = 1$ to $A = -1$ and $A = 1$. The adiabatic surfaces that result from electronic coupling, expressed in terms of *A*, are:

$$E_{\pm} = \lambda \frac{\left(\frac{1}{2}\left(A^2 + 1\right) + \Delta G_0^0\right)}{2} \mp \frac{\left[\left(\lambda A - \Delta G_0^0\right)^2 + 4H_{AB}^2\right]^{\frac{1}{2}}}{2} \tag{2}$$

In the limit of zero driving force, the minima of the lower surface (E_+) are given by;

$$A = \pm\sqrt{1 - 4\frac{H_{AB}^2}{\lambda^2}} \tag{3}$$

It is important to reiterate that ΔG_0^0 is the *diabatic* driving force. That is, the driving force that exists in one ignores the effects of H_{AB}. If ΔG_0^0 is small compared to H_{AB} (strong coupling limit), then the

introduction of the driving force should not cause the minima to move significantly along *A*. Thus, any shift of the minima in E_+ along *A* is due almost entirely to the effects of H_{AB} and (3) provides a good estimation of their positions. We may then use (2) and (3) to find the difference in energy between the two minima for the case of an asymmetric complex. This difference, ΔG_1^0, is the driving force present in the lower adiabatic surface.

$$\Delta G_1^0 = E_+\left(A = +\sqrt{1-4\frac{H_{AB}^2}{\lambda^2}}\right) - E_+\left(A = -\sqrt{1-4\frac{H_{AB}^2}{\lambda^2}}\right) \tag{4}$$

Marcus-Hush theory predicts that, in addition to the stabilization of the ground state potential energy surface by H_{AB}, the products and reactants will also be stabilized with respect to each other. In other words, the adiabatic driving force, ΔG_1^0, will be smaller than the diabatic driving force, ΔG_0^0 (Figure 2.2).

It is this difference between ΔG_1^0 and ΔG_0^0 that allows for the determination of H_{AB} from simple thermodynamic considerations. Since E_+ is a function of H_{AB}, ΔG_0^0 and the reorganizational energy in the symmetric case (λ_{symm}), equation (4) can be rearranged to solve for H_{AB} in terms of only experimental quantities. Making correct choices of positive roots and eliminating insignificantly small terms, we find:

$$H_{AB} = \frac{\lambda_{symm}}{2\Delta G_0^0}\sqrt{\left(\Delta G_0^0\right)^2 - \left(\Delta G_1^0\right)^2} \tag{5}$$

Equation 5 is similar to a relation between the adiabatic $\Delta G°$ and H_{AB} for asymmetric ET systems derived earlier by Brunschwig and Sutin.[4] The important distinction between these expressions is that here we assume that the minima can be accurately described using the expressions for the symmetric case, which is reasonable given the extremely delocalized nature of these complexes.

The procedure for obtaining ΔG_0^0 and ΔG_1^0 has been outlined previously.[44] Briefly, ΔG_0^0 is obtained from the difference between the average $E_{1/2}$ values in the cathodic region of the cyclic voltammogram for the two symmetric analogues of an asymmetric complex, $\Delta\Delta\overline{E}_{red}$. These values are reported in Table 2. For an asymmetric dimer [A—B], the symmetric analogues are [A—A] and [B—B]. ΔG_1^0 is found through a comparison of the intensities of major and minor peaks in the ν(CO) spectra for the mixed-valence (-1) state (*vide supra*). The only value that proves difficult to obtain for the asymmetric case is λ_{symm}. This difficulty arises from the fact that λ_{symm} in (5) is formulated as the reorganization energy for a symmetric CT complex. Because of this, a small correction must be made to this term. This correction is best applied using the expression

$$\lambda_{symm} = \left[\lambda_{asymm}^2 - 2\Delta G_0^0 \sqrt{\lambda_{asymm}^2 - H_{AB}^2}\right]^{\frac{1}{2}} \tag{6}$$

This expresses λ_{symm} in terms of the experimentally determined values λ_{asymm} and ΔG_0^0 as well as the non-experimental term, H_{AB}. The presence of this non-experimental term, however, does not present a major problem. Since the correction to λ_{symm} is expected to be small in the strong coupling/weak driving force limit, we can solve (5) and (6) recursively to obtain H_{AB}. For comparison, we calculate H_{AB} using the relationship normally employed for determination of H_{AB} from the position and shape of the IVCT band (equation 7).[47]

$$H_{AB} = \left(2.06\times10^{-2}\right)\frac{\left(\overline{\nu}_{\max}\cdot\overline{\varepsilon}_{\max}\cdot\overline{\nu}_{1/2}\right)^{\frac{1}{2}}}{r} \tag{7}$$

Values of ΔG_0^0, ΔG_1^0, and K_{eq} are presented in Table 1. Calculated values of H_{AB} using solely (5) or (7) as well as both (5) and (6) recursively are reported in Table 2 along with the values of λ_{asymm}. Values of H_{AB} calculated using only (5) overestimate H_{AB}. (This error arises from the fact that λ_{asymm} is larger than

the corrected λ_{symm}.) Equation (7) is of questionable accuracy in determining H_{AB} in highly coupled CT complexes, in large part due to the difficulty in determining reliable values of *r*. Values of H_{AB} arrived at using (7) are much lower than those that are obtained from the recursive use of (5) and (6). Due to the fact that (6) takes into account the correction to λ_{symm} and that neither (5) nor (6) use the quantity *r*, it is assumed that their recursive use gives more reliable values of H_{AB} than does (7). As expected, the relative magnitudes of H_{AB} reflect the relative magnitudes of $\Delta\Delta G^{0}$ for complexes **1-4** as it is H_{AB} that functions to decrease ΔG* on the way towards complete electronic delocalization.

Table 2.2. λ_{asymm} and H_{AB} for **1-4**, calculated using several methods

L1-L2	λ_{assym} (cm^{-1})	[a] H_{AB} (cm^{-1})	[b] H_{AB} (cm^{-1})	[c] H_{AB} (cm^{-1})
cpy-dmap	10400	5169	4248	1100
cpy-py	10500	5200	4715	1200
py-dmap	11500	5725	5356	1800
BL=mpz	9900	3852	3755	n/a

[a]Calculated using Eq. (5) assuming $\lambda=\lambda_{asymm}$

[b]Calculated using Eqs. (5) and (6) recursively

[c]Calculated using Eq. (7)

2.4 Implications of the values of the thermodynamically obtained H_{AB}

The central assumption made in the preceding derivation of a calculation of H_{AB} based on thermodynamic data is that for near-delocalized complexes like **1-4** motion along the ET reaction coordinate (*X*, or *A* above) of the two minima is governed only by coupling (delocalization): the diabatic driving force is assumed not to influence the position of these minima. In essence, the implicit assumption is that the most important factor is electronic delocalization, which dominates over any small perturbative effect of energetic asymmetry in the adiabatic ground-state potential surface. For near-delocalized mixed-valence complexes, in which H_{AB} (the Marcus-Hush quantification of delocalization) is thousands of wavenumbers in energy, the competing localizing thermodynamic forces of ligand asymmetry will be a

much smaller effect in all but the most extreme cases (for example, asymmetry of metals in a M_1-BL-M_2 complex). Examining Tables 1 and 2 it can be seen that for complexes **2**-**4** H_{AB} is much greater than ΔG_0. For the most highly coupled complexes ΔG_0 is less that 5% of H_{AB}. Since the position of the minima depends on the squares of H_{AB} and ΔG_0 (equation 2) the contribution of ΔG_0 to A in these cases should be quite small. Additionally, as H_{AB} increases the relative importance of ΔG_0 will decrease. This means that the calculations presented here are *more* accurate the closer the complex approaches class III, which is exactly where X-ray estimates of r become the most inapplicable and calculations based on equation 1 become *less* accurate. Thus, it is clear that as complexes approach the localized to delocalized transition, the calculations outlined in this chapter should become increasingly more accurate than those typically employed in the two state model of mixed valence chemistry.

It is important to note that this treatment is only expected to apply to mixed-valence complexes with strongly delocalized mixed-valence states and small asymmetries in the charge center environments, such as minor ancillary ligand differences or assymetric bridging ligands. The main assumption, that motion along the reaction coordinate is determined only by delocalization, agrees well with the nature of all known near-delocalized mixed valence complexes as M_1-BL-M_2 complexes in which the bridging ligand is a central part of the delocalization. The main conduits for electronic delocalization are the two successive M-BL interactions; the favorable nature of these interactions, and the redistributions of charge along the ET reaction coordinate that they lead to, are not expected to be largely affected by minor adjustments to the energy of the M sites. However, it is clear that the energy differences do play a significant role in the effective coupling between sites. From Tables 1 and 2 it is clear that H_{AB} increases with decreasing ΔG_0. This relationship is expected if one considers that the overall coupling between the two clusters involves two successive couplings between both clusters and the bridge. The effective coupling between the bridging ligand and the clusters, J_{AB}, may be written as in equation 10.

$$J_{AB} = \frac{V_{AB}}{\Delta E_{AB}} \tag{8}$$

In equation 10, V_{AB} is the orbital overlap between the cluster and the bridge and ΔE_{ABL} is the energy difference between the coupling orbitals on the cluster and the bridge. Thus, the bridging ligand in these systems is not a passive participant. In a two-site system, M_1-M_2, in which the interactions between charge sites are more direct, asymmetries between the charge sites would be a more significant regulator of the balance of charge between M_1 and M_2.

To this point, the semiclassical Marcus-Hush model has formed the theoretical basis for understanding ET processes in diverse molecular scenarios for generations of researchers, and it continues to underlie the language in which molecular ET events are presented and discussed. Calculation of the two-state H_{AB} for **1-4** is important because it provides a framework for understanding near-delocalized complexes in terms of this common language, and in the specific case of mixed-valence complexes, it allows a direct critical comparison of the case of **1-4** to the bulk of previous research in mixed-valency. The calculation of H_{AB} in strongly-coupled and near-delocalized complexes by a means other than the energy and bandwidth of the IT band (equation 1) and estimation of the electron transfer distance provides an important comparison to previous work and the possibility of a critical evaluation of the shortcomings of a semiclassical two-state model near the localized/delocalized limit in complexes for which more than two electronic sites are important. In particular, the inclusion of more sites is likely to lead to more electronic transitions – transitions that can complicate the shape of the IVCT band. Furthermore, inclusion of additional units that undergo electronic coupling can make determination of the distance of electron transfer even more difficult. Indeed, for complexes such as **1-4** it is difficult to decide whether the electron transfer distance should be associated with a specific distance between the six ruthenium or whether the distance should be taken as the average distance between the two clusters. Additionally, interactions of the clusters with the bridge could result in additional weight being assigned to the metal centers to which the bridge is attached, increasing the difficulty of assigning an electron transfer distance. For **1-4**, it is likely that the thermodynamic calculation of H_{AB} via equations (5) and (6) provides a more realistic evaluation of H_{AB} in these complexes than what is offered by equation (7), despite the fact that our "thermodynamic" calculation of H_{AB} still depends to some extent on the energy of the IT band as λ_{symm} appears centrally in

equation 6. Thus, it is seen that the major advantage of the thermodynamic calculations presented above is the algebraic removal of the distance dependence from H_{AB}.

The unique observation of charge transfer isomers in **1-5**, and the recovery of the thermodynamic parameters necessary for estimating H_{AB} from data other than the IT band, suggests a rethinking of what aspects of Marcus-Hush theory are still valid for mixed-valence complexes near the Class II/III boundary. From Table 2 it is clear that IT band analysis severely underestimates the electronic delocalization in these near-delocalized ruthenium dimers of trimers. It is likely that this is also the case for other bridged mixed-valence systems near the Class II/III boundary. This has been addressed in many other works where the problems associated with the correct determination of the shape of the IVCT band as well as the determination of the charge transfer distance have been acknowledged[11, 17].

Recent experiments [48-50] have shown the central importance of the bridging ligand in determining the electronic structure of symmetric ruthenium dimers of trimers, and a vibronic coupling model which explicitly includes electronic and vibrational participation of the bridging ligand [22, 23, 27, 51] is used to explain these experimental results. Compared to the Marcus-Hush treatment for mixed-valence complexes, the vibronic coupling model predicts different properties for the "IT" electronic absorption band and provides a basis for discussing the role of the bridging ligand in different terms than the bulk of previous work on strongly coupled or near-delocalized M-BL-M mixed-valence complexes.

2.5 Conclusions

Complexes at the Class II/III borderline present an interesting challenge in electron transfer theory. Our thermodynamic calculations yield values of H_{AB} so large that they approach $\lambda_{symm}/2$, indicating that the shape of the lower potential energy surface approaches a single minimum. Certainly a value of H_{AB} equal to $\lambda/2$ is reasonable within the error of the measurements and approximations we used. However, from the infrared spectroelectrochemical observations of the mixed valence isomers it is clear that we are observing two isomers present in solution, indicating the presence of two minima in the lower adiabatic

potential energy surface. Such large values of H_{AB} juxtaposed with the observations of both mixed valence isomers shows that they are at the localized to delocalized transition and firmly establishes our complexes in the class II-III regime.

The thermodynamic calculation for H_{AB} also serves to clear up an important disparity previously noted [35, 52] between the rate constants estimated from the IR spectroelectrochemical lineshape analysis and those calculated using equation 8[5].

$$k_{ET} = \kappa \nu_N \exp\left\{-\left(\Delta G_\lambda^* - H_{AB} + H_{AB}^2 / 4\Delta G_\lambda^*\right)/RT\right\} \tag{9}$$

ΔG_λ^* is estimated to be $\lambda_{symm}/4$, and, making the typical assumptions, $\kappa = 1$ and $\nu = 5.0 \times 10^{12}$. Using H_{AB} calculated from optical parameters we find rate constants on the order of 10^9 s^{-1}, while the rates we estimated from the spectroelectrochemical data are on the picosecond timescale. While there is some degree of uncertainty in our estimates of k_{et}, the mere appearance of dynamically broadened bands in the IR put a lower limit on the rate of electron transfer of 10^{11} s^{-1}.[9, 10, 37] It seems that the large underestimate of k_{et} using the H_{AB} determined from equation 1 most likely is due to the fact that optical methods provide a large underestimation of the magnitude of H_{AB} for highly coupled systems. Use of the thermodynamically derived values for H_{AB} in equation 8 yields an exponential term very close to unity. This results in rate constants that are primarily determined by the nuclear frequency factor with a small correction due to the nature of the ancillary and bridging ligands (which can change the value of H_{AB}). Thus, the rate of electron transfer is expected to be on the order to 10^{12} s^{-1}, which is in agreement with rates previously estimated for these complexes. The nuclear frequency factor used in this equation is defined as the rate at which the system is able to obtain the nuclear coordinates of the transition state. Thus, the value of ν_N is weighted by both vibrational modes of the molecule (intramolecular nuclear rearrangement) as well as the dynamics of the solvent (intermolecular nuclear rearrangement). One would expect, then, that the rates of electron transfer in these systems would show a marked dependence on the dynamics of the surrounding medium. Such a dependence has been observed and is the focus of the next two chapters.[53]

Chapter 3: Determination of ΔH and ΔS for asymmetric class II-III mixed valence systems

3.1 Introduction

In chapter 2 we were able to show that the asymmetric compounds of the type $[Ru_3O(OAc)_6(CO)(L)]_2$-μ_2-pz (where L is a pyridyl ligand and pz is a bridging pyrazine)[44, 45] are class II compounds.[6] The large magnitude of H_{AB} seems to place them in the newly emerged class II-III mixed valency.[17] However, this estimate was reached using data from only a single temperature. The fact that we are able to observe both of the isomers in this system means that there must exist a non-zero energetic barrier to electron transfer. As such, these compounds should show a classic temperature response with respect to the isomer populations. The ability to observe both isomers puts us in the unique position of being able to experimentally determine both the ΔH and the ΔS of electron transfer for highly coupled mixed valence systems.

Here, we look at the temperature dependence of the populations in the mixed valence isomer. Such data enables us to further refine our values for both the energy difference between the isomers and H_{AB} as well as allow us, for the first time, to experimentally determine the value of ΔS for a single electron transfer event.

3.2 Experimental

Synthesis of $[Ru_3O(OAc)_6(^{13}C^{18}O)(cpy)]$-μ-pz-$[Ru_3O(OAc)_6(CO)(dmap)]$ (**1**) has been reported elsewhere.[44] Reduction of **1** was accomplished electrochemically. A solution of the **1** and 0.1 M TBAH was passed through a home built flow-through bulk electrolysis cell[54] where it was reduced. The mixed valence dimer was then collected in a vial. The flow-through cell and vial were kept at a temperature of -40° C by means of a recirculating cooling bath contained in a glovebag under N_2. Following the collection of $\mathbf{1}^-$, it was transferred to a Specac cryostat by canula. The cryostat was kept at -40° C during the transfer,

after which the temperature was changed to the desired value and FTIR spectra were taken. IR spectra were aquired using a Brucker *Equinox 55*.

3.3 Results and Discussion.

Figure 3.1a shows a spectrum taken at 0° C of the mixed valence state of **1**. At first glance this spectrum is quite complex, however, it can be understood through simple thermodynamic considerations. It is known that the orbital energy levels of the clusters are extremely sensitive to the electronic properties of the attached ancillary ligands[46]. In particular, the reduction potentials of the clusters shift more negative (the orbital energy levels increase) with increasing pK_a of the attached ligands. As a result, the cluster to which cpy is attached is lower in energy than the cluster to which dmap is attached. This effect can be represented by a potential energy surface of the mixed valence state Figure 3.1b. Here, the difference in the diabatic energies present in the neutral state is translated into a difference in energies in the adiabatic energies present in the mixed valence state. How these two energy differences are related to the coupling between states (H_{AB}) was addressed in chapter 2.

The difference in energy between isomers means that, in the mixed valence state, the unpaired electron will spend more time on the cluster with cpy than the cluster with dmap. In other words, there will be a larger population of dimers in which the cpy cluster is reduced than dimers in which the dmap cluster is reduced. This population difference is manifested as the different intensities of the ν(CO) bands present in Figure 3.1a.

Using this information, the bandshape of **1** in Figure 3.1a can be understood. In the neutral state only two peaks are present, the stretches associated with $^{12}C^{16}O$ and $^{13}C^{18}O$ attached to neutral clusters. Likewise, the fully reduced dimer also exhibits two ν(CO) bands associated with $^{12}C^{16}O$ and $^{13}C^{18}O$ attached to reduced clusters. Because the CO undergoes π-backbonding with the ruthenium to which it is attached, it is sensitive to the oxidation state of the clusters. Reduction of the clusters moves the CO strech to lower energy by *ca.* 40 cm^{-1}. In the mixed valence state, however, there are four peaks present which are

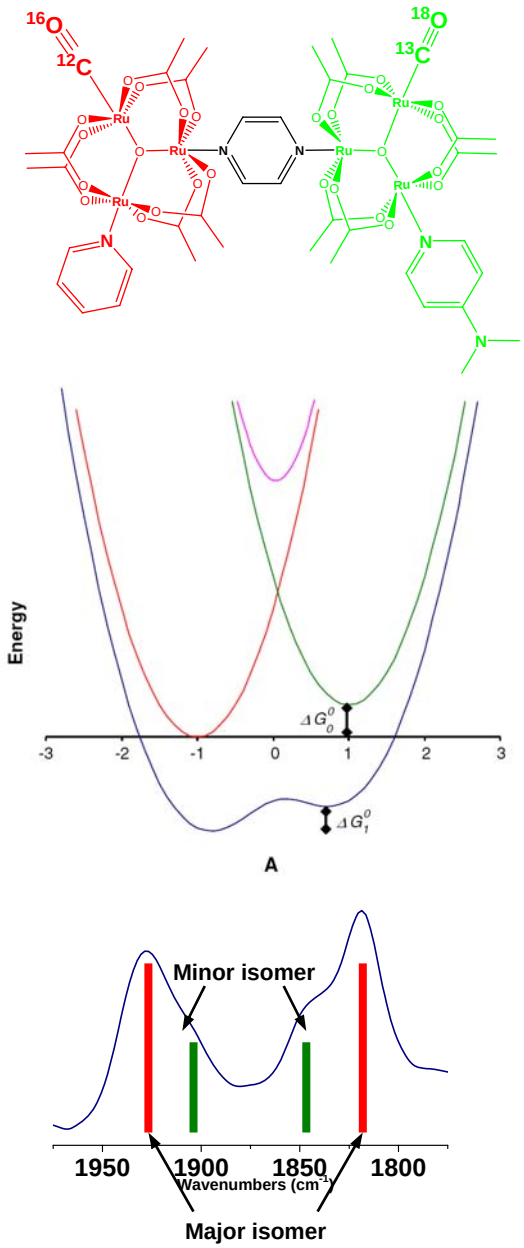

Figure 3.1: a) The asymmetric dimer, **1**. b) The diabatic (green and red) and adiabatic (blue and pink) potential energy surfaces associated with **1**. The red diabatic curve is associated with the lower energy cluster (pyridine substituted) and the blue diabatic curve is associated with the higher energy cluster (dimethylamino pyridine substituted). c) The IR spectra for $\mathbf{1}^{-1}$. The spectum arises from the overlapped spectra of two isomers. The major isomer arises from the electron occupying the pyridine substituted cluster while the minor isomer arises from the electron occupying the dimethylaminopyridine substituted cluster.

located at 1928 cm^{-1}, 1908 cm^{-1}, 1846 cm^{-1}, and 1819 cm^{-1}. The highest energy band is associated with $^{12}C^{16}O$ attached to a neutral cluster. The next higest energy band is associated with $^{12}C^{16}O$ attached to a reduced cluster. The second lowest energy band is associated with $^{13}C^{18}O$ attached to a neutral cluster and the lowest energy band is associated with $^{13}C^{18}O$ attached to a reduced cluster. Thus, the four *positions* of the bands are explained.

With the positions of the bands understood, what remains is to address their relative *intensities*. The intensity pattern observed for **1** in the mixed valence state is explained by invoking the above discussion of the potential energy surfaces associated with the dimer. Using this information we can identify two "mixed valence" isomers. The major isomer is a result of the electron sitting on the cluster with the cpy ligand (the cluster lower in energy). Thus, for this isomer, the $^{13}C^{18}O$ is attached to a reduced cluster and shifts to lower energy (1819 cm^{-1}) while the $^{12}C^{16}O$ is attached to a neutral cluster and remains at 1928 cm^{-1}. In the minor isomer the electron resides on the dmap cluster (the cluster at higher energy). In this case, it is the $^{12}C^{16}O$ that is attached to a reduced cluster (1908 cm^{-1}) and it is the $^{13}C^{18}O$ that is attached to a neutral cluster (1846 cm^{-1}). Thus, the major and minor isomers together give the following pattern; the highest and lowest energy bands arise from the major isomer and are the most intense, while the bands at intermediate energy arise from the minor isomer and are less intense.

Because the energy difference in this complex is great enough to give rise to observable population differences, we should be able to adjust the relative populations by adjusting the temperature, as is predicted by the Boltzmann law. Figure 3.2 displays a series of IR spectra for **1** in the mixed valence state taken at the temperatures +10, 0, -40, and -90 C. There are two items of interest in these spectra. First, as the temperature is cooled from +10 to -90 degrees the contribution to the spectrum from the minor isomers decreases. This is the behavior expected for a system that consists of states at different energy levels whose relative populations follow a Boltzman distribution. By lowering the temperature we are able to force a greater proportion of the population to reside in the more stable, or major isomer. The second item of note is that the peak positions in the spectra do not change substantially with temperature. Thus, any change to the bandshape is attributed to a change in the relative populations of the major and minor isomers.

As in previous studies, we were able to simulate the IR bandshapes of $\mathbf{1}^{-1}$ for all the spectra found in Figure 3.2. This simulation is done using a modified Bloch equation appropriate for the simulation of dynamic IR spectra[9, 10, 36, 37]. This equation takes into consideration (among other things) the separation of the bands being exchanged, the rate of the exchange, and the relative intensities of the bands undergoing exchange. Because the ν(CO) bands all arise from the same molecule the separation between the exchanging bands remain constant. Figure 3.2 shows an example of the experimental data and its fit. Because the ET rate is assumed to remain constant (i.e. the positions of the bands do not change) with changes in temperature, all the spectra seen in Figure 3.3 can be adequately simulated using the same rate constant of k_{et} = 8.5 x10^{11} s^{-1}. Because the bands considered here all arise from similar stretches, we can assume that the difference in intensity directly stems from a difference in population. Thus, the adjustable parameter in these simulations is the relative populations of the major and minor isomers. Because of this, simulating these spectra allows us to obtain estimates of K_{eq} for the spectra in Figure 3.2. Table 3.1 lists the equilibrium constants so obtained at each temperature.

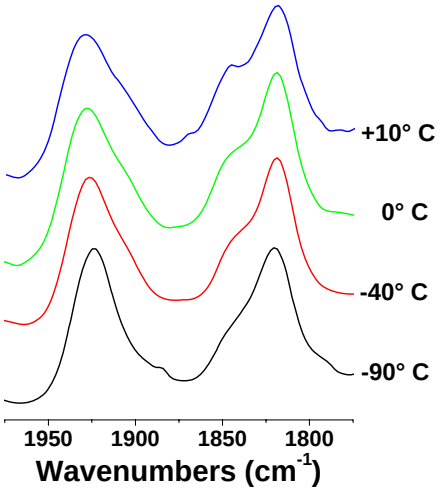

Figure 3.2: Carbonyl stretching region for $\mathbf{1}^{-1}$ taken in CH_2Cl_2 at +10° C, 0° C, -40° C, and -90° C. The assessment of the peak positions are the same as outlined in Figure 3.1. The changes in relative intensities for the major and minor isomers are a result of changes in the relative Boltzmann populations of these species.

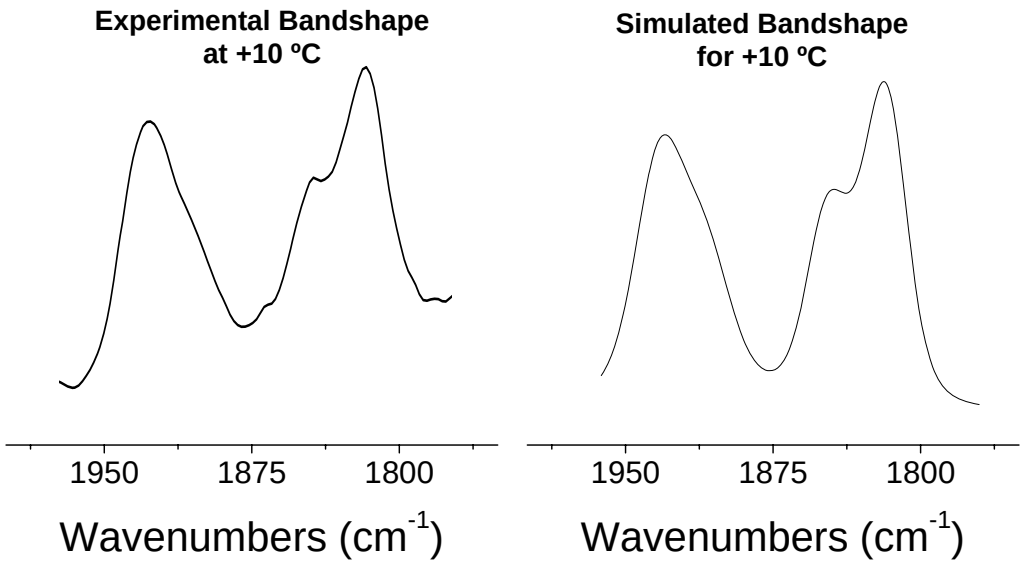

Figure 3.3: Experimental and simulated ν(CO) spectra for $\mathbf{1}^{-1}$ at 0° C.

Table 3.1. Equilibrium constants (K_{eq}) for 1^{-1} at +10° C, 0° C, -40° C, and -90° C. The K_{eq} were obtained through simulation of the spectra in Figure 3.2.

Temperature	K_{eq}
+10° C	1.53
0° C	1.60
-40° C	1.70
-90° C	1.80

Figure 3.4 is a Van't Hoff plot of the data presented in Table 3.1. A linear fit to the data gives a ΔH = 0.64 kJ/mol ± 0.14 kJ/mol (53 cm^{-1}/mol ± 12 cm^{-1}/mol) and a $\Delta S = 1.5 X10^{-3}$ kJ/mol ± 0.6 x 10^{-3} kJ/mol (0.12 cm^{-1}/mol ± 0.048 cm^{-1}/mol) for the exchange of major and minor isomers. Since the exchange of major and minor isomers is effected by the transfer of an electron from one cluster to the other, the ΔH and ΔS found here are those for the ET event. Of note is that, within the resolution limit of the instrument employed, ΔS is 0. This is an expected result, as the two sites between which the electron exchanges are essentially identical. The only intrinsic difference between the two sites is the difference in pyridyl ligands. The major entropic differences that would arise from this difference in ligands stem from differences in their solvation shells and vibrational modes. However, the entropic differences arising from these considerations is expected to be small. Furthermore, these small differences in solvation shells and vibrational modes between the two pyridyl ligands is largely mitigated by the fact that the ET occurs on the time scale of both vibrational motions and solvent dynamics which has the effect of partially averaging the solvent and internal vibrational motions with respect to the ET event. Additionally, as was seen in Chapter 2, H_{AB} is quite large in these complexes and has the effect of decreasing the differences in the vibrational modes between the sites stemming from difference in electron occupancy (H_{AB} has the effect of moving the minima of the potential energy surface towards each other along the reaction coordinate). Thus, the effects of internal vibrational and solvent modes are both time and space averaged with respect to the electron transfer between sites and do not even fully carry the small weight that one would expect from examination of a static picture of the dimer. Therefore it is quite reasonable that, in this case, ΔS is found to be zero.

Because ΔS can be taken to be zero, ΔH provides the value of ΔG for the exchange of an electron between the to ruthenium clusters. This gives a new value for ΔG of 53 cm^{-1}/mol. The previous estimate of ΔG for this dimer was 75 cm^{-1} (Chapter 2). However, this estimate was obtained using bandshapes obtained at a single temperature of -30°. Thus, by taking spectra at several different temperatures, this value has been changed by a factor of 2/3.

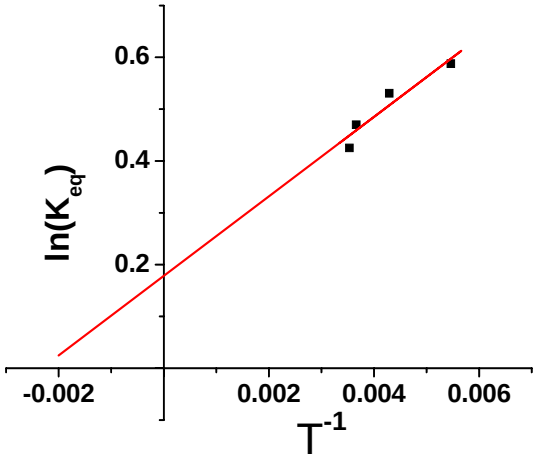

Figure 3.4: Van't Hoff plot for $\mathbf{1}^{-1}$. The red line is a linear fit of the data giving ΔH = 0.64 kJ/mol ± 0.14 kJ/mol (53 cm^{-1}/mol ± 12 cm^{-1}/mol) and a ΔS = 1.5 $X10^{-3}$ kJ/mol ± 0.6 x 10^{-3} kJ/mol (0.12 cm^{-1}/mol ± 0.048 cm^{-1}/mol)

As discussed in chapter 2, knowledge of ΔG in both the diabatic and adiabatic cases allows one to calculate the value of $\boldsymbol{H_{AB}}$ for a complex by way of equation 1.

$$H_{\mathrm{AB}} = \frac{\lambda_{\mathrm{symm}}}{2\Delta G_0^0}\sqrt{(\Delta G_0^0)^2 - (\Delta G_1^0)^2}. \qquad (1)$$

Where λ_{symm} is given by,

$$\lambda_{\mathrm{symm}} = \left[\lambda_{\mathrm{asymm}}^2 - 2\Delta G_0^0\sqrt{\lambda_{\mathrm{asymm}}^2 - 4H_{\mathrm{AB}}^2}\right] \qquad (2)$$

As discussed in Chapter 2, the value of ΔG for this dimer in the diabatic case (ΔG^0_0) was calculated to be 1850 cm^{-1}. The value of ΔH reported here provides an improved estimation of the adiabatic ΔG (ΔG^0_1) used in chapter 2. Using formulas 1 and 2 recursively, we can calculate H_{AB} to be

5368 cm^{-1}. The estimate of H_{AB} for **1** reported in the previous chapter was 5356 cm^{-1}. Thus, even though our estimate of ΔG has changed by a factor of 2/3 our estimate of H_{AB} has changed by much less than 1%. Such a small change in H_{AB} despite such large refinement of ΔG seems to support the accuracy of H_{AB} determined here and in Chapter 2. This adds more validity to the claim that theses dimers reside on the localized to delocalized transition and are class II-III mixed valence complexes.

3.4 Conclusion

Here we discussed the temperature dependence of an asymmetric mixed valence compound. The populations of mixed valence isomers present in this system follow the expected Boltzmann behavior. Specifically, we have shown that the percentage of minor isomer present decreases with temperature.

As a result of this study we have been able, for the first time, to experimentally determine the value of ΔS for an electron transfer event. As expected for nearly symmetric complexes, this value is essentially zero. This reflects the fact that there is essentially no information passed as the electron moves from one site to another. We have also been able to refine our estimate of H_{AB} in these complexes. The extremely small change in the calculated value for H_{AB}, despite a large change in the associated value for the driving force of the ET indicates that the value of H_{AB} presented here is reasonably accurate. This, in turn, supports the assignment of these complexes to the class II-III regime – the regime that covers the localized ($H_{AB} < \lambda/2$) to delocalized ($H_{AB} = \lambda/2$) transition.

Chapter 4: Dynamical solvent control of the electron transfer rates for a class II-III mixed valence system

4.1 Introduction

The firm establishment of the dimers of trinuclear ruthenium clusters, $[(RuO(OAc)_6(CO)(py)]_2$-μ_2-pz, as class II-III compounds together with the ability to determine electron transfer rates from IR bandshape analysis[34, 35] places us in the unique position to investigate the dynamics of class II-III compounds with respect to their environment. The classical definition of class II-III mixed valence states that solvent motions, but not the internal vibrational modes, are time averaged with respect to the electron transfer event. However, these statements are biased upon the solvent independence of IVCT bands. Analysis of UV-vis bandshape only allows one to probe the thermodynamic properties of these systems. Since the dynamics of most (if not all) other class II-III systems have not been determined, many of the descriptions concerning the behavior of class II-III systems center around thermodynamic considerations. In particular, the solvent averaging usually ascribed to class II-III systems is inferred by the solvent independence of λ. However, as λ is the *instantaneous* vertical reorganization energy it can only account for the thermodynamic contributions of the solvent and is unable to account for the dynamics of the system. This is an explicit assumption of the Frank-Condon approximation invoked to describe the transitions between diabatic potential energy surfaces as well as the Born-Oppenheimer approximation used to generate these diabatic curves. Both of these approximations assume that the electron transfer event occurs at a timescale much faster than nuclear motion. Thus, the potential energy difference that an electron must overcome when being excited from one site in a compound to another site (the vertical excitation energy) *cannot* be influenced by the dynamics of the system. Furthermore, the timescale associated with the processes that lead to UV-vis absorption are much faster than that of nuclear motions and as such, dynamic nuclear information cannot be obtained from UV-vis bandshape analysis in the same way that it is obtained from IR studies[9, 10, 37] (which address dynamics explicitly in the position of the band and implicitly in the

shape of the band). Clearly, any analysis of class II-III properties that stems from UV-vis data will exclude information on the dynamics of the nuclear modes involved in electron transfer.

We are particularly interested in the effect of nuclear dynamics of solvent upon the electron transfer. That is, we are interested in how the dynamics of the surrounding medium can affect electron transfer in highly coupled, class II-III systems. Examination of the electron transfer rate expression utilized in the normal Marcus-Hush model of electron transfer[3, 8, 19, 55, 56] shows that nuclear modes (internal and external) are expected to have a large impact in compounds for which H_{AB} is quite large (approaching $\lambda/2$). This expression is;

$$k_{et} = \kappa \nu_N \exp[-(\Delta G_\lambda^* - H_{AB} + H_{AB}^2 / 4\Delta G_\lambda^*)/RT] \quad (1)$$

When H_{AB} approaches $\lambda/2$, then the exponential term approaches unity. In such a case, the kinetics of the electron transfer will be controlled by the value of the pre-exponential term, ν_N, which can be thought of as a nuclear frequency factor that gives the frequency at which the nuclear coordinates (of both the molecule and surrounding solvent) obtain the geometry of the transition state. Thus, this term is the weighted average of all nuclear coordinates that contribute to attainment of the transition state and can be described as;[21]

$$\nu_N = \left[\sum_i \nu^2 E_i \Big/ \sum_i E_i \right]^{1/2} \quad (2)$$

From this analysis it can be seen that electron transfer in highly coupled, class II-III systems should show a large degree of dependence on the dynamics of the solvent in which they are dissolved. Previous work in our lab has shown that the electron transfer does appear to scale with parameters that describe the dynamics of the solvent.[53] This chapter provides a more thorough investigation into which solvent parameters appear

to be controlling the electron transfer rate as well as a detailed analysis of why these parameters should so influence k_{et}.

4.2 Solvent effects on electron transfer rates

Previously, a communication from our laboratory had investigated the solvent dependence of the electron transfer rates in complexes **1**-**4** (Figure 4.1).[53] Here, we present a more complete discussion of the effects of solvent upon the observed electron transfer rate constants, k_{et}, of these complexes. Tables 4.1 and 4.2 present measured values of k_{et}^{-1} for complexes **1**-**4** in acetonitrile, methylene chloride, dimethylformamide, tetrahydrofuran, dimethyl sulfoxide, chloroform, and hexamethylphosphoramide. Figure 4.2 shows ν(CO) bands of $\mathbf{2}^-$ in acetonitrile, chloroform and tetrahydrofuran with the rate constants estimated from bandshape simulation.[57] As can be seen in this figure, more coalesced bandshapes correspond to faster ET rate constants. Additionally, Table 4.1 lists solvent parameters that reflect the time-independent energetic properties of these solvents while Table 4.2 contains parameters that reflect the time-dependent dynamical properties of these solvents. The energetic parameters are the outer-outer sphere reorganization energy (λ_o) commonly employed in the two state model of electron transfer[7, 11], the optical and static dielectric constants (ε_{op} and ε_s), and the solvent microscopic polarity (E_T)[58]. The dynamic parameters are the solvent viscosity (η), the principle moments of inertia ($\mathbf{I}_x$, $\mathbf{I}_y$, and $\mathbf{I}_z$), and solvent relaxation parameters as defined by Maroncelli and co-workers (τ_o, $<\tau>$, and t_{1e}).[59] At the bottom of the columns associated with these solvent parameters is an average R^2 value. This R^2 term was obtained from a linear regression fit to a plot of k_{et}^{-1} versus the parameter for each of the complexes **1**-**4** and was then averaged over all four of the complexes. The R^2 values are provided to help the reader quickly evaluate the degree of correlation between k_{et}^{-1} and the various solvent parameters. Higher R^2 values indicate stronger correlation between k_{et}^{-1} and the parameter of interest. The quantity k_{et}^{-1} is used instead of k_{et} as most of the dynamic solvent parameters are expressed as lifetimes. Using the data gathered in these tables we can begin to discuss the role that solvent plays in highly coupled mixed valence systems undergoing ultrafast electron transfer.

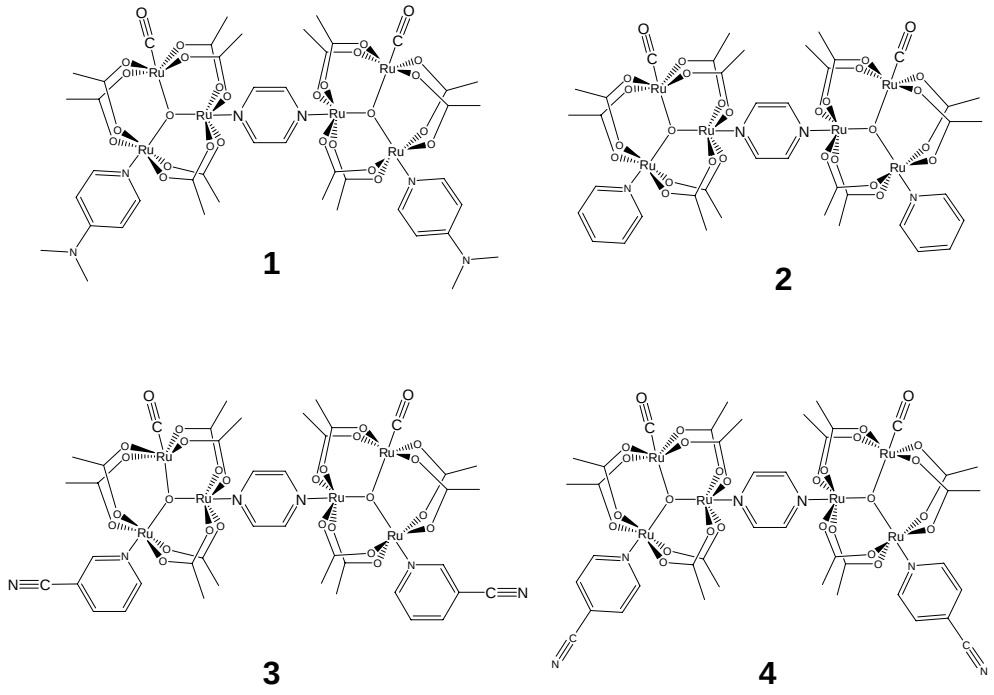

Figure 4.1. Stuctures of $[Ru_3O(OAc)_6(CO)L]_2$-μ-pz where pz=pyrazine with ancillary ligands **1** = 4-dimethylaminopyridine, **2** = pyridine, **3** = 3-cyanopyridine, and **4** = 4-cyanopyridine.

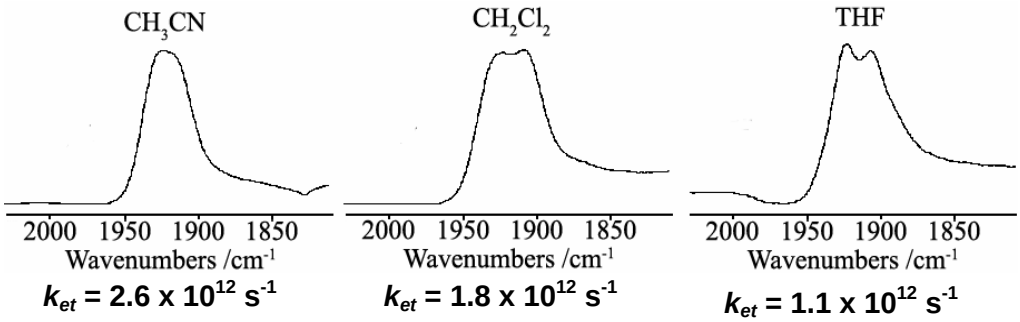

Figure 4.2. IR bandshapes for the ν(CO) band of $\mathbf{2}^-$ in CH_3CN, CH_2Cl_2, and THF. The estimated electron transfer rate (k_{et}) is given below the spectra. More coalesced spectra are associated with faster electron transfer rates.

Table 4.1. k_{et}^{-1} for complexes **1-4** and selected solvent thermodynamic parameters

Solvent	**1** k_{et}^{-1} /ps	**2** k_{et}^{-1} /ps	**3** k_{et}^{-1} /ps	**4** k_{et}^{-1} /ps	ε_s [a]	ε_{op} [b]	$(1/\varepsilon_{op} - 1/\varepsilon_s)$	E_T [c] /kcal mol^{-1}
CH_3CN	0.35(5)	0.38(5)	0.72(10)	0.91(12)	35.94	1.81	0.526	45.6
CH_2Cl_2	0.50(5)	0.57(5)	0.72(12)	0.91(11)	8.93	2.03	0.381	40.7
DMF	0.67(12)	0.77(15)	0.91(10)	1.0(2)	36.71	2.04	0.462	43.2
THF	0.83(15)	0.95(15)	1.0(1)	1.0(1)	7.58	1.98	0.373	37.4
DMSO	0.77(10)	0.87(14)	1.1(1)	0.9(1)	46.45	2.19	0.435	45.1
$CHCl_3$	1.5(2)	1.8(2)	1.9(1)	2.0(1)	4.81	2.09	0.270	39.1
HMPA	1.5(2)	2.2(2)	2.5(2)	3.3(3)	29.30	2.13	0.436	40.9
R^2 [d]	--	--	--	--	**0.040**	**0.280**	**0.191**	**0.169**

Table 4.2. k_{et}^{-1} for complexes **1-4** and selected solvent dynamic parameters

Solvent	**1** k_{et}^{-1} /ps	**2** k_{et}^{-1} /ps	**3** k_{et}^{-1} /ps	**4** k_{et}^{-1} /ps	η [a] / 10-3 Pa s	I_x [b] /g Å^2 mol^{-1}	I_y [b] /g Å^2 mol^{-1}	I_z [b] /g Å^2 mol^{-1}	τ_o [c] /ps	$\langle\tau\rangle$ [c] /ps	t_{1e} [c] /ps
CH_3CN	0.35(5)	0.38(5)	0.72(10)	0.91(12)	0.345	3.31	55.53	55.54	0.12	0.26	0.15
CH_2Cl_2	0.50(5)	0.57(5)	0.72(12)	0.91(11)	0.441	16.2	156.9	169.7	0.25	0.56	0.38
DMF	0.67(12)	0.77(15)	0.91(10)	1.0(2)	0.924	56.8	122.8	172.9	0.38	2	0.67
THF	0.83(15)	0.95(15)	1.0(1)	1.0(1)	0.575	70.5	72.2	125.3	0.43	0.94	0.7
DMSO	0.77(10)	0.87(14)	1.1(1)	0.9(1)	1.991	72.3	73.4	120.5	0.4	2	0.9
$CHCl_3$	1.5(2)	1.8(2)	1.9(1)	2.0(1)	0.058	152.83	152.96	295.2	0.71	2.8	2.3
HMPA	1.5(2)	2.2(2)	2.5(2)	3.3(3)	3.47	474	580	712	0.3	9.9	5.9
R^2 [d]	--	--	--	--	**0.334**	**0.825**	**0.657**	**0.748**	**0.234**	**0.764**	**0.860**

4.3 Electron transfer rate dependence on time-independent solvent parameters

The first parameter to be addressed is the outer-sphere re-organizational energy (λ_o), which is a measure of the energetic contributions of the solvent to the barrier for instantaneous (optically-induced) electron transfer [5].

$$\lambda_o = \frac{(\Delta e)^2}{8\pi}\left(\frac{1}{\varepsilon_{op}} - \frac{1}{\varepsilon_s}\right)\int (D_A - D_B)^2 \, d\tau \tag{3}$$

Here, Δe is the charge transferred, ε_{op} is the optical dielectric constant, ε_s is the static dielectric constant, and D_A and D_B are the dielectric displacement vectors of the precursor and successor complexes, respectively. For electron transfer in a given system in different solvents, Δe^2, D_A, and D_B remain unchanged. The changes to λ_o brought about through changes in solvent are accounted for by the term ($\varepsilon_{op}^{-1} - \varepsilon_s^{-1}$). The parameter λ_o is included in the expression for the barrier to thermal electron transfer (activation energy) as given by equation 1 and the term ($\varepsilon_{op}^{-1} - \varepsilon_s^{-1}$) normally shows good correlation with the observed electron transfer rates for mixed valence complexes. We expected this to be true for **1**-**4**, but this is not the case. Figure 4.3 is a plot of ($\varepsilon_{op}^{-1} - \varepsilon_s^{-1}$) versus k_{et}^{-1}. Examination of Figure 4.3 shows that there is no correlation between λ_o and k_{et}^{-1}. This is surprising, but the data are clear; λ_o does not capture the solvent dependence of the mixed valence ions **1**-**4**. In this important respect, **1**-**4** are behaving as if they were class III (delocalized) systems.

Although λ_o and k_{et}^{-1} are not correlated, it is possible that a single dielectric constant could capture the solvent dependence of complexes **1**-**4**. The static dielectric constant, ε_s, is a measure of the extent to which the solvent is affected by an external electric field. It is given by the following equation.[60]

$$\varepsilon_s = \frac{4\pi}{3} N_o \left(\alpha_o + \frac{\mu^2}{3kT}\right) \tag{4}$$

Here, α_o is the polarizability of the solvent molecules, which accounts for how their electron clouds are deformed by local electric fields, and the μ term accounts for the orientation of the permanent dipole moment of the solvent in response to an applied field. Thus, ε_s should provide a parameter for how the solvent responds to the change in dipole moment that occurs upon electron transfer. However, ε_s only describes the solvent's response when the applied field is either static or oscillates at frequencies less than that associated with the far IR (10^{11} s^{-1}). At oscillations in the field that have frequencies greater than that associated with far IR the orientational term (μ) in equation 4 drops out, as the solvent can no longer keep pace with the changes in the electric field. The dielectric constant that results from the exclusion of the orientational term is termed the optical dielectric (ε_{op}), and is equal to the square of the refractive index of the solvent, n.[60] The ET rates measured for **1**-**4** are on the order of 10^{11} s^{-1} and, because of this, it is not surprising that k_{et}^{-1} and ε_s show no correlation (Table 1). Because the ET rate is fast, ε_{op} is expected to be a better parameter for comparison with k_{et}. However, as can be found in Table 1, the correlation between ε_{op} and k_{et}^{-1} remains quite poor. It should be noted that even though there is some frequency dependence of the dielectric constants, they remain static parameters (they account for the magnitude of the solvent response to the applied field and not the dynamics of this response). In any case, it is easily seen that no clear correlation exists between the dielectric constants of solvents and k_{et}^{-1}.

Despite the fact that λ_o, ε_{op}, and ε_s have failed to explain the solvent dependence exhibited by complexes **1**-**4**, it is difficult to depart from the assumption that the major contribution to the rate of electron transfer will stem from the reorganization of the solvent's nuclear coordinates following the shift in charge associated with electron transfer. Thus, we consider another parameter that may capture this contribution. A logical conjecture is that the electron transfer correlates with solvent polarity. Clearly, the polarity of the solvent should reflect the strength of the response of the solvent to a change in charge distribution following an electron transfer event. This response to a change in the local electronic environment could be accounted for by the microscopic polarity (E_T) of the solvent. However, Figure 4.4 (a plot of k_{et}^{-1} versus E_T) shows that ET rates in our complexes do not depend on solvent polarity.

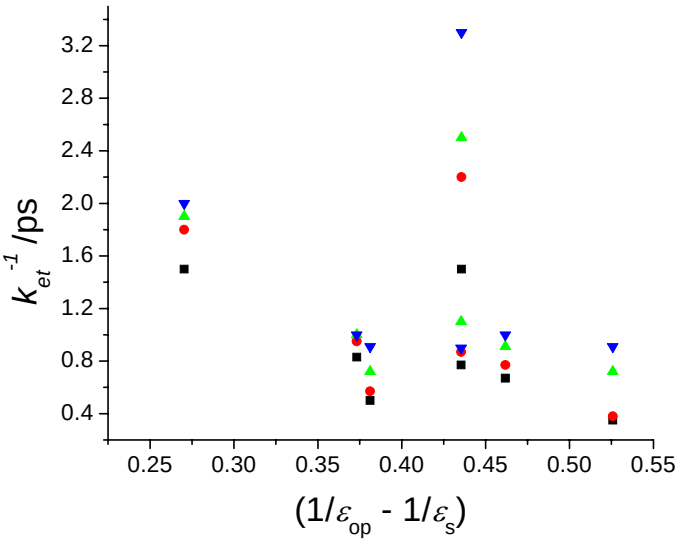

Figure 4.3. Plot $(1/\varepsilon_{op} - 1/\varepsilon_{s})$ -- the variable portion of the outersphere reorganization energy, λ_{out} -- versus the lifetime for electron transfer, k_{et}^{-1}, for complexes **1**(■), **2**(●), **3**(▲), and **4**(▼). The average of the R^2 values for this plot is 0.191.

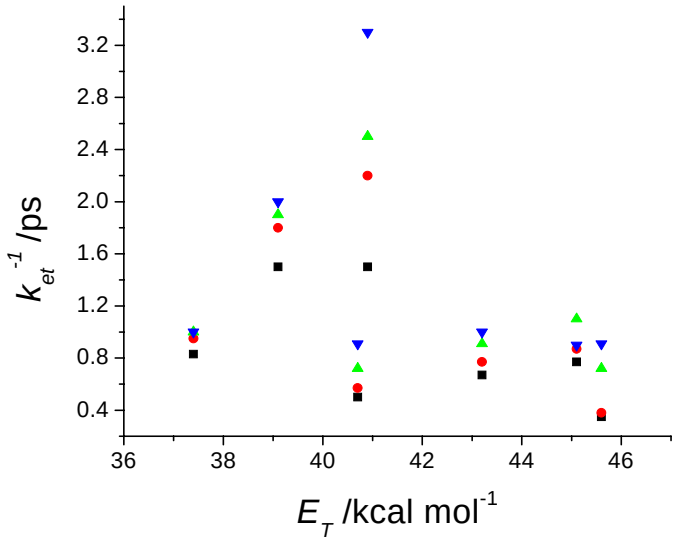

Figure 4.4. Plot of the micoscopic polarity of the solvent, E_T, versus the lifetime for electron transfer, k_{et}^{-1}, for complexes **1**(■), **2**(●), **3**(▲), and **4**(▼). The average of the R^2 values for this plot is 0.169.

Up to this point it has been shown that there is no good correlation between k_{et}^{-1} and either λ_{out}, ε_{op}, ε_s, or E_T. Thus, there appears to be no connection between the strength of solvent response and changes in the local fluctuating electric field around **1-4**. That is, the energetics of the solvent's response to changes in electric dipole seem to have no influence on k_{et}. Reference to equation 1 suggests the boundary conditions for this type of behavior to be observed.

For strongly coupled systems ($H_{AB} = \lambda/2$) the exponential term will be close to zero and the value of the exponential function approaches unity. For nearly activationless electron transfer, it is the pre-exponential term (ν_N) that will dominate the expression for k_{et}. The pre-exponential term is the weighted average of all internal vibrational modes that contribute to electron transfer and nuclear reorganization *as well as* the solvent modes that allow for reorganization of the solvent durring the ET event. We see why normal assumptions about solvent reorganization fail to capture the solvent dependence of **1-4**. The parameters λ_{os}, ε_{op}, ε_s, and E_T, all quantify different time-independent thermodynamics of the solvent contribution, which, when the value of the exponential term is *not* near zero, have a large impact on the electron transfer rate. However, in the highly coupled case when the exponential approaches unity, the pre-exponential frequencies control the rates of ET. We therefore turn our attention away from the static thermodynamic properties of the solvents and towards the *dynamic* properties of the solvents.

4.4 Electron transfer rate dependence on time-dependent solvent parameters

A simple solvent parameter that we can use as a metric for solvent dynamics important in fluidity is the solvent viscosity, η. Viscosity is a function of the rate at which a fluid's velocity changes over distance (dv/dx) and, as such, is a measure of the restriction of translational motion. In polar solvents with more restricted motion, it is expected that ν_N and, as a result of this, k_{et} will decrease in value. This general trend is observed in Figure 4.5, which is a plot of solvent viscosity versus k_{et}^{-1}. While the correlation between these two parameters is by no means excellent, it is vastly improved over those found in Figures 4.3 and 4.4 and provides a satisfying agreement with the intuitive reasoning presented above. The poor correlation most likely stems from the fact that while there is certainly some degree of translational motion

of the solvent in response to the ET, it seems more likely that the major reorganizational movement is that of rotation of the dipole. That is, following the change in the charge distribution associated with ET the solvent needs to rotate such that its dipole moment is correctly oriented with respect to this new charge distribution. Indeed, this picture is supported by work done by Stratt and co-workers.[61,62] Simulation and analysis of solvation spectra for dipolar solutes in polar solvents showed that the rotational rearrangement of the solvent molecules accounts for the major contributions to solvation of the solutes as well as the observed timescales of solvation. In contrast, they found that translational motion of solvation is largely universal amongst differing solvents and did not account for the observed differences in the timescale of solvation. This supports the idea that differences in the dynamics of solvent (and the effects that these dynamics will have on the overall dynamics of a system) are largely a result of rotational motion of the solvent. Relying on the assumption that rotational motions are the most important for initial solvent reorganization, Weaver has derived an expression for ν_N that depends solely on the rotational motion of the solvent [21].

$$\nu_N = (2\pi\tau_{rot})^{-1} \tag{5}$$

Here, τ_{rot} is termed the "solvent-phase inertial rotation time." This parameter attempts to explain the rotation of molecules within a dielectric medium. While rotational motion probably plays into the physical property of viscosity, it should be a minor contribution. The term τ_{rot} should correlate with the electron transfer rates. This parameter, however, is not straightforward to obtain for all solvents in our study. We turn instead to a simpler parameter that quantitatively addresses the rotational motion of solvent, namely the principle moments of rotational inertia.

The rotational moments of inertia (**I**) for solvent molecules can be calculated using commercial software [63] and are expected to provide a useful measure of the ease of dipole reorientation. Clearly, the rate of rotation is inversely proportional to the rotational inertia of the solvent molecules. Because the rate of electron transfer is controlled by the dynamics of the solvent and the rotational reorientation of the solvent dipole is required to accommodate the movement of the electron, we expect to find a strong

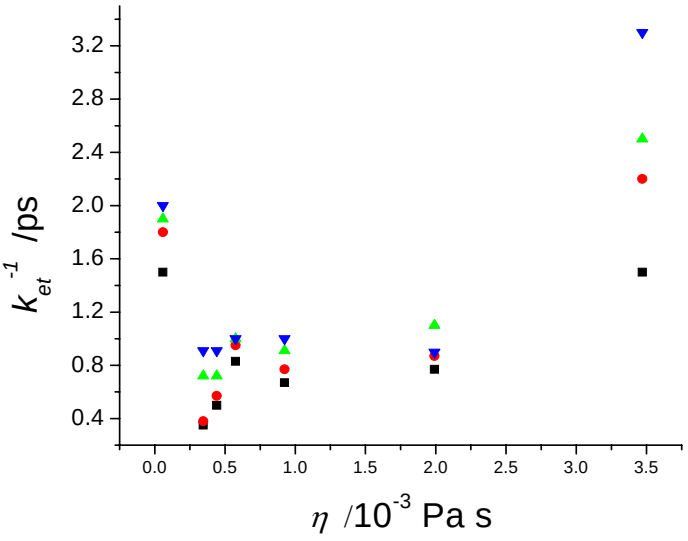

Figure 4.5. Plot of solvent viscosity, η, versus the lifetime for electron transfer, k_{et}^{-1}, for complexes **1**(■), **2**(●), **3**(▲), and **4**(▼). The average of the R^2 values for this plot is 0.334.

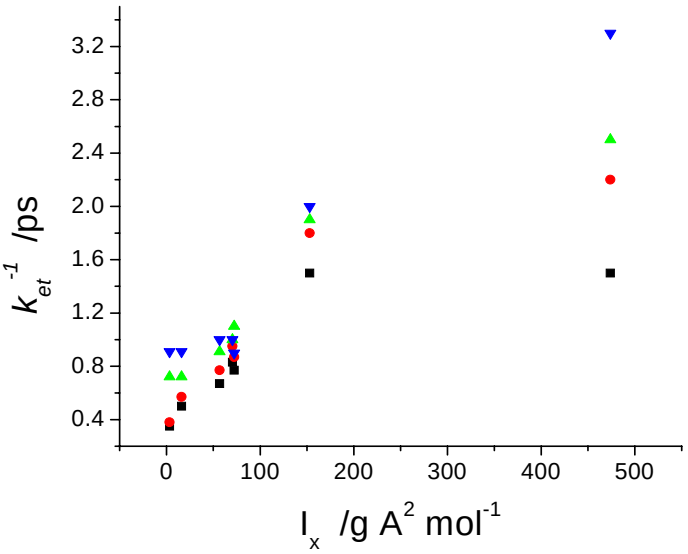

Figure 4.6. Plot of the moment of inertia along the solvent's *x*-axis, $\mathbf{I_x}$, versus the lifetime for electron transfer, k_{et}^{-1}, for complexes **1**(■), **2**(●), **3**(▲), and **4**(▼). The average of the R^2 values for this plot is 0.825.

correlation between the moments of inertia of the solvent and the electron transfer rates of complexes **1**-**4**. Examination of Table 2 shows that $\mathbf{I}_x$, $\mathbf{I}_y$, and $\mathbf{I}_z$ all have good correlations with k_{et}^{-1}. However, $\mathbf{I}_x$ shows the strongest correlation. A plot of $\mathbf{I}_x$ versus k_{et}^{-1} is shown in Figure 4.6 in order to demonstrate the trend. $\mathbf{I}_x$ is defined as the smallest principle moment of inertia and, as such, rotation along this axis is expected to be easiest. To a first approximation, rotation of the solvent by exerting a force resulting from the change in an external dipole should be principally about the "easy" axis. Thus, it is quite satisfying that $\mathbf{I}_x$ shows the strongest correlation with k_{et}^{-1}.

It is clear from Figures 4.3-4.6 as well as the data presented in Tables 1 and 2 that k_{et} is affected by the dynamics of the solvent. However, the moments of inertia only account for rotation of the solvent. While rotation should play the major role in the reorganization of the solvent, translational modes are most certainly involved. Translational movement is required for the solvent to realize the geometric coordinates that minimize the potential energy resulting from the interaction of their dipoles with the mixed-valence system. Thus, it would be useful to compare k_{et}^{-1} with parameters that take into account both the rotational and translational motions of the solvent in response to the movement of charge. Maroncelli's work on solvent relaxation dynamics has provided these parameters [59]. The work by Maroncelli and coworkers is the most comprehensive on solvent relaxation to date. This group measured the time-resolved multiexponential Stokes shift in the fluorescence of Coumarin 153 in a wide range of solvents. The fastest responses were attributed to solvent rotational motion. This motion is ascribed to the reorientation of the solvent dipole in order to stabilize the new charge distribution in Coumarin 153. The slower times were attributed to translational motion to attain the most stabilized excited state. Maroncelli calculated three characteristic solvent relaxation times for most common solvents. The first, τ_0 is the instantaneous response before solvent motion evolves. It deals with exceptionally fast timescales. The second, $<\tau>$, is the average lifetime of all components observed in the solvent response and accounts for the behavior of the solvent over long time periods. The third, t_{1e}, is the time required for the solvent response function to reach $1/e$ and may be thought of as encompassing the total evolution of solvent dynamic response to changes in local electronic environment. Of these three parameters, τ_o shows the worst correlation with k_{et}^{-1} while t_{1e} provides the best (k_{et}^{-1} versus t_{1e} is plotted in Figure 4.6). This is not wholly unexpected. The

parameter τ_o deals with the time before the solvent motion gets underway and may be considered an instantaneous polarizability. These are not expected to contribute significantly to the attainment of the transition state and, hence, to the value of ν_N. The values of $<\tau>$ are, in general, slower than our measured ET rates and, as a result, were not expected to be strongly correlated with k_{et}^{-1}. The fact that $<\tau>$ does show good correlation with k_{et}^{-1} may indicate that slower solvent motions need to be included in the total solvent response to ET in **1-4**. Finally, t_{1e}, as a parameter enveloping the full range of solvent dynamics provides the best correlation to k_{et}^{-1} of the solvent parameters we have explored. This is very reasonable if the total ensemble response of the solvent is to be considered when investigating the solvent dependence of ultrafast electron transfer.

Referring back to Tables 1 and 2, we are now prepared to make a few comments on the general trends that emerge in the correlation between k_{et}^{-1} and solvent parameters. First, it is clear that there are poor correlations between k_{et}^{-1} and solvent parameters that are mostly thermodynamic in nature (such as λ_{out}, ε_{op}, and ε_s). Second, parameters (such as $\mathbf{I}_x$ and t_{1e}) that address important dynamic solvent properties show good correlations with k_{et}^{-1}. The solvent parameters that show the strongest correlations with k_{et}^{-1} are ones that correspond to the fast movement of solvent in response to an external force (change in dipole). These parameters are $\mathbf{I}_x$ and t_{1e} and they show extremely similar correlation, suggesting that they address very similar dynamical processes of the solvent.

Given the form of equation 1 and the fact that solvent thermodynamic parameters provide poor correlation with observed k_{et}^{-1} while solvent dynamics provide excellent correlation with observed k_{et}^{-1}, it seems justified to assume that it is the solvent dynamics that are controlling the electron transfer rates of complexes **1-4** *via* the pre-exponential term. This pre-exponential control is a result of the fact that the solvent modes are included in the pre-exponential term and the fact that the electronic coupling, H_{AB}, in these complexes is large enough (approaching $\lambda/2$) that the value of the exponential approaches unity and the rate of electron transfer should be controlled by the value of ν_N.

As seen in equation 2, ν_N contains contributions from solvent modes and Weaver's derivation of ν_N in equation 5 seems to indicate that the solvent dynamics are expected to be major contributors to ν_N in fluid solution. However, the solvent dynamics are expected to be much slower than the internal vibrational

modes of the molecule that contribute to ET. For comparison, it is known that the ν_{8a} mode of the bridging pyrazine is strongly coupled to the ET event in these complexes [64] and, therefore, should be figured into the pre-exponential term. The frequency of this vibration is 4.8 x 10^{13} s^{-1} while the relaxation "frequency" of even the fastest solvent we have used (acetonitrile) is 6.7 x 10^{12} s^{-1} (using t_{1e}). Clearly the relaxation of the solvent is a process that limits the electron transfer rate of the complexes. Thus, if it were possible to de-couple the solvent dynamics from the electron transfer event, we would remove the "solvent friction" from the system and *increase* the overall ET rate.

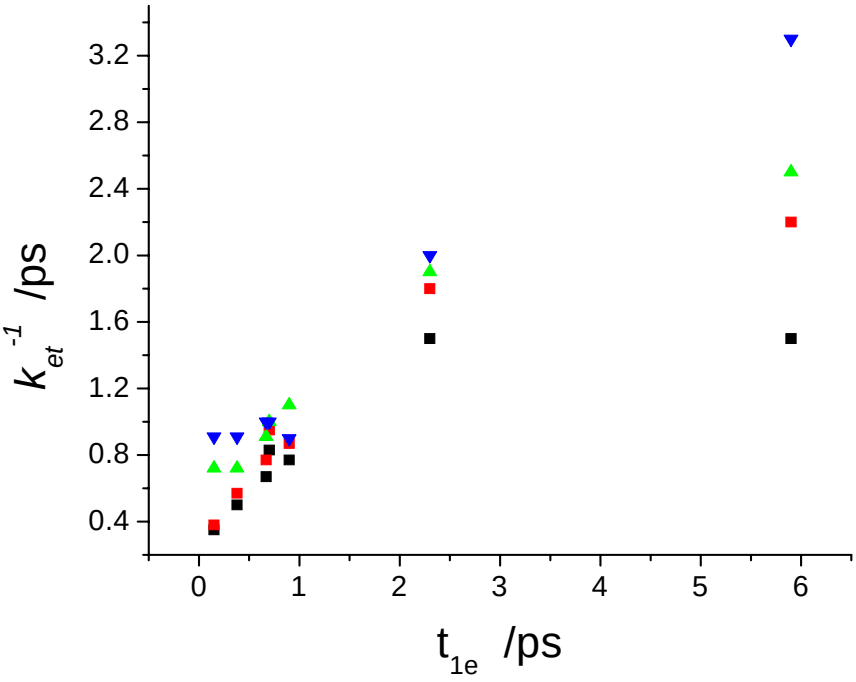

Figure 4.7. Plot of the characteristic solvent relaxation time, t_{1e}, versus the lifetime for electron transfer, k_{et}^{-1}, for complexes **1**(■), **2**(●), **3**(▲), and **4**(▼). The average of the R^2 values for this plot is 0.860.

4.5 Conclusions

The work presented in this chapter has shown that, for complexes **1-4**, the solvent dynamics are controlling the ET rate via ν_N. It is clear, then, that for **1-4** the solvent environment is *not* averaged as is predicted for class II-III compounds.[17] Even though the estimated ET rate (10^{12} s^{-1}) is in the correct time regime to be intermediate between solvent (10^{11} s^{-1}) and vibrational (10^{13} s^{-1}) modes, it appears that residual solvent dynamics play an important part in determining the value of k_{et}. By considering many models of solvent dynamics, it is apparent that it is the inertial properties of the solvent (the factors that govern the solvent's most rapid movements) that dictate the rate of ET. Thus, we are forced to conclude that the current definition of class II-III does not fully capture the solvent dependence of such systems. This stems from the use of λ as a measure of the solvent dependence, which can only measure the dependence on static, thermodynamic, properties (ie. $1/\varepsilon_{op} - 1/\varepsilon_s$). While ε_{op} does carry some information concerning dynamics , this information is lost at a timescale *much* slower than the k_{et} expected for class II-III systems (10^{11} s^{-1}). Because of this, it is unsurprising that λ could be observed to be solvent independent, but that k_{et} would maintain some degree of solvent dependence.

As a result of the considerations presented in this chapter, we propose a new definition for class II, class II-III, and class III mixed valency. Class II may be defined as the case in which solvent thermodynamic properties still contribute to the electron transfer rate (λ will be solvent depedent in this case). Class II-III may be defined as the case in which thermodynamics no longer control k_{et} (λ will be solvent independent in this case) but k_{et} still shows some dependence on solvent dynamics. Class III, then, is the case in which *both* thermodynamic and dynamic properties of the system are averaged. This provides a much more experimentally accessible definition of class I, II-III, and III. This is especially true in the case of large metal complexes where the dynamics of the solvent are much more homogeneous than the dynamics of vibrational modes of the complex, which can easily stretch over several orders of magnitude ($\sim 10^{12}$ s^{-1} to $\sim 10^{15}$ s^{-1}) – raising questions concerning the correct timescale to employ for discussions of electronic delocalization. Since class II-III attempts to address properties of mixed valence systems that reside on the localized to delocalized transition, a clear marker for this transition should be employed.

Solvent dynamics provide a very well defined, consistant, and physically satisfying metric for this transition.

Because complexes **1-4** show dependence on solvent dynamics, if one could change the dynamics of a particular solvent, one would expect to observe concurrent changes in k_{et}. Such effects are the focus of the next chapter, where the effects of freezing the solvent upon k_{et} are investigated.

4.6 Experimental

Complexes used in this study were of the type $[Ru_3O(OAc)_6(CO)L]_2$-μ-pz where pz=pyrazine with ancillary ligands **1** = 4-dimethylaminopyridine, **2** = pyridine, **3** = 3-cyanopyridine, and **4** = 4-cyanopyridine, Figure 4.1. Complexes **1-4** were prepared as described previously.[65] Complex **5,** $Ru_3O(OAc)_6(CO)(4\text{-cpy})_2$, was obtained as a side product during the synthesis of complex **4**.

Solvents for this study were chosen such that the mixed valence state of the complex is soluble and is stable over a wide range of temperatures. For the optical cryostat studies, acetonitrile and methylene chloride were dried over basic alumina with a custom dry solvent system. 10 mM solutions of each dimer were chemically reduced to the mixed valence state with 1.1 molar equivalents of cobaltocene (E°'= -1.33V vs. Fc/Fc^+)[66] in an inert atmosphere. Spectra of mixed valence dimers were recorded on a Bruker Equinox 55 FTIR in a flow through optical cryostat (Specac, model number 21525). The sample cell, consisting of CaF_2 windows with pathlength of 0.1mm, is contained in a vacuum jacketed housing. Addition of liquid nitrogen to the cooling compartment followed by heating to the desired temperature with a computer-controlled thermocouple/heating coil regulates temperature in the sample cell. Solvents for the use in IR spectroelectrochemistry were dried and distilled by the usual methods. The IR spectroelectrochemical responses were measured in a sixth-generation home built cell mounted onto a specular reflectance unit. The cell has been described in detail elsewhere [67]. Simulation of IR spectra to estimate ET rate constants was preformed with VibexGL, a program for the simulation of IR spectra of exchanging systems [57].

Chapter 5: Electron transfer rates in class II-III mixed valence systems in solid media: Decoupling of the solvent and electronic motions

5.1 Introduction

As discussed in the previous chapter, the electron transfer rate (k_{et}) of highly coupled mixed valence systems is dependent on the dynamics of their environment. In particular, it was shown that, to a large extent, the dynamics of solvent motion and reorientation in response to a change in dipole dictate the rate of electron transfer (ET) in these complexes. It is not unreasonable then to think of this interaction as "solvent friction." That is, the reorientation of the solvent dipoles is slow enough that it imposes an dynamic "drag" on the ET event, which does not allow the system to obtain the transition state at the same frequency that it would, were the solvent not be so heavily coupled to the ET. That is, the system is slowed down from its innate – or purely intramolecular – frequency. Thus, if one could somehow remove the solvent contribution to the pre-exponential term, ν_N, then one could reasonably expect the electron transfer rate to increase.

One way to remove the solvent contribution to the pre-exponetial term is to remove the solvent from the system. While this may be the most direct approach, it is also experimentally problematic. The mixed valence ion is not expected to possess a high vapor pressure. As such, gas phase IR of the mixed valence complex is currently experimentally unobtainable in our laboratory. Measurement of k_{et} in crystals of the mixed valence ion would yield solvent free rates, however, the results may be complicated by interacting ET centers, where the dipoles from one exchanging system may influence the barrier to ET of another system and *vice versa*. Thus, determination of k_{et} in an ordered solid phase may not accurately reflect k_{et} following the simple removal of the solvent term from ν_N. Instead we turned to more delicate methods for removing the solvent contribution to ν_N.

In Chapter 4, it was established that the major dynamic motions of the solvent that contribute to ν_N should be rotational (or librational) in nature and that translational motion must make up a minor contribution. Thus, all we must do is find a way to fully arrest the rotational (and perhaps even the translational) motion of the solvent. As the solid state of matter is expected to have very little of either of these two motions, it is clear that freezing of the solvent should have the effect of removing the solvent contribution to ν_N. Thus, the transition of a system of our mixed valence ion in solution from liquid to solid would be accompanied by the removal of the solvent "friction" form the electron transfer rate. This, in turn, would result in an increase in the observed electron transfer rate (as evidenced by IR bandshape coalescence).

5.2 Decoupling of solvent modes from rates of electron transfer

It has been predicted that the de-coupling of the solvent modes from the electron transfer rate may be achieved by freezing the solvent in which the electron transfer is occurring.[68] The main effect of this de-coupling is that solvent dipolar reorientation will no longer play a dynamic role in the reorganization of the system and ν_N will consist only of a weighted average of intramolecular vibrations. When solvent friction is removed, the pre-exponential is expected to increase from 10^{12} s^{-1} to 10^{13} s^{-1}. The interesting and counter-intuitive result that must follow from this is that the rate of electron transfer is expected to *increase* as the solvent temperature decreases. However, this increase in rate should only occur near the freezing point of each solvent and then change no further (i.e. solvent modes decouple once frozen and remain uncoupled.) Using **1**, **2** and **4** in methylene chloride (mp = -92 C°) and acetonitrile (mp = -44 C°), FTIR spectra were collected from 25° C to the freezing point of each solvent. In all cases, as the temperature of the system was decreased from 25 °C to just above the freezing point of the solvent, non-Arrhenius behavior of the electron transfer rate was observed (a slight increase in estimated rate constants occurred at lower temperatures). This is consistent with very low barriers to ET. As the freezing point of the solvent was approached, a dramatic increase in the coalescence of the ν(CO) bands was observed. Lowering the temperature past the freezing point of the solvent resulted in no further coalescence or change in the IR spectra. Figures 5.1 and 5.2 show ν(CO) spectra of **4** at several temperatures in methylene chloride and

acetonitrile, respectively. It is clear that as the solvent freezes, the ν(CO) bandshape coalesces and that beyond the freezing point of the solvent no further coalescence occurs. Complex **4**, which has the slowest exchange rate of **1**-**4**, shows the most dramatic change in coalescence. Complexes **1** and **2**, which show more coalesced ν(CO) spectra at 25° C compared to **4**'s do not show as striking an increase in the bandshape coalescence. Tables 5.1 and 5.2 summarize simulated electron transfer rates for **1**,**2**, and **4** as a function of temperature, up to the freezing point, in methylene chloride and acetonitrile, respectively.

Recall that it was shown in chapter 3 that the mixed valence complexes **1**-**4** show slower k_{et}'s in "slower" solvents (i.e. those with longer dipolar relaxation lifetimes). How then does freezing the solvent produce faster k_{et}'s? Freezing the solvent causes the dynamic solvent modes to decouple from very fast ET. This can be seen by consideration of the expression for the electron transfer rate given in equation 1.

$$k_{et} = \kappa \nu_N \exp[-(\Delta G_\lambda * - H_{AB} + H_{AB}{}^2 / 4\Delta G_\lambda *) / RT] \quad (1)$$

In this equation, κ is the electron transmission coefficient and is taken to be 1 for highly coupled mixed valence systems such as those being studied, ν_N is the pre-exponential frequency factor and accounts for the frequency at which the systems (both internal and external) nuclear coordinates obtain the transition state, ΔG* is the activation energy for electron transfer, and H_{AB} is the electronic coupling between the two redox sites. It is expected that the freezing of the solvent will have the largest effect upon the nuclear frequency factor, as incorporating the solvent in to a solid matrix will affect the nuclear motions of the solvent. Equation 2 was introduced by Weaver to describe the relative contribution of nuclear modes to the pre-exponential term.

$$\nu_N = \left[\sum_i \nu^2 E_i \Big/ \sum_i E_i \right]^{1/2} \quad (2)$$

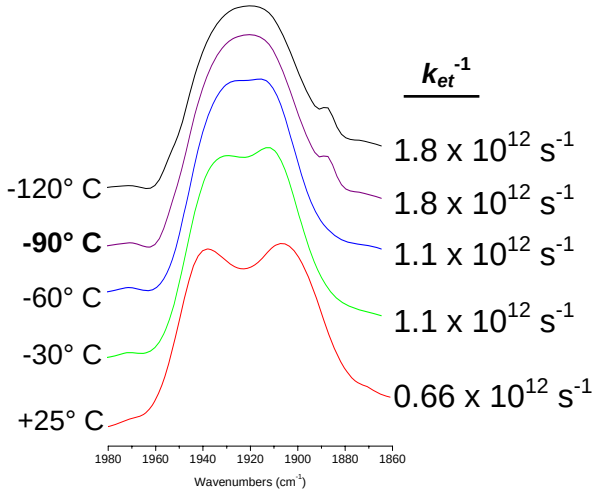

Figure 5.1. IR bandshape for ν(CO) of mixed valence **4** in CH_2Cl_2 as a function of temperature. The bandshape shows increasing coalescence as the freezing point of the solution is approached (ca. -95° C). To the right of each spectrum are listed the electron transfer rates obtained from simulation of that spectrum.

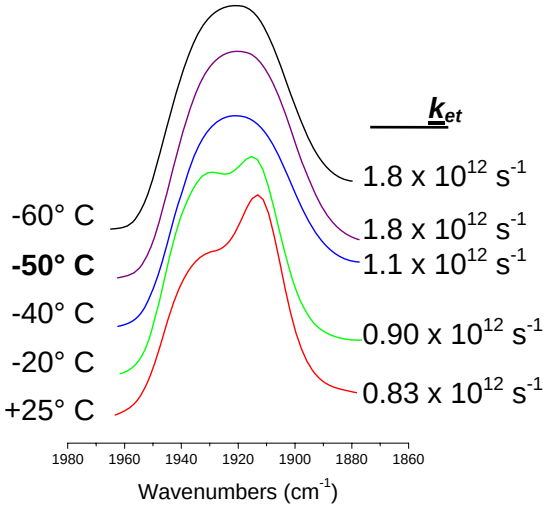

Figure 5.2. IR bandshape for ν(CO) of mixed valence **4** in CH_3CN as a function of temperature. The bandshape shows increasing coalescence as the freezing point of the solution is approached (ca. -44° C). To the right of each spectrum are listed the electron transfer rates obtained from simulation of that spectrum.

Table 5.1. k_{et} [a] for complexes 1,2 and 4 in CH_2Cl_2

	Temperature / ºC				
	25	**-40**	**-60**	**-80**	**-90**
1	2.00	2.00	2.30	2.30	**3.50**
2	1.36	1.77	1.79	2.10	**2.50**
4	1.05	1.10	1.15	1.40	**1.46**

[a]Values of k_{et}^{-1} are given in units of 10^{12} s^{-1}. Uncertainties are 0.02 x 10^{12} s^{-1}.

Table 5.2. k_{et} [a] for complexes 2 and 4 in CH_3CN

	Temperature / ºC				
	25	**-20**	**-30**	**-40**	**-50**
2	1.63	1.66	1.80	1.90	**2.00**
4	0.83	0.90	1.09	1.80	**1.80**

[a]Values of k_{et}^{-1} are given in units of 10^{12} s^{-1}. Uncertainties are 0.02 x 10^{12} s^{-1}.

One can see that as the solvent mode's frequency decreases (as they are incorporated into a solid matrix) their contributions to ν_N will dramatically decrease. Thus, the ET rate should show little dependence on solvent dynamics once the solvent in frozen. Once the dependence on solvent dipole reorientation is lifted, faster internal modes dominate ν_N, k_{ET} increases as a result, and we expect the ν(CO) bandshapes to reflect this increase in ET rate. Examination of Figures 5.1 and 5.2 shows that the spectra of complex **4** are indeed more coalesced following the freezing of the solution. Because the timescale associated with the freezing of solvent molecules is expected to be much slower than ET, the mixed valence ions observed in an IR experiment should exist in "averaged" solvent environments upon freezing. This averaging is how valence trapping is avoided at low temperatures.

It is worth commenting on one further ramification of freezing the solvent. Examination of Figures 5.1 and 5.2 shows that once the solvent is frozen the coalesced bandshapes in these two solvents are nearly identical. This, in turn, must mean that the rate of electron transfer is nearly identical for

complex **4** in both solvents *once they are frozen*. This is a striking feature of these figures, especially since the bandshapes (and electron transfer rates) are very different when the solvents are fluid. This is consistent with removal of solvent dynamical terms from ν_N upon freezing the solvent, leaving only the internal vibrational modes of the molecule. Thus, the freezing of both methylene chloride and acetonitrile has the effect of equalizing the ν_N term for these solvents. Remembering that k_{et} is under pre-exponential control (because the exponential term is nearly unity for these complexes) we then see that freezing of the solvents must produce nearly identical electron transfer rates in different solvents. This is verified by the spectra in figures 5.1 and 5.2.

One possible complication of estimating electron exchange rate constants by simulating IR bandshapes is the intrinsic temperature dependence of the contributing bandshapes. It is well known that IR bandshapes change with temperature – especially following the freezing of the solvent where locking the solute into a solid matrix can greatly increase the contribution of inhomogeneous broadening.[9] Because of this, it is important to determine the contributions of IR bandshapes, independent of electron exchange. In order to rule out effects stemming from changes in temperature and state of the solvent reference spectra of the Ru_3 monomer, **5**, were taken in the neutral and minus one states in methylene chloride from 25° C through -190° C and in acetonitrile from 25° C to -100° C. The monomer was used so that neutral and fully reduced clusters could be obtained (the ruthenium dimers are unstable in the fully reduced, -2, state). The peak position and full-width-at-half-maximum values were measured for ν(CO) bands in CH_2Cl_2 and CH_3CN and are reported in Tables 5.3 and 5.4, respectively. As the solvent temperature decreased broadening of all the ν(CO) bands was observed, accompanied by a shift in the peak position. In all cases the shift in peak position was less than 6 cm^{-1} from the starting value over the temperature range investigated. Neither the shift in position nor the changes in the FWHM were sufficient to account for the spectra observed in Figures 5.1 and 5.2. This result confirms that the increase in coalescence we observed upon freezing solutions of mixed valence ruthenium dimers is due to an increase in the rate of dynamic electron exchange, not the intrinsic temperature dependence of IR bandshapes.

Now that the increase in k_{et} with decreasing temperature is shown not to be an artifact, we must comment on one further point of interest for this temperature dependence. While such non-Arrhenius

behavior has been observed before it is usually explained in terms of a stable intermediate that is not realized at significant concentrations except at low temperatures (the non-Arrhenius behavior is a result of relative populations of the species throughout a mechanism)[69] or in terms of significant contributions from tunneling channels[70]. The non-Arrhenius behavior observed here, however, is fundamentally different. It is observed through a *direct* modification of the pre-expenential term for a single elementary reaction. That is, the pre-exponential term is observed to increase with decreasing temperature! This, in turn, must mean that we are altering the fundamental molecular process that leads to the attainment of the transition state. Indeed, this appears to be exactly what is happening; freezing of the solution decouples solvent modes from the electron transfer and fundamentally changes the overall pathway for attainment of the transition state.

5.3 Conclusions

The ET rate in highly coupled mixed valence ruthenium dimers of trimers is found to increase upon freezing of the solvent. The increase in k_{et} is observable as an increase in coalescence of ν(CO). This behavior is a direct consequence of the large magnitude of H_{AB}, but it equally relies on the fact that though it is large, H_{AB} remains less that λ/2. The large value of H_{AB} places the rate of ET under pre-exponential control and ensures that it will be sensitive to changes in solvent dynamics. The fact that H_{AB} is less than λ/2 means that full delocalization is not yet obtained and that changes in k_{et} may be observed. The increase in rate observed upon freezing is ascribed to decoupling of solvent modes from the ET event (removal of the solvent contribution to ν_N). The removal of the solvent modes from ν_N (and the subsequent increase in k_{et}) has two very important ramifications. First, the k_{et} in various frozen solvents is expected to be indentical for indentical mixed valence species. This is because once the solvent modes are removed ν_N is entirely determined by internal vibrational modes, which are largly unaffected by the temperature. Secondly, the increase in k_{et} at the freezing point represents a sort of non-Ahrenius behavior – one in which the fundamental mechanism of a single elementary reaction is altered. As a final point, it should be stated that the behavior observed in freezing media adds support to the claim that the solvent is controlling the ET rate (i.e. the solvent is *not* averaged with respect to the ET event) for highly coupled class II-III complexes.

Chapter 6: Changes in electronic coupling in class II-III systems as a driving force for chemical interactions

6.1 Introduction

In chapters 2 and 3 we saw how the synthesis of asymmetric mixed valence complexes have allowed for many properties of mixed valence systems to be determined for the first time. In particular, they have allowed for the observation of the separate mixed valence states (mixed valence isomers) that were previously degenerate and, as such, indistinguishable. Furthermore, the ability to determine the equilibrium constants relating the two mixed valence isomers allowed for the determination of the adiabatic energy difference between the two charge configurations. Together with information about the diabatic energy differences, this allowed for an accurate determination of H_{AB}. Such determination allows us to confirm that these complexes reside on the border between class II and class III mixed valence complexes.. Indeed such large electronic coupling, together with the fact that the two mixed valence isomers are observable, seems to place such complexes firmly in the newly created class II-III. Beyond this, asymmetric complexes have allowed us to experimentally determine both ΔH and ΔS. In the case of the enthalpy, we reached the satisfying conclusion that the heat of activation is very low – as it must be if the electron transfer is to occur on the picosecond timescale. In the case of entropy, it was found that ΔS is close to zero, which also agrees nicely with intuitive reasoning concerning the complex.

To date, we have only looked at mixed valence complexes possessing static asymmetry, however, we now relate the effects of dynamically induced asymmetry. By "dynamically induced asymmetry" we mean asymmetry that is not permanently manifest via connectivity of the molecule (ie. ligand substitution) but, which can be realized through a non-covalent interaction with some other chemical species. Thus far, we have only investigated complexes that possess inherent substitutional asymmetry in their molecular structures. We now turn to complexes that are inherently *symmetric*, but which, through interaction with

their environment, can become asymmetric. Specifically, we are interested in the system comprised of $[Ru_3O(OAc)_6(CO)(ppy)]_2$-μ-pz (**1**) and calix[6]arene (Figure 6.1). It is known that calixarenes interact with aromatic molecules in a host-guest manner.[71-73] Thus, it is expected that calix[6]arene will complex with **1** through interaction with the 4-phenyl pyridine ligands. The discussion of the effect of this interaction is framed by the understanding of potential energy surfaces gained through the study of mixed valence isomers can be used to explain the effects of dynamic symmetry breaking on symmetric mixed valence complexes.

In particular, this discussion relies heavily on knowledge of the effects of H_{AB} upon the potential energy surfaces associated with intramolecular electron transfer as well as the expected magnitude of the electronic coupling (H_{AB}). From discussions of the proceeding chapters, it is clear that these ruthenium dimers of trimers must be highly coupled, residing on the precipice of delocalization (H_{AB} approaches λ/2). For our complexes λ is on the order of thousands of wavenumbers and so when H_{AB} approaches the delocalized limit H_{AB} must be quite large. H_{AB} does not just represent a degree of electronic coupling, but also a magnitude of resonance stabilization. Indeed, the lower potential energy surface is found to be stabilized by an amount equal to H_{AB}. Thus, H_{AB} represents a source of free energy for the system and

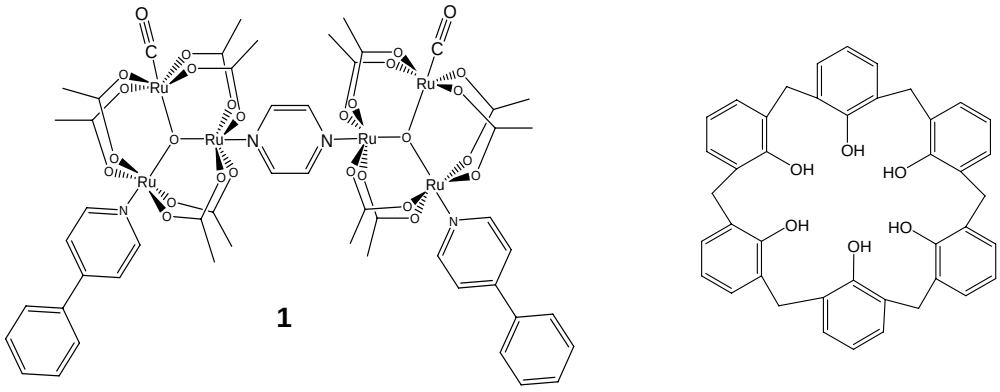

Figure 6.1. (left) Structure of $[Ru_3O(OAc)_6(CO)(ppy)]_2$-μ-pz (**1**) and (right) structure of calyx[6]arene.
increases or decreases in its value which are concomitant with a chemical event can be viewed as contributing to the overall driving force for the event.

6.2 Electronic effects of the binding of calix[6]arene to $[Ru_3O(OAc)_6(CO)(ppy)]_2$-$\mu_2$-pz

The electrochemistry of **1** was investigated using both cyclic voltammetry (CV) and differential pulse voltammetry (DPV). In the anodic region, the dimer undergoes two reversible two-electron oxidations at +0.158 V $[(Ru^{III}Ru^{III}Ru^{II})_2 \rightarrow (Ru^{III}Ru^{III}Ru^{III})_2]$ and at +0.951 V $[(Ru^{III}Ru^{III}Ru^{III})_2 \rightarrow (Ru^{IV}Ru^{III}Ru^{III})_2]$. In the cathodic region, the two ruthenium clusters are reduced sequentially, giving rise to two reversible one-electron reductions at -1.126 V $[(Ru^{III}Ru^{III}Ru^{II})_2 \rightarrow (Ru^{III}Ru^{II}Ru^{II})(Ru^{III}Ru^{III}Ru^{II})]$ and -1.500 V $[(Ru^{III}Ru^{II}Ru^{II})(Ru^{III}Ru^{III}Ru^{II}) \rightarrow (Ru^{III}Ru^{II}Ru^{II})_2]$. That the reduction of the clusters occurs sequentially is indicative of electronic communication between the clusters. This has been observed in analogous pyrazine bridged mixed-valence complexes.[34, 35] The degree of splitting ($\Delta E_{1/2}$) is a qualitative measurement of the degree of electronic communication, or coupling (H_{AB}^2/λ) between clusters.[74] In this case, the value of $\Delta E_{1/2}$ is 374 mV, corresponding to a conproportionation constant, K_c = 2.18 x 10^6. These values are comparable to those reported previously for similar mixed valence dimers.[34, 35]

In order to study the effects of calixarene binding on the electronic properties of **1** a titration of calix[6]arene into a solution of **1** was performed. Table 6.1 summarizes the electrochemical data obtained during this titration, while Figure 6.2 shows the forward (top) and reverse (bottom) DPV of **1** at the beginning (zero equivalents of calix[6]arene) and endpoint (6 equivalents of calix[6]arene) of this titration. There are three transformations that are immediately obvious from this data. First, the position of the first reduction, $E_{1/2}(1)$, changes very little upon the addition of calix[6]arene, shifting more negative by only 2 mV. Second, the potential of the second reduction, $E_{1/2}(2)$, experiences a comparatively large positive shift upon addition of calix[6]arene, a total of 19 mV. Third, the separation between the two reduction events ($\Delta E_{1/2}$) is found to decrease upon the addition of calix[6]arene, changing in magnitude from 374 mV to 352 mV. There are two types of electronic perturbations which give rise to these three observed effects:

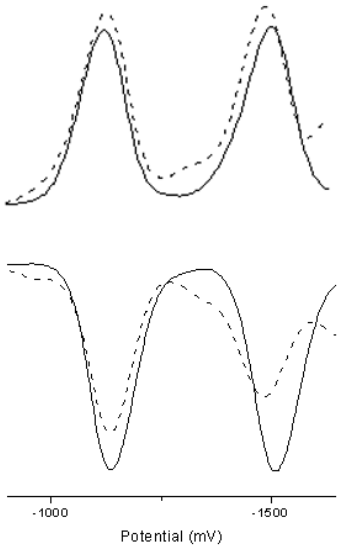

Figure 6.2: Forward (top) and reverse (bottom) DPV of 2 mM **1** with 0 eq of calix[6]arene (solid lines) and 6 eq. of calix[6]arene (dashed lines).

Table 6.1. Values for $E_{1/2}(1)$, $E_{1/2}(2)$, and $\Delta E_{1/2}$ for complex **1** as a function of the equivalents of calix[6]arene present.

Equivalents of Calix[6]arene	$E_{1/2}(1)$	$E_{1/2}(2)$	$\Delta E_{1/2}$
0	1.126	1.5	0.374
0.2	1.13	1.502	0.372
0.4	1.131	1.504	0.373
0.6	1.133	1.505	0.372
0.8	1.132	1.504	0.372
1	1.133	1.504	0.371
2	1.13	1.489	0.359
3	1.13	1.483	0.353
4	1.13	1.484	0.354
5	1.131	1.484	0.353
6	1.128	1.481	0.353

(1) The change in the intrinsic reduction potentials of the clusters, *i.e.* inductive effects from changes in the pK_a of the ppy ligand upon interaction with calix[6]arene[46] and; (2) Changes in the conproportionation equilibrium constant, $\mathbf{K_c}$, owing to changes in the stability of the mixed valance ion caused by electronic delocalization.

The most straightforward contribution to the change in reduction potentials arises from the decrease in $\Delta E_{1/2}$ (effect 2 above). As $\Delta E_{1/2}$ decreases the first and second reduction waves are expected to move towards each other by equal amounts. Thus, each wave contributes one-half of the total $\Delta\Delta E_{1/2}$ and the first wave moves more negative by 11 mV while the second wave moves more positive by 11 mV. While the shifts in potential due to $\Delta\Delta E_{1/2}$ are easily unraveled, the physical origin of these shifts cannot be understood without first discussing the direct electronic effects of calix[6]arene binding to **1**. These effects are a direct result of the changes in cluster orbital energies upon binding of calix[6]arene. The orbital energy levels of the clusters are extremely sensitive the electronic nature of the attached ancillary ligands.[24] The binding of calix[6]arene to the ppy ligand is expected to perturb the electronics of the ppy, which, in turn, brings about a change in the reduction potential of the clusters. Given the total change in the positions of the reduction waves and the contribution arising from $\Delta\Delta E_{1/2}$, we can extract the degree to which the energy levels of the clusters are adjusted by the binding of calix[6]arene. For $E_{1/2}(1)$, the total potential shift upon exposure of **1** to calix[6]arene was -2 mV. Recalling that the contribution from $\Delta\Delta E_{1/2}$ was -11 mV the binding of calix[6]arene must move the potential of $E_{1/2}(1)$ by +9 mV. A similar analysis of $E_{1/2}(2)$ reveals that the binding of calix[6]arene shifts the potential of the reduction positive by +8 mV. Thus, taking into consideration the contribution from $\Delta\Delta E_{1/2}$, the total shift for $E_{1/2}(2)$ is observed as +19 mV. From these simple considerations, it is evident that the change in potential due to calix[6]arene binding is essentially the same for both $E_{1/2}(1)$ (+9 mV) and $E_{1/2}(2)$ (+8 mV). This is expected as the electronic process associated with these potentials is the addition of an electron into identical orbitals on two different clusters. Since the same orbital is involved in both reductions, the effect of calix[6]arene upon each is expected to be similar.

In view of the overall weak binding of calix[6]arene to **1**, it is important to have independent evidence that this interaction is occurring. In a 2D NOESY NMR experiment the proton of calix[6]arene

para to the hydroxyl group was observed to interact with the most distal proton on the ppy ligand. This experiment was performed on a 400 MHz ^{1}H-NMR spectrometer with a mixing time, τ_M = 1 s, and mole ratios of calix[6]arene to **1** of 2:1. This clearly shows that the interior cup of the calix[6]arene is interacting with the 4-phenylpyridine ligand in a host-guest manner. This study confirms calix[6]arene binding, but the low intensities of the ^{1}H-NOESY cross peaks also highlight that this binding is very weak and reversible. The weak nature of the binding of calix[6]arene to neutral **1**, we will show, is a benefit in this study. The weak interaction of calix[6]arene and **1** is found to be *required* to observe cooperative binding behavior (*vide infra*).

The fact that the electrochemical potential shifts that arise from calixarene binding are positive indicates that the binding of calixarene to the clusters has a stabilizing effect on the cluster to which it binds. This can be seen by examining a simple square scheme for calixarene binding (Figure 6.3). The shift in the reduction potential for a complex that undergoes a binding event is related to the binding constant by the equation;

$$(E_b - E_u)\frac{nF}{RT} = \ln\left(\frac{K_{red}}{K_{ox}}\right) \quad (1)$$

Where $\boldsymbol{E_u}$ is the reduction potential of the complex in its unbound state, $\boldsymbol{E_b}$ is the reduction potential of the complex in its bound state, $\boldsymbol{K_{ox}}$ is the binding constant for the complex in its oxidized state, and $\boldsymbol{K_{red}}$ is the binding constant for the complex in its reduced state. From equation 1, it can be seen that a positive shift in reduction potential means that $\boldsymbol{K_{red}}$ is larger than $\boldsymbol{K_{ox}}$. That is, the binding event is more favorable when the complex is in its reduced state. This, in turn, means that the reduced cluster must be more stabilized by the binding of calixarene than neutral cluster ($\boldsymbol{\Delta G_{red}}$ is greater than $\boldsymbol{\Delta G_{ox}}$). Thus, in the reduced state, the binding of calixarene has the effect of lowering the energy (reduction potential) of the cluster to which it is attached.

Once the overall effects of the non-covalent binding of calix[6]arene to the mixed valence complex are understood in terms of the separate changes in intrinsic reduction potential and changes in

electron exchange stabilization, the origin of $\Delta\Delta E_{1/2}$ is easily explained. It has been hypothesized that electronic communication between clusters in the pz bridged mixed valence complexes proceeds through the LUMO of the pz.[48] The LUMO of the pz is higher in energy than the cluster's orbitals that are involved in inter-cluster electronic communication. Since the calix[6]arene has the effect of lowering the orbital energies of the clusters to which it is attached, the energy gap between the clusters and the pz bridge will increase. This, in turn, will lead to smaller effective coupling and less electronic communication between the clusters, reflected by a decrease in $\Delta E_{1/2}$ – as is observed by electrochemical methods.

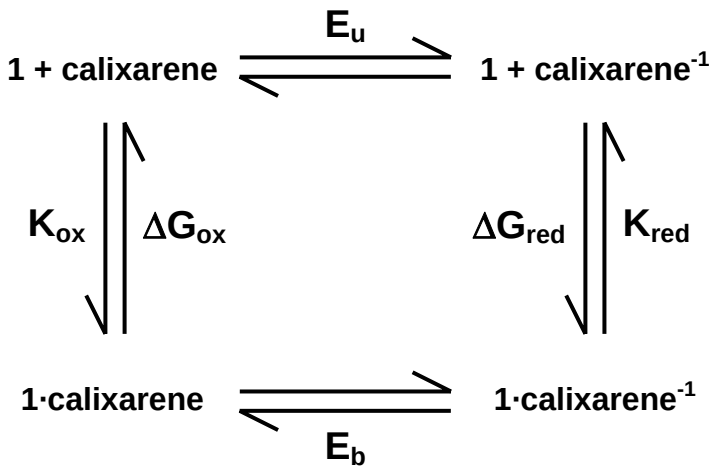

Figure 6.3: Square scheme for the binding of calix[6]arene to **1** and the reduction of the bound and unbound dimer. The scheme presented is only for the first binding event, though the results are generally applicable for the binding of the second calixarene.

6.3 Cooperative binding of calix[6]arene to $[Ru_3O(OAc)_6(CO)(ppy)]_2$-μ-pz – direct thermodynamic effects.

There is one important effect that is a result of the modulation of electronic coupling by calix[6]arene binding. This is best illustrated by plotting $\Delta E_{1/2}$ versus equivalents of calix[6]arene (Figure 6.4). The most striking aspect of this graph is the strong sigmoidal shape of the curve, which is indicative of cooperative binding. In the current system, each dimer contains two separate sites for the binding of calix[6]arene and the shape of the curve in Figure 6.4 suggests that binding of one calix[6]arene positively influences the binding of the second. Thus, **1** must be more stable with two calix[6]arenes bound than with just a single calix[6]arene bound. This result is unexpected for two reasons. First, in previous studies which investigated the binding of hosts to multiple sites of the same molecule, the binding events have been observed to be *negatively* cooperative.[75] That is, the binding of the first host interferes with the binding of the second. This is often attributed to steric hindrance between the hosts. In our complexes the hosts (calixarenes) are sufficiently separated spatially that steric interactions are not expected to play a major role in the binding of the second calixarene. However, the elimination of the steric considerations merely removes the reasoning for negative cooperation, it does not explain the observed positive cooperation. The second reason why observation of positive cooperativity is surprising is that there is direct thermodynamic opposition to it. Binding of the calixarene *decreases* $\boldsymbol{\Delta E_{1/2}}$. Thus, binding of the calixarene lowers the resonance stabilization of the mixed valence dimer. This is partially compensated by the average decrease in cluster reduction potentials that reflects the stabilizing influence of host-guest complex formation. Overall, however, the changes in (a) intrinsic reduction potentials and (b) $\Delta E_{1/2}$ lead to a shift in reduction potential that is *negative*. Thus, what we are observing is positive cooperativity for an event that is overall energetically uphill. It is clear that the cooperative binding of calixarene cannot be explained through any direct effects.

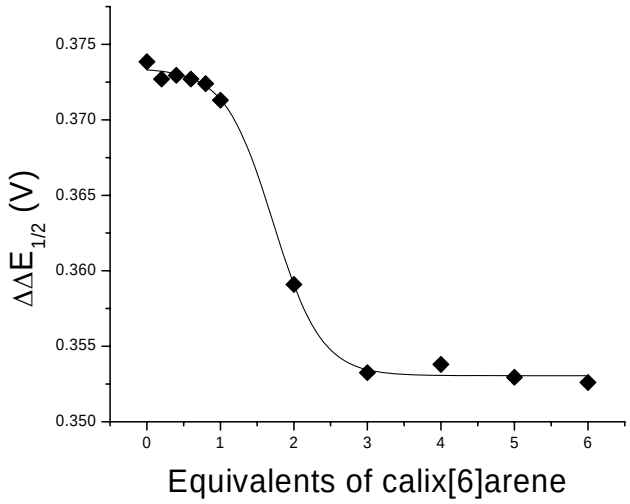

Figure 6.4: Plot of $\Delta E_{1/2}$ vs equivalents of calix[6]arene. The sigmiodal curve is fit with an $R^2 = 0.9985$ and a $\chi^2 = 1.987 \times 10^{-7}$. R^2 is a relative measure of correlation, the better the correlation between the curve and the data, the closer the value of R^2 is to one. χ^2 is a measure of statistical significance, the lower the value of χ^2, the more significant the fit.

The cooperative binding of calixarene can be explained however, if one considers the energy of the potential energy surfaces associated symmetric and asymmetric mixed valence ions of uncomplexed and complexed **1,** respectively. In particular, the resonance stabilization – or the difference between the diabatic and adiabatic surfaces for the dimer – requires comment. The energy of the lower potential energy surface, $\mathbf{G_1}$, is given by the equation[7],

$$G_1 = \tfrac{1}{2}\{(G_b + G_a) - [(G_b - G_a)^2 + 4H_{AB}^2]^{\frac{1}{2}}\} \qquad (2)$$

Where $\boldsymbol{G_a}$ and $\boldsymbol{G_b}$ are the energies of the reactants and products in the diabatic case (in this case the energy difference between the two clusters in the dimer) and $\boldsymbol{H_{AB}}$ is the effective electronic coupling matrix which mixes the wavefunctions of the reactants and products. In the diabatic case, the wavefunctions are not mixed and $\boldsymbol{H_{AB}}$ is equal to zero. Thus, the stabilization afforded by the electronic coupling, $\boldsymbol{\Delta G_1}$, can be

obtained by subtracting the lower diabatic potential energy from the lower adiabatic energy. This is given by,

$$\Delta G_1 = G_1(adiabatic) - G_1(diabatic) = \tfrac{1}{2}\{(G_b - G_a) - [(G_b - G_a)^2 + 4H_{AB}^2]^{\frac{1}{2}}\} \qquad (3)$$

In the symmetric dimer (G_b-G_a) equals zero and ΔG_1 is equal to $-H_{AB}$. In the asymmetric case, the (G_b-G_a) terms remain and it can be seen by inspection that the value of ΔG_1 will be more endergonic than $-H_{AB}$. Specifically, the difference in resonance stabilizations between the asymmetric and symmetric dimers, $\Delta\Delta G_1$, is given by,

$$\begin{aligned} \Delta\Delta G_1 &= \Delta G_1(asymmetric) - \Delta G_1(symmetric) \\ \Delta\Delta G_1 &= \tfrac{1}{2}\{(G_b - G_a) - [(G_b - G_a)^2 + 4H_{AB}^2]^{\frac{1}{2}}\} + H_{AB} \end{aligned} \qquad (4)$$

Previously, we have reported the properties of asymmetric Ru_3 dimers, which gave rise to the observation of mixed valence isomers.[44, 45] We have also reported thermodynamic estimates of H_{AB} for these dimers.[49] If the assumption is made that the H_{AB} for the symmetric dimers is similar to those calculated for their closely analogous asymmetric dimers, then we can arrive at a numerical estimation for the value of $\Delta\Delta G_1$. Using H_{AB} equal to 4250 cm^{-1} and G_b-G_a equal to 1850 cm^{-1} (the values for the dimer in which L = dmap (4-dimethylaminopyridine) and L' = cpy (4-cyanopyridine)) one obtains a value for $\Delta\Delta G_1$ of 825 cm^{-1} (9.87 KJ/mol). That is, the lower potential energy surface for the asymmetric dimer is expected to be higher in energy than the potential energy surface for the symmetric dimer by 825 cm^{-1}. Thus, it is clear that the introduction of an asymmetry destabilizes the mixed valence ion by a significant amount.

It should be noted that the above calculations are by no means intended to be exhaustive as we have not calculated, *ab initio*, the potential energy surfaces for these dimers. Rather, the results presented above are meant to demonstrate the effect of the symmetry of a molecule upon potential energy surfaces in general. Because of this, the conclusions reached here are generally applicable to all mixed valence

systems with a reasonably strong degree of electronic coupling. Namely, the property of symmetry can have a strong effect on the energetics of a mixed valence system undergoing electron exchange.

Given that the introduction of asymmetry can have the effect of decreasing resonance stabilization in these complexes, we can now formulate an explanation for the origin of the coopertivity observed for the binding of calix[6]arene to **1** (Scheme 6.1). In its uncomplexed state, with no calix[6]arene bound, **1** is a symmetric dimer (Scheme 6.1, stage A). The binding of a single calix[6]arene to **1** necessarily introduces an asymmetry to the dimer (Scheme 6.1, stage B). This has the effect of decreasing the resonance stabilization in the dimer. Binding of a second calix[6]arene restores symmetry to **1** (Scheme 6.1, stage C). Thus, substantial resonance stabilization is restored as a result of the binding of the second calix[6]arene. It can now be seen why the initial interaction of calix[6]arene with neutral **1** must be small in order for the system to behave in the way that we observe. It is known that the binding constants are related to the change in energy associated with the binding event by the equation $\Delta G = -RT\ln(K_{eq})$. The change in energy associated with electronic delocalization derived in equation 4 is related to a change in binding constant for calix[6]arene, eq. 5.

$$\Delta\Delta G_1 = -RT\ln\left(\frac{K_{eq1}}{K_{eq2}}\right) \quad (5)$$

Here, K_{eq1} is the binding constant associated with the binding of the first calix[6]arene to **1** (introducing an asymmetry) and K_{eq2} is the binding constant associated with the binding of the second calix[6]arene to **1** (restoring symmetry). In the previous section we showed that a reasonable estimate of the resonance destabilization, $\Delta\Delta G_1$, caused by symmetry breaking induced by binding of a single calix[6]arene was 825 cm^{-1}. This assumed value of $\Delta\Delta G_1$ and equation 5 show that the binding of the second calix[6]arene is a factor of 54 times stronger than the binding of the first. Thus, even though calix[6]arene interacts weakly with **1,** we can expect that the binding of the second calix[6]arene is reasonably strong. We conclude that if

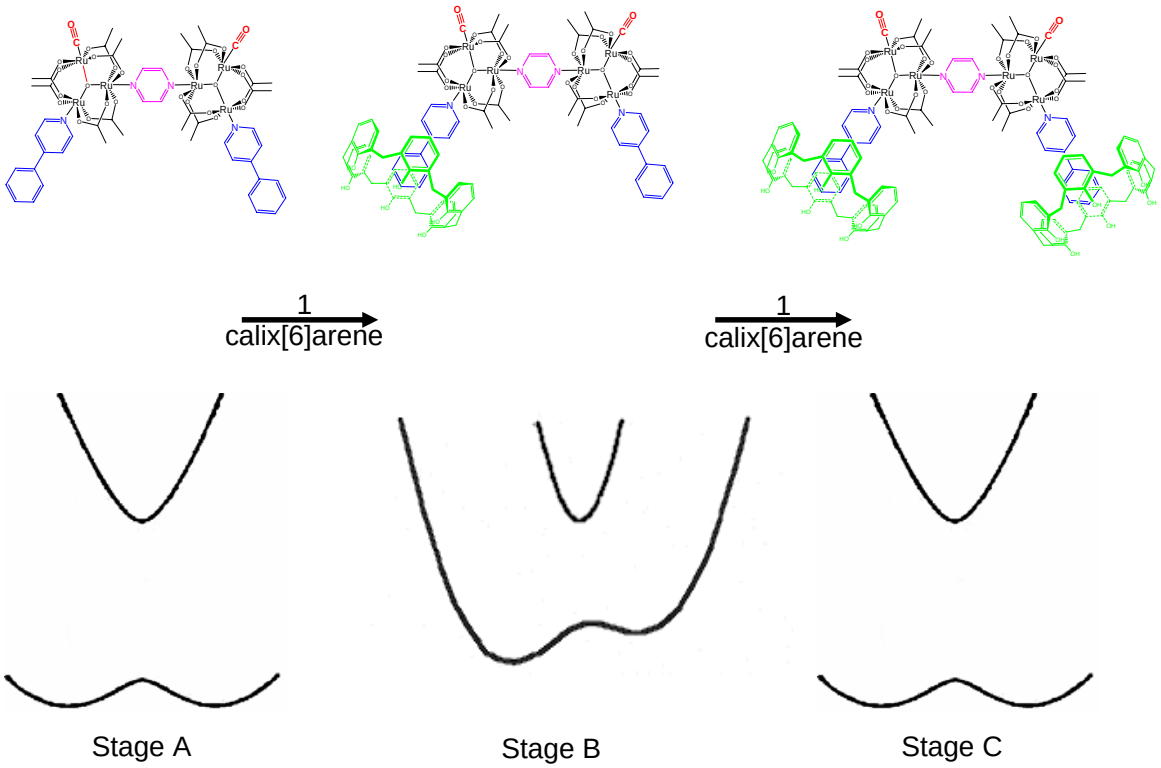

Scheme 6.1: In stage A, the dimer, $[Ru_3O(OAc)_6(CO)(ppy)]_2$-μ-pz, is in its symmetric uncomplexed form. In stage B, a single calix[6]arene has bound to the dimer. This binding is driven by the stabilization of the individual cluster to which it binds. However, the binding also introduces an asymmetry and, as a result, decreases the resonance stabilization of the mixed valence ion. In stage C, a second calix[6]arene has bound to the cluster. This restores the symmetry of the dimer and increases the resonance stabilization. Thus, the binding of the second dimer is driven by both the stabilization of the individual cluster to which it binds and the stabilization of the mixed valence isomer. The additional stabilization of the mixed valence isomer is the "extra" driving force that gives rise to the cooperative binding of calix[6]arene to -$[Ru_3O(OAc)_6(CO)(ppy)]_2$-μ-pz. In this scheme, the reaction coordinate for the potential energy surface is that of all internal nuclear motions as well as solvent modes that must change during the course of the reaction. These coordinates are not quantitatively specified, but are meant as a general indication as to the profess of the reaction (ie. The products and reactant both have individual minima that can be moved between via a high energy intermediate, transition, state.)

the initial interaction were too strong, we would not observe the sigmoidal curve (Figure 6.4) at such high molar ratios of calix[6]arane to **1**.

In summary, the binding of the first calixarene is driven by the stabilization of the cluster to which it binds. This is observed in the electrochemistry as the collective shift of the reduction waves by about +9 mV (*vida supra*). The binding of the second calixarene is driven by this same energy; however, it is also driven by the increase in resonance energy that is realized upon restoration of symmetry to the cluster. It is this additional driving force accompanying the binding of the second calixarene, which leads to the observation of cooperative binding evidenced by the shape of the curve in Figure 6.4.

6.4 Coopertive binding of calix[6]arene to $[Ru_3O(OAc)_6(CO)(ppy)]_2$-μ-pz – effects of changes to electronic delocalization

There is another, equally valid way to consider how the restoration of symmetry provides a driving force for the complexation of calix[6[arene to **1**. In this picture, one must consider the dynamics of the electron motion within the mixed valence complex. As expected, rates of electron transfer shows exponential dependence on the magnitude of the transition state energy. In general the rates of thermally activated processes are described by;

$$k_{et} = Ae^{\frac{-\Delta G^*}{RT}} \tag{6}$$

where ΔG* is the activation energy, R is the gas constant, T is the temperature, and A is a frequency factor that describes how often the systems obtains the transition state (analogous to ν_N from chapter 2).

Thus, for complexes with higher barriers to electron transfer, the rate will be slower. In such cases, one can speak of the electron as being less delocalized than in cases where the electron trasfer is faster (lower barrier to electron transfer). Thus, the rate of electron transfer (the height of the barrier to electron transfer) serves as a qualitative measure of the extent of electronic delocalization. In turn, the

magnitude of electronic delocalization serves as a qualitative measure of the degree of stabilization of the mixed valence isomer (the greater the electronic delocalization, the greater the stabilization). Therefore, one can make the general statement that he higher the barrier to electron transfer, the slower the electron transfer will be, the less delocalized the system will be, and the smaller the electronic stabilization will be. It is clear, then, that we can relate the relative stabilization of a particular complex to that of its barrier to electronic delocalization.

In Marcus-Hush theory, the barrier to electronic delocalization is given in general by,

$$\Delta G^{*}_{asymm} = \frac{\lambda}{4} + \frac{\Delta G°}{2} + \frac{(\Delta G°)^2}{4(\lambda - 2H_{AB})} - H_{AB} + \frac{H^2_{AB}}{(\lambda + \Delta G°)} - \frac{H^4_{AB}\Delta G°}{(\lambda + \Delta G°)^4} \qquad (7)$$

Where λ is the vertical reorganization energy, $\Delta G°$ is the adiabatic (in the absence of coupling) difference in energy between A and B, and H_{AB} is the electronic coupling element that functions to mix the electronic wavefunctions of A and B. In the symmetric limit, when $\Delta G°=0$, equation 7 simplifies to,

$$\Delta G^{*}_{symm} = \frac{\lambda}{4} - H_{AB} + \frac{H^2_{AB}}{\lambda} \qquad (8)$$

The difference in activation energy between the symmetric and asymmetric cases, $\Delta\Delta G^{*}$, is given by;

$$\Delta\Delta G^{*} = \Delta G^{*}_{asymm} - \Delta G^{*}_{symm} = +\frac{\Delta G°}{2} + \frac{(\Delta G°)^2}{4(\lambda - 2H_{AB\,asymm})} + \frac{H^2_{AB\,asymm}}{\lambda + \Delta G°} - \frac{H^4_{AB}\Delta G°}{(\lambda + \Delta G°)^4} - \frac{H^2_{AB\,symm}}{\lambda} \qquad (9)$$

The values of ΔG* for the symmetric analogs of this asymmetric dimer, in which L'=L''-dmap and L'=L''=cpy, are calculated to be 268 cm^{-1} and 123 cm^{-1} (0.77 KJ/mol and 0.35 KJ/mol), respectively. These values were obtained using the assumption that $H_{ABsymm} = H_{ABasymm}$. It is obvious that the activation energy for electron transfer in assymetric complexes can be much larger than that encountered in

symmetric complexes. Since the rate of electron transfer is exponentially dependent on the activation energy (normal Arrhenius behavior), we can expect that electron transfer in symmetric mixed valence species will be faster than in their asymmetric analogues leading to greater resonance stabilization in the symmetric versus the asymmetric dimer. This is the same result that we reached through consideration of the potential energy surfaces associated with the symmetric and asymmetric complexes. Namely, a gain or loss of resonance stabilization – arising from the movement of an electron within a molecule (k_{ET}) – can arise from a gain or loss of symmetry within a mixed valence system. In turn, this change in resonance energy can function as a driving force for supramolecular assembly.

6.5 Conclusions

We have demonstrated the ability to control electronic coupling between metal sites through small non-covalent interactions at ancillary positions on the coupled metal clusters. We have shown how relatively weak interactions at distal positions in a complex can give rise to large electronic effects within the complex, confirming that highly coupled borderline class II-III complexes are extremely sensitive to their environment. There are several implications of this result. First, electronic coupling is a dynamic property of mixed valence systems, not a static one. Thus, it can be changed and manipulated dynamically through tertiary interactions with the mixed valence complex. Second, since electronic coupling is dynamic, it must have a timescale associated with it. That is, changes to H_{AB} are not instantly realized by the mixed valence system, but must be given time to evolve. It seems reasonable that this timescale would be limited by the rate of ET (in class II complexes) or vibrational modes (in class III complexes) or some weighted contribution of both (in class II-III) complexes). It is clear that understanding of fundamental ET processes would benefit from experimental determination of this timescale. Third, there is a strong implication for the related fields of supramoleular chemistry and molecular electronics. Specifically, the resonance stabilization resulting from electronic mixing (H_{AB}) is an energy that one can utilize as a driving force for chemical interactions. The invocation of electronic delocalization as a driving force for reactions is not unknown. Indeed, it is commonly taught in organic chemistry that a reaction which leads to an

aromatic product will have a large driving force associated with it.[76] However, we believe that this is the first time that electronic delocalization has been invoked to explain a chemical interaction in mixed valence chemistry. The end result of this argument is that during the self-assembly of a "communicating" system one *must* consider the dynamics of the environment and the influence that the environment will have on the energetic landscape of the system. (This idea will be discussed more generally for the case of molecular electronics in the next chapter.) Additionally, the translation from a chemical to an electronic signal is a concept that will prove useful in the design and construction of molecular electronic devices.

6.6 Experimental Methods

Synthesis

The synthesis of the dimer, $[Ru_3O(OAc)_6(CO)(ppy)]_2$-μ-pz (**1**), proceeds by the coupling of two trinuclear clusters. First, 1 eq. of $[Ru_3O(OAc)_6(CO)(H_2O)_2]$[77] is stirred with 0.8 eq of ppy in a 1:1 mixture of methylene chloride and methanol for two days to yield $[Ru_3O(OAc)_6(CO)(ppy)(H_2O)]$, which was purified on a silica column using 1% methanol in chloroform. To $[Ru_3O(OAc)_6(CO)(ppy)(H_2O)]$ was added 20 eq. of pyrazine (pz) in methylene chloride and the reaction stirred for 30 minutes. The solvent was then removed to a minimal volume and approximately six-times that volume of hexanes was added. The solution was filtered and $[Ru_3O(OAc)_6(CO)(ppy)(pz)]$ was collected as a precipitate. Equal molar quantities of the clusters $[Ru_3O(OAc)_6(CO)(ppy)(H_2O)]$ and $[Ru_3O(OAc)_6(CO)(ppy)(pz)]$ were then stirred in chloroform for 2 days, yielding the dimer of interest, $[Ru_3O(OAc)_6(CO)(ppy)]_2$-μ-pz (**1**), which was purified on a Bio-Beads SX-3 size exclusion column packed in chloroform. Anal. Calcd for $C_{52}H_{58}N_4O_{28}Ru_6$: C, 34.82; H, 3.26; N, 3.25. Found: C, 34.86; H, 3.53; N, 2.78. ^{1}H NMR (400 MHz, $CDCl_3$): δ 2.00 (s, 12H, acetate), 2.14 (t, 12 H acetate), 2.23 (s, 12 H, acetate), 7.56 (t, 2 H, phenyl), 7.64 (t, 4 H, phenyl), 7.89 (d, 4 H, phenyl), 8.25 (d, 4 H, pyridine), 9.02 (d, 4 H, pyrazine), 9.23 (d-unresolved, 4 H pyridine).

Measurements

Cyclic voltammetry and differential pulse voltametry were performed using a Bio-analytical systems CV-50W potentiostat. Electrochemistry was performed in dichloromethane in the presence of 0.1 M tetrabutylammonium hexaflourophosphate (TBAH). The working electrode was a gold disc (3 mm diameter), the counter electrode was a platinum wire, and the reference electrode was the ferrocene/ferrocenium couple.

Acknowledgements

Much of the material in this chapter comes directly from a manuscript entitled, "Charge Gating and Electronic Delocalization over a Dendrimeric Assembly of Trinuclear Ruthenium Clusters," by Benjamin J. Lear and Clifford P. Kubiak, which has been published in Inorganic Chemistry (2006), 45(18), 7041-7043.

Chapter 7: Electronic delocalization as a driving force for chemical interactions

7.1 Introduction

In the last chapter, we saw how changes in electronic coupling can provide a driving force for a chemical reaction. Such driving forces are of interest to the fields of supramolecular chemistry and nanotechnology. Research in the field of supramolecular chemistry is concerned with the creation of new constructs by the assembly of individual chemical species in which the components are held together reversibly by "soft" intramolecular forces, not covalent bonds. Such species are of interest to the fields of nanotechnology, molecular electronics, biomimetic chemistry, and catalysis. Because supramolecular chemistry is concerned with the assembly of two or more chemical species, the types of intermolecular forces that drive the formation of supramolecular structures are of fundamental interest. Examples of well-known and often utilized forces in the assembly of supramolecular structures are van der Waals forces, π stacking (as in the interaction of calixarenes with aromatic molecules)[71-73], dipole-dipole or dipole-induced dipole interactions (found in charge transfer complexes)[78], hydrogen bonding (used for the specific base pairing in nucleic acids)[79, 80], and ionic bonding. Recently, we reported the results presented in the last chapter[81], where we concluded that the supramolecular structure reported there was driven by a different kind of force: that of electronic delocalization. While it is well known that electronic delocalization provides thermodynamic stabilization to chemical species[3-5, 7, 82], we believe this is the first example where the energy associated with electronic delocalization is used as a driving force for the formation of multiple-component supramolecular constructs. Here we extend our model of resonance-driven supramolecular assembly to the stabilization of molecular nanostructures by current flow.

Building on past work in our laboratory[83], we have recently published a study comparing the conductance of a single organic molecule to the conduction of the same molecule undergoing an electron donor-acceptor interaction with another molecule.[84] These measurements were taken using Tao and co-

workers mechanical break junction[85]. Briefly, a self assembled mono-layer (SAM) of tetramethylphenylenediisocyanide (TMPDI) is formed on a Au(111) surface. An STM tip under bias is then brought to the surface in such a way that the conduction of a single TMPDI can be measured. The conductance of individual TMPDI molecules is taken thousands of times and a histogram is constructed from which the conductance is obtained. Figure 7.1 shows histograms for TMPDI and the TMPDI-TCNE complex. For TMPDI alone, the conductance was found to be 6 x 10^{-4} G_0 (where $G_0 = 2e^2/h$ or about 77μS). This is similar to previous observations for other conjugated organic systems. This was expected as the electronic properties of aromatic systems are expected to be quite similar. However, the addition of tetracyanoethylene (TCNE) to the system described above increased the conduction dramatically. Indeed, the addition of TCNE caused a 50-fold increase in conduction, giving a value of 320 x 10^{-4} G_0 – the largest observed to date for a molecular system.

Such a large increase in conductance can only be the result of a large change in the electronic structure of TMPDI – the molecule through which the current passes. This change in electronic structure is brought about by the interaction of TCNE with TMPDI. TCNE and TMPDI are able to interact with each other to form a charge transfer (CT) complex. In this case, the TMPDI acts as an electron donor, donating a partial electronic charge to the electron acceptor, TCNE, to give the CT complex, $TMPDI^{\delta+}/TCNE^{\delta-}$.[86] The formation of the CT pair appears to significantly alter the density of states near the Fermi level, thus increasing the conductance.

CT interactions are well known in chemistry[86-89]. When the donor and acceptor form a CT pair, there arises a new band in the electronic spectrum not present in the spectrum of either the donor or acceptor. This new band is termed the charge transfer band[90, 91] and corresponds to the excitation of an electron from the donor to the acceptor. With such a distinct marker for the formation of a charge transfer band, it is possible to determine the equilibrium constant for the formation of CT complexes. For strong CT interactions, such as hexamethylbenzene and TCNE, the equilibrium constant is ca. 21 M^{-1}. For a weak pair such as benzene and TCNE, the equilibrium constant is 0.12 M^{-1}.[89] For the present pair, TMPDI and TCNE, the equilibrium constant was too small to be determined by UV-visible spectroscopy. Despite the fact that the equilibrium constant appears to be quite small, the addition of TCNE has a clear and

unambiguous impact on the conduction of TMPDI. The conductance histograms for TMPDI in the presence of TCNE clean (Figure 7.1), suggesting that the CT complex persists even though its expected stability is comparable to k_BT. The question then arises, why do we see such clean statistics for an interaction that is quite weak? Here, we attempt to answer this by considering the effects of passing current through the system.

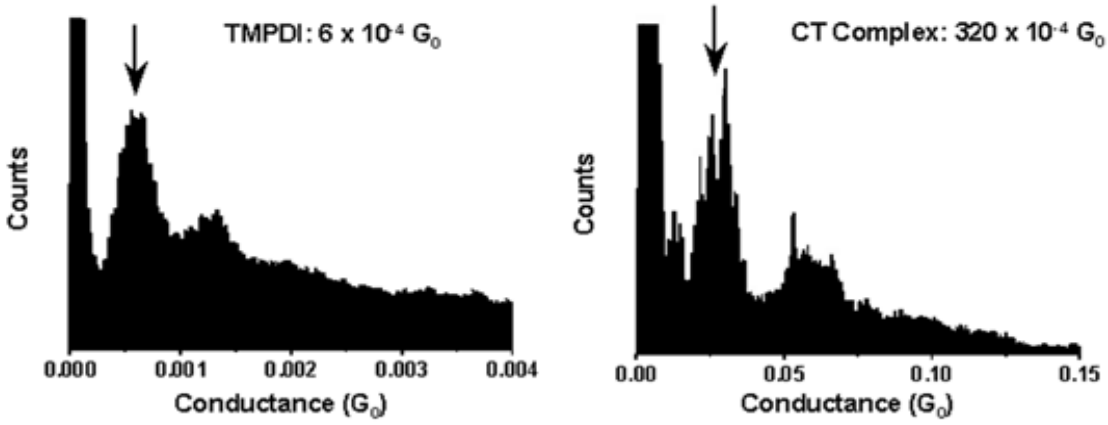

Figure 7.1: Conductance histograms of (a) TMPDI and (b) the TMPDI/TCNE CT complex. The conductance of the TPMDI in the CT complex is 50 times that of the TMPDI alone.

7.2 Change in conductance as a driving force for chemical interactions

Figure 7.2 is a schematic of the conductance experiment described above. It is drawn at the point at which conduction occurs through a single TMPDI molecule. The rectangle represents the electrode surface that contains the SAM of TMPDI and the triangle represents the STM tip. The TMPDI molecule is drawn bridging the two electrodes. In the language of intramolecular electron transfer[7, 56, 82], we may consider the negative terminal of the power source to be the donor, the positive terminal of the power source to be the acceptor and the two wires bridged by the TMPDI are the bridge. For the rest of the chapter, we will refer to the bridge as just the TMPDI, as this is the only segment of the bridge that is likely to change its properties upon exposure to TCNE. The wires are expected to maintain the same properties of metallic conduction for all conditions of the experiment. Under a potential bias, the current passing

through the TMPDI flows from the acceptor to the donor. This, of course, means that electrons are flowing from the donor to the acceptor through the TMPDI. In addition, as the experiment is run under constant bias, current also flows through the power source from the donor to the acceptor (again, this means that electrons traveling from the acceptor to the donor). Current is typically expressed in units of coulombs per second, however, it is equally valid to write current as electrons per second. As we have seen, the current flowing across TMPDI from acceptor to donor (electrons flowing from donor to acceptor) can be thought of as k_{ET}, or forward electron transfer rate. Current flowing from donor to acceptor within the power source (electrons flowing from acceptor to donor) can then be considered as the "back electron transfer rate", or k_{BET}. With this description of the experiment in mind we can develop an explanation for the origin of the strong binding of TCNE to TMPDI from the perspective of intramolecular electron transfer.

Figure 7.3 is a square scheme which examines the binding of TCNE to TMPDI and the conduction through TMPDI. Moving across the top and then the right side of the square scheme, we see that TCNE can bind to TMPDI, after which current is passed through the system (the CT complex is present at the start of the experiment). Alternatively, by moving along the left side and then the bottom of the scheme, current can be flowing before TCNE binds to TMPDI (the CT complex is not present at the start of the experiment). In both cases we can assume that the flow of current is associated with some change in energy, ΔG. The change in energy associated with the flow of current on the right side of the scheme is labeled ΔG_D, while the change in energy associated with the flow of current on the left side of the scheme is labeled ΔG_C. Likewise, the binding events also have a change in energy associated with them and for the top and bottom of the scheme these changes are ΔG_A and ΔG_B, respectively. Because ΔG is a state function, any path from the top left to the bottom right of the scheme in Figure 7.3 must involve the same change in energy and, thus, we arrive at the equation;

$$\Delta G_A + \Delta G_D = \Delta G_B + \Delta G_C \tag{1}$$

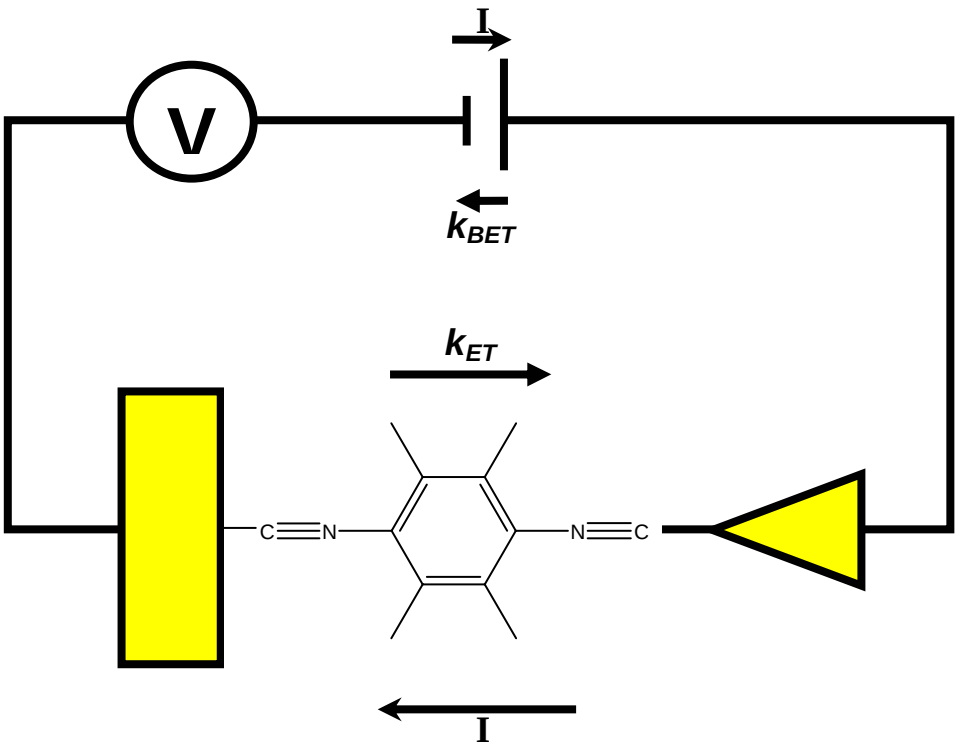

Figure 7.2: A schematic diagram of the break-junction conductance experiment. A TMPDI molecule is attached to a gold surface (rectangle). A STM tip (triangle) is then repeatedly brought into contact with the surface and pulled away. Current is passed through the system and monitored throughout this process.

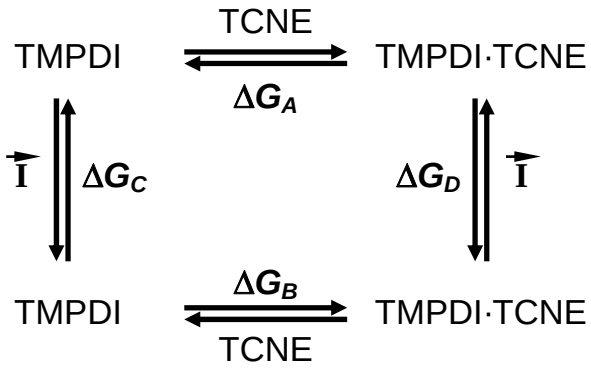

Figure 7.3: Square scheme depicting the various sequences possible for the formation of the CT complex and the passing of current. The CT complex can form when no current is flowing (corresponding with a change in energy of ΔG_A) after which current is passed through the system (corresponding to a change in energy of ΔG_D). Likewise, current can be passed through the system when there is no CT complex present (corresponding to a change in energy of ΔG_C) after which the CT complex forms (corresponding to a change in energy of ΔG_B). Because ΔG is a state function, the total change in energy from top left to bottom right is the same no matter which path is taken. Thus, $\Delta G_A + \Delta G_D = \Delta G_B + \Delta G_C$.

The change in energy associated with a chemical equilibrium is given by $\Delta G = -RT\ln(K_{EQ})$, making this substitution into equation 1 and rearranging yields;

$$RT\ln\left(K_{EQ_A}\right) - RT\ln\left(K_{EQ_B}\right) = RT\ln\left(K_{EQ_C}\right) - RT\ln\left(K_{EQ_D}\right) \tag{2}$$

Here we have assumed that we can treat the passage of current as an equilibrium condition. If we assume that the system is held at constant potential throughout the experiment, this assumption is valid. This means that there is steady-state current flowing across the molecule from the acceptor to the donor and through the power source from the donor back to the acceptor. Again, there is forward (donor to acceptor) and back (acceptor to donor) electron transfer. The principle of detailed balance[92, 93] states that the equilibrium constant for the electron transfer can be written as the ratio of the two associated rate constants. Specifically $K_{EQ} = k_{ET}/k_{BET}$. Substitution of this relationship into equation 2 gives us;

$$RT\ln\left(K_{EQ_A}\right) - RT\ln\left(K_{EQ_A}\right) = RT\ln\left(\frac{k_{ET_C}}{k_{BET_C}}\right) - RT\ln\left(\frac{k_{ET_D}}{k_{BET_D}}\right) \tag{3}$$

Rearrangement followed by cancellation of RT gives;

$$\ln\left(\frac{K_{EQ_A}}{K_{EQ_B}}\right) = \ln\left(\frac{k_{ET_C}k_{BET_D}}{k_{ET_D}k_{BET_C}}\right) \tag{4}$$

It is important to note that k_{ET} and k_{BET} being discussed here are the *intrinsic* rate constants and not the *observed* rates of electron transfer.

While is certainly likely that there is some back electron transfer through the TMPDI, the degree to which this occurs should be negligible with respect to the same process occurring within the power source in the experimental set up. Thus, all back electron transfer can be assumed to proceed via the power

source contained between the two terminals. Likewise, the forward electron transfer can be assumed to proceed, to a good approximation, solely through the TMPDI. Because of this, k_{ET} and k_{BET} can be treated separately – especially with regard to changes in their value upon the formation of the CT complex. Since the back electron transfer (k_{BET}) proceeds through the power source both when TCNE is bound and unbound to TMPDI and because TCNE is not expected to interact with the power source to any appreciable extent (in the experiment under discussion, the power source was not exposed to TCNE), the rate constant of the reverse electron transfer is expected to be unchanged by the introduction of TCNE to the system. Therefore, $k_{BETC} = k_{BETD}$ and equation 4 becomes,

$$\ln\left(\frac{K_{EQ_A}}{K_{EQ_B}}\right) = \ln\left(\frac{k_{ET_C}}{k_{ET_D}}\right) \tag{5}$$

Because the back electron transfer is not affected by the binding of TCNE, any change in current must be a result of a change in the value of k_{ET}. In other words, measurement of a change in current is the same as a measurement of a change in the value of k_{ET}.

From equation 5 we see that the binding constants of TCNE to TMPDI and the current passage through TMPDI are related. The square scheme can then be read in the following ways; when TCNE binds to TMPDI current flows more readily or when current flows, TCNE binds to TMPDI more strongly. Thus, it is seen that an increase in current in the TCNE/TMPDI system drives the formation of the CT complex. In other words, the passage of current can be used to create a driving force for supramolecular assembly. This driving force can be explicitly and quantitatively determined. By re-substituting the relationship $\Delta G = -RT\ln(K_{EQ})$ we arrive at;

$$\Delta G_A - \Delta G_B = RT\ln\left(\frac{k_{ET_C}}{k_{ET_D}}\right) \tag{6}$$

The quantity ΔG_A-ΔG_B then represents the *additional* change in energy brought about by CT complex

formation during the passage of current. For the TCNE/TMPDI system, which experienced a 50-fold increase in conduction upon formation of the CT complex, $\Delta G_A - \Delta G_B = 9.4$ KJ mol^{-1}. This value is the driving force for complex formation due to the passage of current. Clearly, current can provide a substantial amount of driving force to a chemical system.

The above discussion assumed both that the system was in equilibrium throughout the experiment (the applied voltage did not change) and that the back electron transfer rate (within the power source) does not change upon TCNE binding to TMPDI. A bit of thought will show that these two conditions are mutually exclusive. With an increase in current, a system must experience a voltage drop unless the rate of electron transfer within the power source increases. Thus, both of these conditions cannot be satisfied simultaneously and the system must either not be in equilibrium (the applied voltage changes upon CT complex formation) or the back electron transfer through the power supply must change. In the case that the back electron transfer remains unchanged following the CT complex formation (the applied voltage changes) then the basic assumptions above are still valid. The system is still in equilibrium before and after the binding (the voltage is constant at the two limits of CT complex formation) but during the formation, the complex is not in equilibrium. However, we are just considering the system with and without CT complex and, as a result, we can consider these two limits – limits in which the system will be in equilibrium. Thus, the use of equilibrium constants in equation 2 remains valid. In the case that the back electron transfer rate changes (the voltage remains constant throughout the entire experiment) then the one cannot use the simplifying assumption that measurement of the current through the molecule can be used to directly calculate the driving force that the increase in current provides (equations 5 and 6). In this case, equation 6 gives an upper limit for the driving force for increasing in current (a lower limit for driving forces stemming from a decrease in current). If more accurate values for the driving force associated with changes in conductance are desired, then measurements of the electron transfer rate through the power supply would be required.

Despite these two major concerns (only one of which was shown to pose any real problems) it is clear that the effect remains real – changes in current within a system undergoing a chemical interaction can provide a driving force for the interaction. Though the above theory has been developed for the specific

case of TCNE/TMPDI, equation 6 (and its implications) should be generally applicable to chemical interactions in systems experiencing conduction through one of the species involved in the interaction. We are very excited about the implications this has for the fields of molecular electronics and supramolecular chemistry.

7.3 Conclusions

We have shown that a chemical interaction that results in a change in current in an electrical system will have a driving force associated with it that is proportional to the degree (and sign) of the change in current. The relationship between change in current and driving force has been developed using simple thermodynamic and kinetic relationships. In particular, we have discussed current as the rate of electron transfer between the terminals of a molecular electronic construct. This approach to current raises an interesting corollary. Because current can be treated as multiple electron transfer events, we may conclude that an increase current across a wire means an increase in the electron transfer rate. Faster electron transfer rates, in turn, are indicative of a more electronically delocalized system. Thus, we are left with the conclusion that it is *electronic delocalization* that provides the driving force for chemical interaction in molecular electronics and that the conclusions drawn here can be applied to other systems that are able to experience changes in their degree of electronic delocalization.

The identification of electronic delocalization as a driving force for supramolecular chemistry is new to the field. We believe that the ideas presented here are generally applicable to the assembly of chemical devices. In particular, these results are relevant to the field of molecular electronics, where the theory presented here provides the groundwork for a new paradigm in the design of molecular electronics. Molecular electronics are built in order to pass current, thus, current is readily available to be used as a driving force for assembly of molecular electronic devices. The direction is clear. When constructing supramolecular devices for molecular electronics the passage of current during their assembly can greatly increase the percentage yield and the strength of interaction of the devices allowing for the use of interactions previously thought too weak to give robust formations. Conversely, the passage of current can be used to disrupt molecular interactions that increase the resistivity of a system, creating reversible

systems using interactions that were previously thought too strong to be reversible. Furthermore, as the devices will only experience additional forces that affect assembly where current is being passed, the driving force will allow for directed assembly at those areas in which current in being passed. Similar results have been reported previously for electrochemically created polymers[94, 95], however, the work presented here is more general as it involves a bi-molecular system with tunable properties such as size, conduction, and selectivity of interaction and is widly applicable to many other systems. Lastly, it is possible that dynamic interactions that are sensitive to the degree of current being passed through the system could be used for the construction of molecular logic devices.

Chapter 8: Charge transfer and charge re-organization in a dendritic assembly of trinuclear ruthenium clusters

8.1 Introduction

All of the work discussed so far in this thesis (with the exception of Chapter 7) has dealt with dimers of trinuclear ruthenium clusters of the type $[Ru_3O(OAc)_6(CO)(L)]_2$-μ_2-BL (BL = bridging ligand) which, in the mixed valence state, provide a sensitive probe of ground state electron transfer (ET) in the class II-III regime [26]. The ability to effect small electronic changes within the cluster assemblies by varying the bridging and ancillary ligands has allowed an in depth study into the effects of small electronic perturbations upon the ET rate (k_{et}), the electronic structure, and electronic coupling in these complexes.[50, 96] Using these dimers, we have reported the first observations of "mixed valence isomers,"[44, 97] which provided the ability to experimentally evaluate the Marcus-Hush potential energy surfaces associated with ET.[49] They have also allowed for determination of ΔH and ΔS, study into the dynamic environmental effects, and the use of the energy associated with electronic delocalization as a chemical driving force for supramolecular assemblies incorporating these highly coupled mixed valence systems.

Given the ability of these "dimers of trimers" to probe ET, we now extend our work to study electron transfer across greater distances and between multiple sites. Effects of electron transfer between multiple sites have been considered[98] and many compounds proposed in order to probe these effects, but few have been reported and none, to my knowledge, have the ability to probe k_{et} for such constructions. To this end, We have synthesized the 0^{th} generation ligand-centered dendrimer (LCD), $[Ru_3O(OAc)_6(CO)(L)]_3$-μ_3-2,4,6-tri-(4-pyridyl)-s-triazine[4] (Figure 1) and here is presented its synthesis, electronic characterization and a discussion of its electronic behavior.

8.2 Synthesis

This 0^{th} order dendrimer was prepared by mixing three equivalents of $Ru_3O(OAc)_6(CO)(py)(H_2O)$[99] with one equivalent of 2,4,6-tri-(4-pyridyl)-s-triazine (tz)[100] for three days in chloroform, followed by purification on a Biobeads S-X1 (Bio-Rad) size exclusion column. The compound was obtained as a blue-purple powder upon recrystallization from CH_2CL_2 with hexane. [Ru3O(OAc)6(CO)(L)]3-m3-2,4,6-tri-(4-pyridyl)-s-triazine·**$CHCl_3$**. Yield 34%. Anal. Calcd for $C_{74}H_{86}Cl_3N_9O_{42}Ru_9$: C, 31.86; H, 3.11; N, 4.52. Found: C, 32.06; H, 2.98; N, 4.52. ^{1}H NMR (400MHz, $CDCl_3$): δ 1.91 (s, 18H, Acetate), 2.10 (s, 18H, Acetate), 2.16 (s, 18H, Acetate), 8.04 (t, 6H, pyridine), 8.14 (t, 3H, pyridine), 8.93 (d, 6H, triazine), 9.05 (d, 6H pyridine), 9.24 (d, 6H, triazine). IR (KBr disk): 3399 cm^{-1} (s), 2968 cm^{-1} (w), 2931 cm^{-1} (w), 1946 cm^{-1} (s), 1608 cm^{-1} (s), 1572 cm^{-1} (m), 1578 cm^{-1} (m), 1421 cm^{-1} (s), 1373 cm^{-1} (w) 1349 cm^{-1} (w), 689 cm^{-1} (w).

8.3 Electrochemistry

The electrochemistry of LCD was investigated using cyclic voltammetry (CV) and differential pulse voltammetry (DPV).[101] In the anodic region, the CV of LCD contains two separate, reversible three electron reduction waves (0.95 V and 0.17 V), corresponding to the oxidation of the three metal clusters ($Ru^{III}Ru^{III}Ru^{III}/Ru^{III}Ru^{III}Ru^{IV}$ and $Ru^{III}Ru^{III}Ru^{II}/Ru^{III}Ru^{III}Ru^{III}$ respectively). However, in the cathodic region, the reduction of the three metal clusters is not a concerted process. Instead, the reductions are split into two distinct reversible redox processes. Similar behavior has been observed in the CV of the dimers of trimers[1]. Based on a comparison of integrated current obtained from DPV, the waves at -1.24 V and -1.36 V are assigned to a one and two-electron reduction, respectively, and correspond to the reduction of one of the clusters followed by a concerted reduction of the other two clusters. This degree of splitting corresponds to a $\boldsymbol{K_c}$ = 1.56 x 10^4. The last electrochemical event that we observe in the CV (-1.79 V) is the reduction of the bridging tz ligand. The fact that the reduction potential is quite close to that of the cluster's means that the tz ligand can be considered a "non-inocent" ligand (ie. The ligand can participate in the

redox chemistry of the complex). This is a fact that will play a crucial role in the discussion of the electronic properties and behavior of complex **1**.

Once the eletrochemsitry of the complex was understood, the next step was to characterize its spectroelectrochemical (SEC) response. The large value of K_c, while not a conclusive indication of **1** belonging to class II-III, promises values of H_{AB} large enough to observe dynamic effects in the IR spectra of **1**.

8.4 Infrared Spectroelectrochemistry

The IR SEC response of LCD in the region of the carbonyl stretching frequency at low temperature (-30 C) is shown in Figure 1a[102]. As the potential is brought suffecietly negative to reduce LCD (-0.95 V vs. Ag wire)[54], we observe a decrease in intensity of the ν(CO) at 1940 cm^{-1} until it is no longer present in the spectrum. At the same time we observe the growth of a new band at 1895 cm^{-1}. Based on previous work [35], we assign the band at 1940 cm^{-1} to ν(CO) of a neutral cluster and the lower energy band to the ν(CO) of a reduced cluster. Taking into consideration these assignments, the progression of spectra shown in Figure 1a corresponds to the reduction of the three outer clusters of LCD. The smooth progression from neutral to fully reduced (-3 overall charge) proceeded without a stable, mixed valent, intermediate. Such a species would exhibit some degree of fractional reduction (-1 or -2 overall charge) observable as ν(CO) intensities present at both the reduced and neutral frequencies simultaneously. This is at odds with the observed electrochemical measurements, which seemed to indicate that the singly reduced (-1) species would be a stable mixed valence ion. However, the electrochemistry was performed at room temperature, while the above SEC was obtained at -30° C. We considered that there was some unanticipated temperature dependence of the SEC response of the LCD. In order to probe this, SEC of the LCD was taken at room temperature.

At room temperature the response of LCD to reducing potentials is indeed more complex. Initially, at -1.05 V (vs. Ag wire) a reduction in intensity of the high energy ν(CO) band is observed accompanied by the appearance of the low energy ν(CO) band, a progression associated with the reduction of the outer metal clusters (Figure 1b). However, this evolution of the spectrum ceases at the point when the ratio of

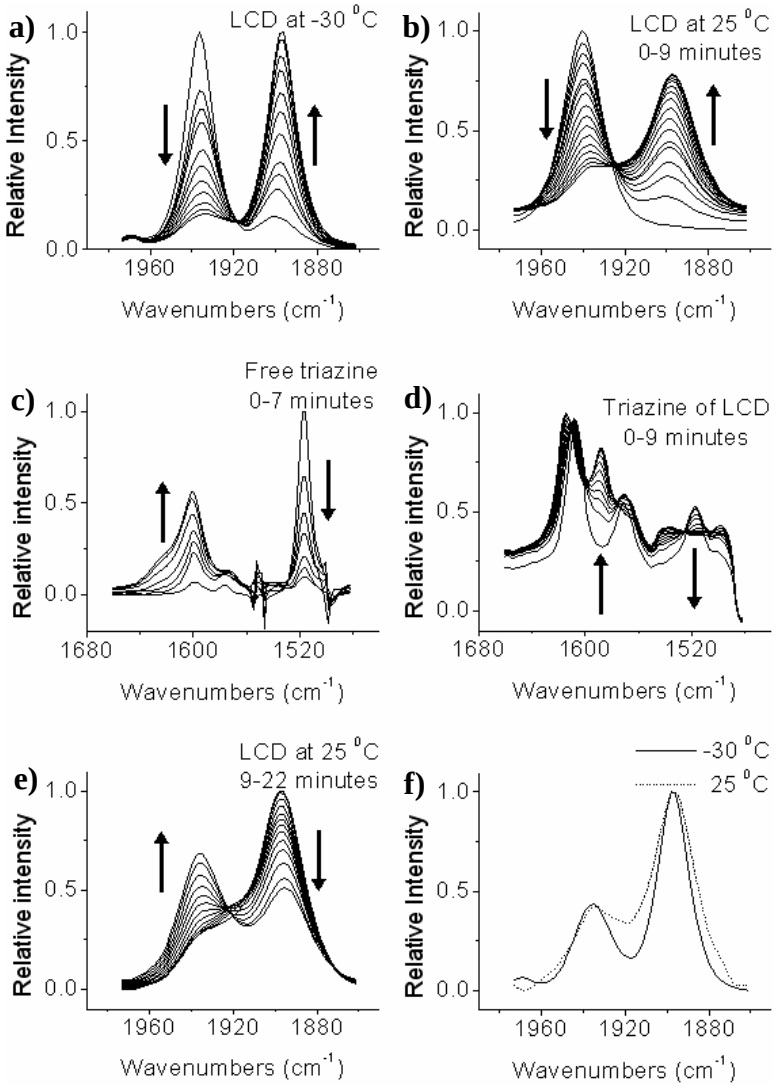

Figure 8.1. Spectroelectrochemical response of (a) LCD at -30 C and -0.95 V, (b) LCD at room temperature and -1.05 V, (c) 2,4,6-tri-(4-pyridyl)-s-triazine at room temperature and -1.20 V, (d) LCD at room temperature and -1.05 V, (e) LCD at room temperature and -1.05 V, and (f) a comparison of spectra at the LCD at both -30 C and room and temperature. All potentials are versus a Ag wire.

intensities of the high energy and low energy bands is 1:2. This indicates that reduction of LCD has stopped at the point at which only two of the outer clusters are reduced. This is an unexpected behavior since the CV of LCD reveals that reduction of the second and third clusters in LCD occurs concurrently. Thus, at a potential sufficient to reduce two of the clusters, all three clusters should be reduced. In effect, we observed a two electron process spectroscopically when a three electron process is predicted electrochemically.

This result may be explained by considering the SEC response of "free" tz to reduction. For the purposes of our study, we are only concerned with the band at 1515 cm^{-1}, as this is the only band arising from tz that is both intense enough in LCD to be useful and does not overlap with bands associated with the ruthenium clusters. Upon reduction this band is found to disappear (Figure 1c) as a new band grows in at 1600 cm^{-1}. Using these spectroscopic signatures, we find that in LCD at room temperature, reduction of the central triazine occurs concomitant with the reduction of the outer clusters (Figure 1d). Thus, at room temperature, the initial reduction of LCD *is* a three-electron process. However, the process does not yield a species having three reduced clusters. Rather, the end point of reduction, as observed spectroscopically, is a species that contains two reduced clusters and a reduced triazine.

Maintaining an applied potential of -1.20 V, the next event observed in the SEC response of LCD at room temperature is also unexpected (Figure 1e). Here, the lower energy band is seen to decrease in intensity while the intensity of the high energy band increases. This is a progression of spectra associated with oxidation of the ruthenium clusters. Given that the potential applied has not changed from that used to effect the initial reduction of LCD (Figure 1b), what is occurring is an *oxidation* event at a *reducing* potential.

At the point at which this reversal in electrochemical response is observed, a difference arises between the room and low temperature spectra (Figure 1f). Here, the low temperature spectra was taken at a point during the electrochemical response of LCD such that the intensity ratio of the 1940 cm^{-1} band to the 1895 cm^{-1} band was the same as that seen in the final spectra in Figure 1b (the initial room temperature spectroelectrochemical response of LCD). The most striking difference between these spectra is the "extra" intensity present in the room temperature spectrum between the high and low energy ν(CO) bands.

This extra intensity is an expected result of dynamic exchange on the IR timescale and was predicted by Turner and coworkers when they adapted the Bloch equation used in dynamic NMR for use in dynamic IR.[37]

Just as in dynamic NMR, the bandshapes in dynamic IR hold information as to the rate of the dynamic process occurring.[36] In this case the dynamic process is ET between the outer clusters of LCD and simulation of the spectra provides an estimation of the rate of electron exchange (Figure 2).[103] The low temperature spectra is adequately reproduced in the limit of stopped exchange – that is assuming a k_{et} of less than 10^{11}. The best fit of the simulated spectra to the room temperature spectra is achieved assuming $k_{et} = 1.1 \times 10^{12}$. The only chemical difference between LCD at low temperature and room temperature is that the species at room temperature contains a reduced tz, while the tz at low temperature retains intensity in the band at 1515 cm^{-1}, indication that it remains unreduced. Thus, it appears the reduction of the tz functions as an electronic "switch," turning on ET across the molecule.

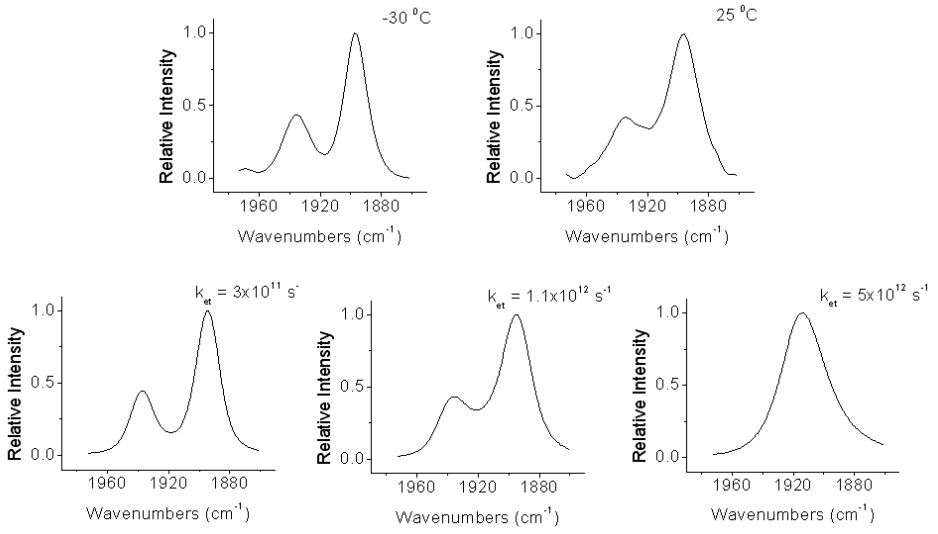

Figure 8.2. (a) ν(CO) band of LCD at -30 C. (b) ν(CO) band of LCD at room temperature. (c-e) Simulated ν(CO) band assuming an electron transfer rate of 3×10^{11} s^{-1}, 1.1×10^{11} s^{-1}, and 5×10^{11} s^{-1}, respectively.

8.5 Discussion

The reversal in electrochemical behavior of LCD can be understood by considering that the reduction potential of the ruthenium clusters is found to decrease with increasing electron donation strength of the attached ligands[46]. Since the radical anion tz is expected to be a much stronger electron donor than the neutral tz, reduction of tz pushes the reduction potential of the clusters to lower potential. This has the effect of trapping the electron on the tz, since upon the lowering of the reduction potential of the clusters the tz anion is no longer a strong enough reducing agent to reduce the attached clusters. Additionally, the applied potential is now no longer negative enough to reduce the third and final ruthenium cluster. Recalling that the second and third clusters undergo concerted reduction (as observed in the CV), it follows that if the potential is not negative enough to reduce the third cluster it is no longer sufficient to maintain the reduction of the second cluster. Accordingly, one of the clusters, which had just been reduced, is now oxidized as is observed in the room temperature SEC response (Figure 1e).

There is a further reason why the electron, once on the tz, may become trapped. The last two chapters have shown how electronic delocalization can provide a driving force for chemical interactions. In mixed valence systems this interaction is most easily quantified by considering the stabilizing effect that, through the action of H_{AB}, electronic coupling has upon the ground state molecular wavefunction. It was found that in cases where a chemical interaction is found to increase the electronic coupling, this interaction is driven in part by the increase in electronic delocalization the interaction affords. For the same complex, increases in electronic coupling must necessarily be accompanied by decrease in the barrier to electron transfer ΔG^*. This in turn means that the observed electron transfer rate should increase as a result of increased electronic coupling. Thus, the increase in electron transfer rate observed concomitant with the reduction of the tz indicates that the reduction of tz has the effect on increasing the electronic coupling in the LCD. This increase in coupling could account, in part, for the stability of this reduced tz.

The above discussion of the SEC response of the LCD at room temperature relies heavily upon the effects a tz radical would have upon the electronic of the LCD. Thus, it is critical to evaluate the probable likelihood and dynamics of reducing the tz bridge. The probability of obtaining a reduced tz can be evaluated assuming a Boltzmann distribution, where the percentage of the system with an electron on the tz

is given by exp(-ΔG/RT) where ΔG is the energy required to promote an electron from the reduced cluster to the tz in the triple reduced LCD. The value of ΔG can be obtained from the electrochemical data and is equal to 430 mV (3468 cm^{-1}), which gives a relative population of reduced tz of 3.9 x 10^{-10}. While this population is small, as we have seen, once the electron occupies the tz there is sufficient thermodynamic reasons why it would become trapped on the tz. Thus, the question of the possibility of a reduced tz becomes one of kinetics. That is, it remains to be shown that a significant number of reduced clusters could transfer an electron to the tz within the experimental timescale (*ca.* 10 min). Since the transfer of an electron from the cluster to the tz is an intramolecular electron transfer we can use the expression for the rate constant introduced in chapter 1, equation 3. Namely, $k_{et} = \kappa \nu_N \exp[-(\Delta G_\lambda^*)/RT]$. The typical value assmed for ν_N is 5 x 10^{12} s^{-1} and, since there is expected to be significant coupling between the cluster and the tz, κ can be set to 1. The fastest rate of ET to the cluster is in the absence of an activation barrier. In this case the activation energy (ΔG*) equals the free energy change for the reaction (ΔG). Remembering that the ΔG for this reaction is 3468 cm^{-1}, we arrive at a k_{et} = 2.0 x 10^3 s^{-1} in the absence of an activation barrier. In most physical systems there exists a non-zero activation barrier and this would act to slow down the reaction. However, there must exist some coupling between the cluster and the tz, since the mixed valence ion exhibits picosecond ET. This coupling would act to decrease any intrinsic barrier that would be present in the uncoupled system. Thus, the assumption that ΔG* is zero is not fully unreasonable and it gives us a reasonable framework from which to proceed. The rate constant calculated above can be assumed to be first order and because of this the half-life associated with this rate can be calculated to be 3.5 x 10^{-4} s. With this half-life within the timescale of the measurement (10 min) essentially one hundred percent of the population would be expected to contain a reduced tz. This again assumes that the reduced triazine becomes trapped such that the electron transfer from the cluster to the bridge is irreversible. We feel that there is compelling evidence that this could be the case. Thus, if the above assumptions are valid, it is likely that one could obtain a reduced tz, dynamically speaking, in the triply reduced LCD.

Given that the reduced tz is both thermodynamically and dynamically feasible, Scheme 1 is forwarded as a mechanism which accounts for the SEC response of LCD upon reduction at room temperature. The first two steps of Scheme 1 bring together the data obtained from CV and SEC. First, all three clusters of

LCD are reduced (step **1**), as indicated by CV, but this is followed by a rapid intramolecular ET (step **2**), in which one of the outer clusters donates an electron to the tz, giving rise to LCD species observed spectroscopically in Figures 1b and 1d. The reduced tz pushes the reduction potential of the clusters more negative (resulting in an increase in the resonance stabilization of the complex) giving rise to their oxidation at the applied potential (step **3**). This is the effect observed in Figure 1e.

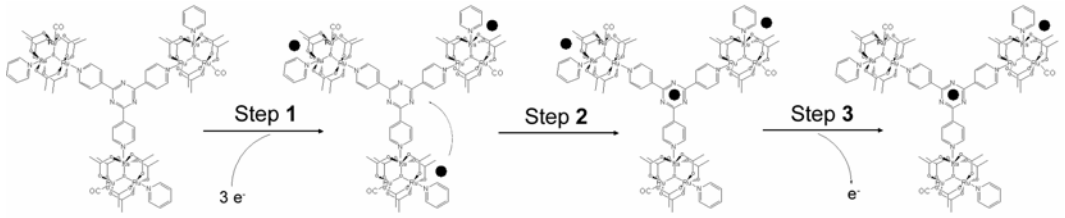

Scheme 8.1. The LCD initially undergoes a three-electron reduction (step 1). An intramolecular electronic reorganization follows in which one of the reduced clusters donates an electron to the triazine ligand (step 2). Upon its reduction, the triazine pushes the reduction potential of the clusters more negative, resulting in the subsequent oxidation of one of the clusters (step 3).

8.6 Conclusions

The 0th generation dendrimer presented here is well behaved upon reduction at low temperatures, giving easy-to-interpret spectra albeit the response is in contradiction to the observed room temperature electrochemical behavior. However, at room temperature, this dendrimer exhibits some unusual electrochemical behavior. This unexpected behavior includes; intramolecular electronic reorganization, reversal of the electrochemical behavior of LCD to an applied potential, and an electrochemically controlled switching event. There have been many other reports of gated ET, in which molecular dynamics[104-108], pH[109, 110], magnetism[111], ion size[112], and light[113] function as the gate. While gating of ET is by no means novel, we believe this is the first case in which ET appears to be gated by an electronic event within the molecule. All of the complex behaviors exhibited by **1** can be understood through knowledge of these clusters electrochemical properties and simple applications of Boltzman's law and the Marcus-Hush

model for intramolecular ET. In the end, the complex electrochemical behavior can be seen as arising from just a few well understood and simple phenomena. The ability for all these phenomena to interact owes to the use of non-innocent ligands in a complex that is sensitive to its ligand field and can experience a large degree of electronic coupling. Thus, it is once again shown that the large value of H_{AB} is able to allow for unusual behavior in mixed valence complexes on the class II/class III border line.

Acknowledgements

Much of the material in this chapter comes directly from a manuscript entitled "Origins of cooperative noncovalent host-guest chemistry in mixed valence complexes," by Benjmain J. Lear and Clifford P. Kubiak, which has been published in Journal of Physical Chemistry B (2007), 111(24), 6766-6771.

Chapter 9: Intermolecular electron transfer to and from highly coupled mixed valence complexes.

9.1 Introduction

The common theme that has emerged in this thesis is the secondary effects that are a result of a highly coupled mixed valence system. In chapters 2 and 3 it was shown that strong delocalization can have the effect of decreasing the diabatic free energy for electron transfer in asymmetric systems. In chapters 4 and 5 the consequences of near delocalization (near zero activation energy) were explored with respect to thermodynamic versus kinetic control of the electron transfer rate. In chapter 6 and 7 it was discovered that delocalization provides driving force for chemical interactions. In chapter 8, it was demonstrated that the energy associated with delocalization can provide sufficient driving force to stabilize as the ground state what would normally be thought of as an excited state of a mixed valence complex. In all of these examples, the delocalization of the electron leads to interesting and complex behavior of the complex undergoing delocalization. However, we have neglected the most basic effect of delocalization – the stabilization of the orbitals in which the electron resides. That is, the electron in the adiabatic ground state wavefunction of a mixed valence compound is lower in energy than the electron would be in either of the corresponding diabatic wavefunctions. Interestingly, the amount that the minima of the ground state wavefunction is stabilized is exactly equal to H_{AB} for symmetric compounds. This can easily be shown by considering the equation for the energy of the ground state adiabatic wavefunction (G_A) for mixed valence complexes (equation 1).[4, 7]

$$G_{Adiabatic} = \frac{1}{2}\left\{(G_a - G_b) - \left[(G_a - G_b)^2 - 4H_{AB}^2\right]^{1/2}\right\} \quad (1)$$

Where G_a and G_b are the energies associated with the reactant and product diabatic wavefunctions. For symmetric complexes there is no driving force, $G_a = G_b$, and equation 1 reduces to equation 2.

$$G_{Adiabatic} = G_a - H_{AB} \quad (2)$$

Remembering that G_a is the energy of the diabatic wavefunction then the difference between the diabatic and adiabatic wavefunctions (the stabilization of the ground state adiabatic wavefunction) is given by equation 3.

$$\Delta G = G_{diabatic} - G_{Adiabatic} = H_{AB} \quad (3)$$

Thus, for compounds where H_{AB} is large, the stabilization of the electron in the mixed valence state should be significant.

The evidence for this stabilization can easily be seen in the cyclic voltammograms of mixed valence species. For such species, the reduction (or oxidation) of the two redox centers is separated by a potential that is roughly equal to $2H_{AB}$ (the first electron goes into the adiabatic ground state wavefunction and the second electron into the adiabatic excited state wavefuntion). There are many factors that contribute to the potential separation of these redox waves and the value of the separation cannot be used to quantitatively determine the value of H_{AB}. Despite these limitations, the contribution to this electrochemical splitting is largely due to H_{AB} for highly coupled complexes and the degree of separation between these redox processes give one a qualitative measurement of the extent of stabilization afforded the electron in the ground state wavefunction. For complexes **1**-**3** (Figure 9.1), the extent of electronic coupling has been shown to be quite large[35, 44] and the splitting observed in the CV for the reduction of these complexes is correspondingly substantial.

One question that arises when the adiabatic potential energy surfaces are considered is this; does the electron enter into the adiabatic wavefunction or does it enter into the diabatic wavefunctions after which the system evolves to the adiabatic wavefunctions? At first glance the splitting observed in the CV appears to answer this question, surely the electron enters into the adiabatic wavefunction or else why would we observe splitting? That is, if the system was diabatic when the electron entered into the system,

then neither redox site would feel the effects of the other and we would expect their reduction to occur concurrently. However, the situation is not quite so clear as this. For most cyclic voltammotry (CV) experiments the current is swept at a rate of approximately 100 mV/s. This means that it takes 0.001 s to sweep across a potential of 1 mV. In this time, the solvent (who's fastest reorganization movements have a lifetime of ps[59]) and the internal vibrations may progress through billions of conformations. Therefore, during the time required for the instrument to scan through a potential of 1 mV, the electron transfer system and the surrounding medium has the ability to explore roughly a billion different nuclear configurations. It is quite likely that during this time, the complex will be able to find the most stable nuclear configuration for the ground state adiabatic wavefunction. Thus, it is possible that for any electron that is placed into the diabatic wavefunctions the system will be able to undergo electronic coupling and find the lowest energy configuration on a timescale that is *much* faster than that of CV. With this in mind, it is quite easy to understand how, when a potential is reached that is isoenergetic with the adiabatic minima, an electron that is placed into the diabatic wavefunctions may become trapped in the complex (though delocalization of it) and not transfer back to the electrode from which it came. In this case a peak in the current would be observed in the CV at a potential associated with the reduction of the adiabatic wavefunction despite the fact that the electron is actually entering in the diabatic wavefunction.

Clearly, an experiment with a timescale significantly faster than CV is required to answer the question of where an electron initially enters a mixed valence complex – into a diabatic or adiabatic wavefunction. In order to address this question we have devised a system to determine the energy of the electron upon entering and exiting a mixed valence complex. This system is composed of zinc tetraphenylporphyrin (ZnTPP) and complexes **1**-**3**. ZnTPP is photo-excited to generate the excited state singlet which rapidly undergoes intersystem crossing to give the excited state triplet. In the presence of **1**-**3** (which act as quenchers) the decay of ^{3}ZnTPP can be used to determine the rate of electron transfer (k_{et}) from the porphyrin to the mixed valence system, which generates a radical cation, ZnTPP$^+$, and the mixed valence ions **1**$^-$, **2**$^-$, and **3**$^-$. The rate of the back electron transfer (k_{BET}) from the reduced **1**-**3** to the ZnTPP$^+$ can be monitored by observing the recovery of the ground state ZnTPP.

It is known that the electron transfer rates for intermolecular electron transfer exhibit an exponential dependence on the driving force for the reaction.[114] Thus, the rates of the forward and back electron transfer can then be used in order to determine the relative energies of the orbitals of **1**-**3** that the electrons enters into and leaves from The driving force for electron transfer may be obtained from electrochemical studies of **1**-**3** and, in combination with observations of the k_{et} should allow us to determine whether adiabatic or diabatic orbitals are involved.

In addition to this information it is possible that further unusual behaviors may be exhibited by these complexes. Because the coupling of the two ruthenium clusters in these complexes is mediated by the π* orbital of the pz (which lies higher in energy than that of the LUMO of the clusters) the cluster with the highest reduction potential (**3**) also has the largest magnitude of electronic coupling. This, in turn, means that this complex will be the most stabilized. If the stabilization of **3** is sufficient it is possible that the adiabatic wavefunction for **3** will be lower than that for **2**. Likewise, it is possible that the adiabatic wavefunction for **3** will be lower than that for **1**. In this case, the series of rates for **1**-**3** for electron transfers involving the adiabatic ground state wavefunction will be reversed from that expected based on the inductive energetic considerations.

In order to help calibrate our measurements of the electron transfer rates and to facilitate our interpretation of them the k_{et} and k_{BET} will also be determined for a series of pyrazine monomers (complexes **7**-**9**), pyridyl monomers (complexes **10**-**12**), as well as a series of dimers (complexes **4**-**6**) bridged by diazobicyclooctane (dabco). These complexes are shown in Figure 9.1. It has been previously shown that the dabco bridged dimers show greatly reduced electronic coupling between the clusters.[50] Thus, these additional nine complexes will allow us to probe the electron transfer rates for complexes similar to **1**-**3**, but whose electronic structures are not complicated by the extremely large coupling found in complexes **1**-**3**. The monomers allow us to calibrate the clusters energy dependence on the ancillary ligands and in the complete absence of electronic coupling while the dabco dimers allows us to account for the effects of two clusters which are in close proximity to each other. No matter what is observed, we stand to gain significant insight into the nature and evolution of the mixed valence complex as it is first formed.

pyrazine bridged dimers

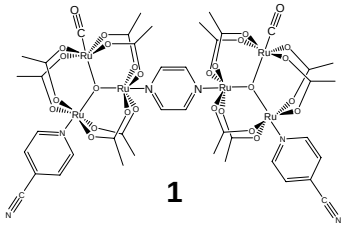

1

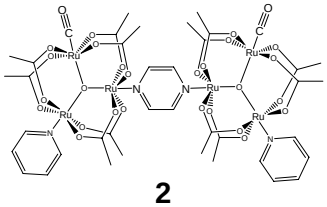

2

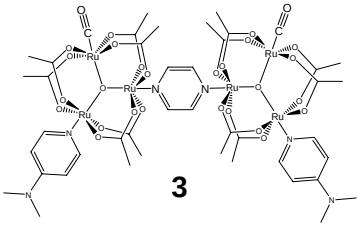

3

dabco bridged dimers

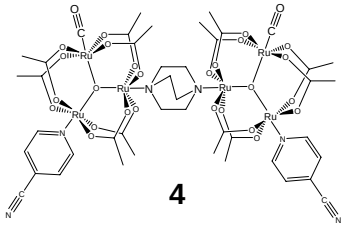

4

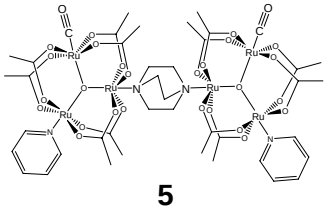

5

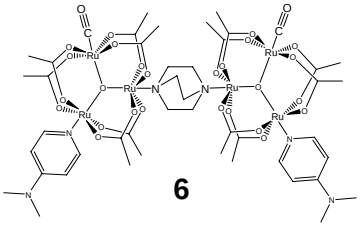

6

pyrazine monomers

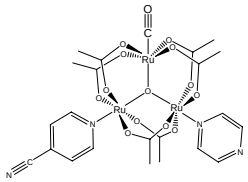

7

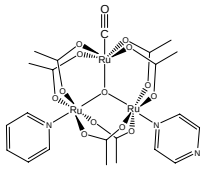

8

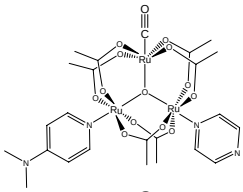

9

pyridyl monomers

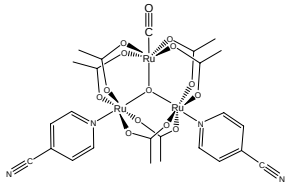

10

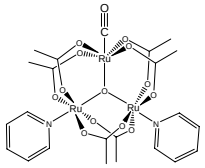

11

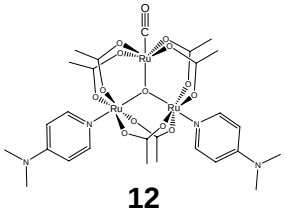

12

Figure 9.1. Complexes **1**-**12** used for this study grouped by type of dimer and type of monomer.

9.2 Experimental

Complexes **1**-**9** were synthesized according to the literature.[50] Complexes 10-12 were prepared by dissolving $RuO(OAc)_6(CO)(H_2O)_2$ in a 1:1 mixture of methanol and methylene chloride. To this was added 20 equivalents of the appropriate pyridine ligand and the reaction was stirred for 30 minutes. The reaction mixture was then rotovaped to dryness, the solid dissolved in a minimal volume of chloroform, and excess hexanes added. The solution was then filtered and the precipitate collected and dried under vacuum. Acetonitrile used for determination of extinction coefficients was used as received from Fisher Scientifics. Extinction coefficients for complexes **1**-**12** were obtained using serial dilutions in CH_3CN and are summarized in Table 9.1.

The laser system employed for the kinetics study has been described elsewhere.[115] All solutions were deoxygenated prior to measurements. Baseline decay curves of ZnTPP in CH_3CN were obtained for each complex. Following the addition of one of the complexes **1**-**12** UV-vis spectra were taken so that the concentration of the porphyrin and ruthenium complex could be obtained. The excited state ZnTPP was generated by excitation at 555 nm. Decay curves were taken at either 470 nm or 400 nm and the data collected using an oscilloscope recording 100000 data points that were averaged over 1000 scans.

Electrochemical studies were performed in acetonitrile with 0.1 M tetrabutylammonium hexaflourophosphate. The acetronitrile was purified and dried prior to use. Measurements were taken using a BAS CV-50 computer controlled potentiostat and potentials are reported versus ferrocene/ferrocienium. The redox potentials for the reduction of complexes **1**-**12** are reported in Table 9.2.

9.3 Electron transfer from excited state porphyrin to ruthenium complexes.

Figure 9.2 shows a set of absorption decay curves taken at 470 nm for 1.0×10^{-5} M ZnTPP in the presence of 0 mM to 4.13×10^{-5} M **2**. It has been shown that the absorption at 470 nm is diagnostic for the ^{3}ZnTPP excited state.[116] Decay lineshapes are typical of those obtained for ^{3}ZnTPP in the presence of any of the complexes **1**-**12**. The curves can be fit to a single exponential from which a decay constant is obtained. These decay constants correspond to an observed electron transfer rate for the forward electron

Table 9.1.
Extinction coefficients for one of the maximums in the UV-vis spectra for complexes **1**-**12**.

Complex	λ (nm)	ε (M^{-1} cm^{-1})
1	607	15090
2	606	12290
3	608	23820
4	582	9200
5	580	5360
6	581	10120
7	597	7310
8	602	6050
9	592	6910
10	594	5890
11	584	4440
12	587	5810

Table 9.2.
Potentials for the reduction of the clusters from $Ru^{III}Ru^{III}Ru^{II}$ to $Ru^{III}Ru^{II}Ru^{II}$ for complexes **1**-**12**.

Complex	E (V)	ΔE (V)
1	-0.895 -1.145	0.250
2	-0.978 -1.285	0.307
3	-1.021 -1.403	0.382
4	-1.198	-
5	-1.365	-
6	-1.473	-
7	-1.114	-
8	-1.139	-
9	-1.199	-
10	-1.062	-
11	-1.277	-
12	-1.485	-

transfer (k_{obs}). The k_{obs} obtained for each concentration of the quencher (ruthenium complex) can be used to generate a Stern-Volmer (SV) plot (Figure 9.3). The slope of this plot gives the intrinsic electron transfer (k_{et}) rate for the forward electron transfer process (from ^{3}ZnTPP to the complex). Table 9.3 lists the k_{et} extracted from the SV plots for each complex as well as the driving forces associated with the electron transfer from ^{3}ZnTPP to each complex. The driving forces are estimated from electrochemical data (*vide infra*). Figure 9.4 provides a graphical representation of the relative electron transfer rates. There are many trends present in Table 9.3 and Figure 9.4 that warrant further comment.

The first trend to consider is how the k_{et} values relate to inductive electronic effects. As expected, the electron transfer rates are found to decrease with increasing electron donor strength of the attached ancillary ligands. Increases in donor strength function, by way of inductive effects, to raise the energy level of the clusters to which they are attached.[46, 50, 116] The higher energy means that there will be less driving force for the electron transfer from ^{3}ZnTPP to the complex and, as a result, the k_{et} will be slower. Thus, for the pyridyl monomers (**10**-**12**), the pyrazine monomers (**7**-**9**), and the pyrazine bridged dimers (**1**-**3**) we observe the electron transfer rate for the compound containing cpy is greater than that for the compound containing py, which is greater than that for the compound containing dmap. This is also the trend expected from the electrochemical considerations, where potentials for reduction move to more positive values (more driving force for electron transfer) for the series dmap < py < cpy. This trend does not hold for the dabco bridged dimers where it is observed that the electron transfer rate to the py containing complex is slow compared to that of the dmap containing dimer – a result that is not expected from consideration of the inductive effects of the ancillary ligands.

Next it is worth comparing the trends between analogous species of different series (e.g. all the cpy containing compounds). Here it is found that the pyrazine monomers (**7**-**9**) have faster electron transfer rates than their analogous pyridyl monomers (**10**-**12**). This implies that pyrazine monomers are lower in energy than pyridyl monomers. In other words, the pz has an overall stabilizing effect upon the clusters to which it is attached, which is expected as the pz is a weaker base than the pyridyl ligands. The next fastest electron transfer is experienced by the pyrazine bridged dimers. Thus, it is the first assumption that these dimers are lower in energy than are the analogous monomers. However, this assumption is complicated by

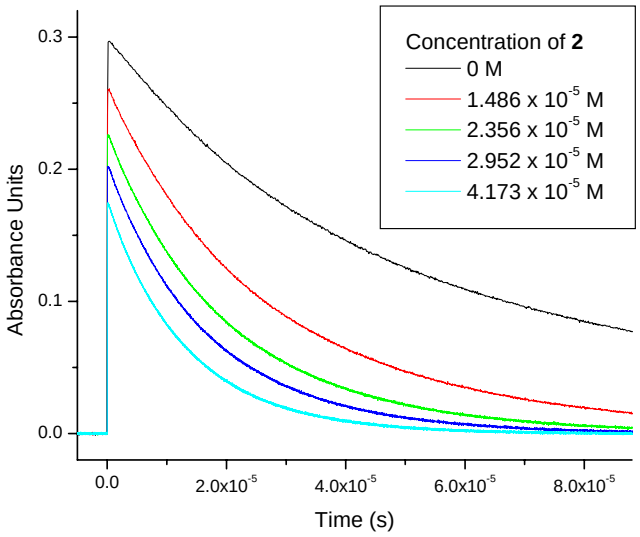

Figure 9.2. Decay curves for ^{3}ZnTPP in the presence of various concentrations of **2**. The ^{3}ZnTPP was generated by excitation at 555 nm and the decay monitored at 470 nm.

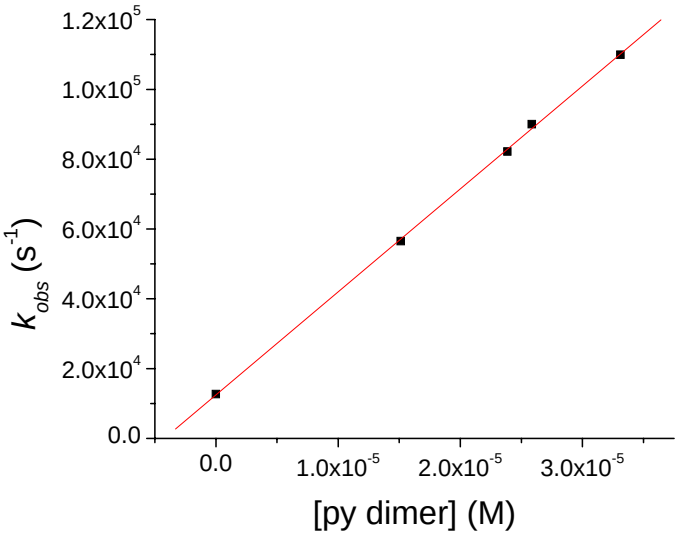

Figure 9.3. Stern-Volmer plot of k_{obs} versus the concentration of **2**. The intrinsic rate of the electron transfer process (k_{et}) from ^{3}ZnTPP to **2** is given by the slope of a linear fit to the data. In this case k_{et} = 1.54 x 10^9 s^{-1}.

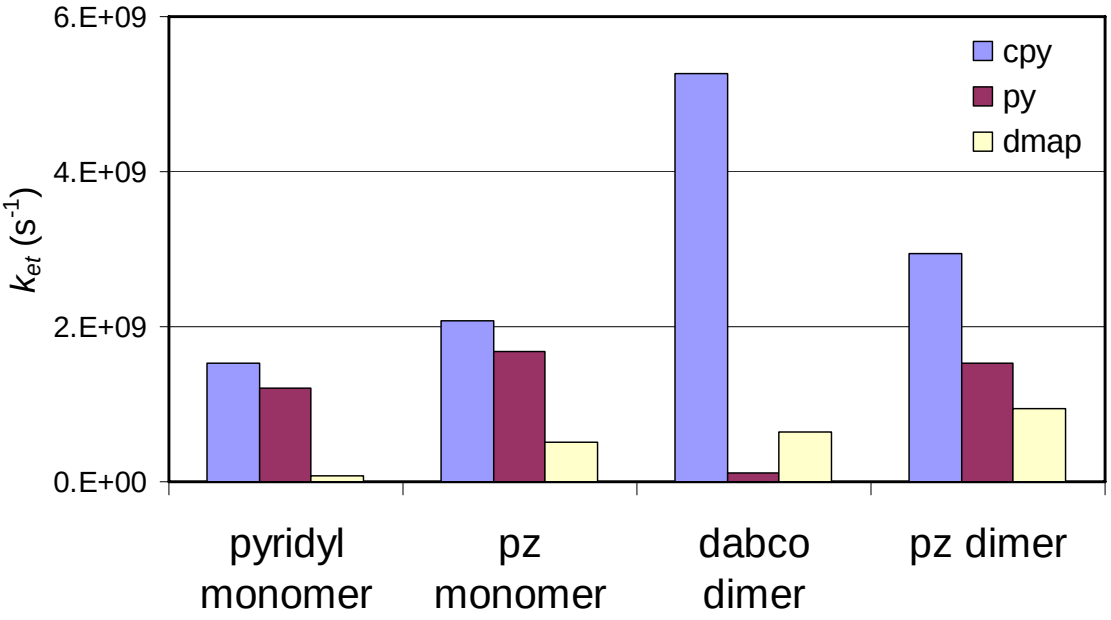

Figure 9.4. Graphical representation of the forward electron transfer rates from ^{3}ZnTPP to complexes **1**-**12**.

the fact that each dimer contains two separate electron acceptors and it is possible that this statistically increases the effective concentration of quencher and accounts for the observed increase in k_{et} of the dimers. However, it seems unlikely that this local quencher concentration difference should affect the electron transfer rates significantly. All encounters of electron donor and electron acceptors can be taken to involve only one donor and one acceptor, since the collision of three bodies is expected to be quite rare.[93] Additionally, for each collision, only one electron can be transferred to one acceptor. Thus, once a dimer becomes reduced it must diffuse away and encounter another ^{3}ZnTPP before it can be reduced another time. Since the electron transfer is bimolecular and occurs in solution, then the fastest electron transfer rate would be on the order of 10^{10} s^{-1} (diffusion controlled).[93, 114] This means that it would take a period of at least a tenth of a nanosecond before the dimer could encounter another donor. If the electron entered into a diabatic wavefunction, then during this time it is expected that the electron would become delocalized to some extent and the second electron transfer event would be met with a higher barrier to electron transfer. Since the extent of electronic coupling is quite large in these dimers, the corresponding additional barrier to the second electron transfer event would also be large. Because of this, one would expect a significant difference between the rates of the first and second electron transfer, which would lead to decay curves that were strongly bi-exponential (two decay constants). If the electron entered into an adiabatic wavefunction, then the large difference between the energy of the ground and excited wavefunctions would also be expected to lead to bi-exponential curves in the event of two electron transfer events from ^{3}ZnTPP to **1**-**6**. For all complexes, **1**-**12**, the decay curves observed for the forward electron transfer were mono-exponential and, as such, it can be concluded that the local electron acceptor concentration difference in the dimers does not contribute to the difference in electron transfer rate between complexes **1**-**3** and **10**-**12**. Additionally, this means that the dimer acceptors (**1**-**6**) do not accept two electrons from two separate ^{3}ZnTPPs. Again, the general trend observed for the monomers and the pz bridged dimers is disrupted by the dabco dimer, where it is observed that the cpy dimer is associated with the fastest electron transfer of all the complexes, the py dimer is associated with the slowest electron transfer of all the py containing complexes, and the dmap dimer is associated with an electron transfer rate intermediate between the pz monomer containing dmap and the pz bridged dimer containing dmap.

It is known that the rate of electron transfer should increase with increasing driving force for electron transfer.[114] The driving force can be obtained using the reduction potentials for the $Ru^{III}Ru^{III}Ru^{II}$ → $Ru^{III}Ru^{II}Ru^{II}$ couple. Table 9.2 lists the potentials for this redox event for complexes **1**-**12** and Table 9.3 lists the driving force for electron transfer as well as the values of k_{et} for **1**-**12**. For the pyrazine bridged dimers, this process is split into two separate processes for the two trinuclear clusters. Figure 9.6 shows a cyclic voltammogram (CV) of **3**. The redox events of interest occur at -1.021 V and -1.403 V. The degree of splitting (0.382 V) is a qualitative measurement of the electronic coupling between the two clusters. If the electron is being transferred to an adiabatic potential energy surface then the lower energy redox event (the first redox wave) must be used when estimating the driving force for electron transfer. However, if the electron first enters into a diabatic wavefunction, then the potentials obtained from the waves in the CV may no longer be used for calculation of the driving force as the redox events in the CV do not correspond to reduction of the diabatic wavefunctions. Instead, one must use the diabatic energies. In an earlier paper, we proposed that this may be done by averaging the potentials associated with the two split processes. In the case of complexes **1**-**3**, the diabatic potentials associated with them are -1.020 V, -1.132 V, and -1.212, respectively. These potentials give a driving force for electron transfer of -0.510 eV, -0.398 eV, and -0.318 eV, respectively. Figure 9.7 depicts the driving force for electron transfer from ^{3}ZnTPP to complexes **1**-**12**, included in this graph is the driving forces associated with the adiabatic and diabatic wavefunctions for **1**-**3**.

Comparison of Figure 9.4 with Figure 9.7 allows one to address whether the electron is entering into an adiabatic or diabatic wavefunction. From Figure 9.7 it can be seen that the driving force for the ground state adiabatic wavefunction of the dimers is greater for all of the dimers than for any of the associated monomers. Thus, if the electron were entering into the adiabatic wavefunction one would expect that the k_{et} from ^{3}ZnTPP to **1**-**3** would be faster than the k_{et} for any other complex. However, examination of Figure 9.4 shows that this is clearly not the case. The electron transfer rate to the py dimer is slower than for any of the cpy monomers and the electron transfer rate from the cpy dimer is much slower than for any of the py and cpy monomers. These observations are not at all in agreement with the trends that would be predicted using the adiabatic driving forces. However, these observed trends in k_{et} do

Table 9.3. k_{et} for the forward electron trasfer from ^{3}ZnTPP to complexes **1**-**12** as well as driving force (DG) associated with this reaction.

Complex	k_{et} (s^{-1})	ΔG (eV)	$\Delta G_{diabatic}$ (eV)
1	2.95E+09	-0.635	-0.510
2	1.54E+09	-0.552	-0.398
3	9.49E+08	-0.509	-0.318
4	5.27E+09	-0.332	-
5	1.16E+08	-0.165	-
6	6.43E+08	-0.057	-
7	2.07E+09	-0.416	-
8	1.68E+09	-0.391	-
9	5.03E+08	-0.331	-
10	1.53E+09	-0.468	-
11	1.21E+09	-0.253	-
12	7.72E+07	-0.045	-

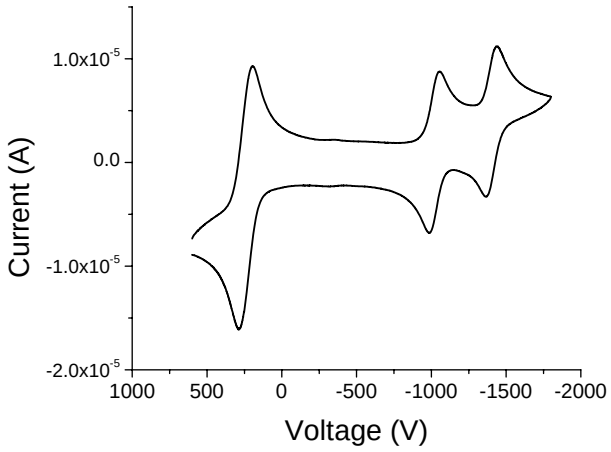

Figure 9.5. Cyclic voltammogram of **3**. The oxidation of the two clusters occurs concurrently while the reduction of the clusters is split into two one electron processes. The two reduction processes correspond to the introduction of an electron into each of the adiabatic wavefunctions. The energy of the diabatic wavefunction may be obtained by averaging the two energies of the adiabatic wavefunctions.

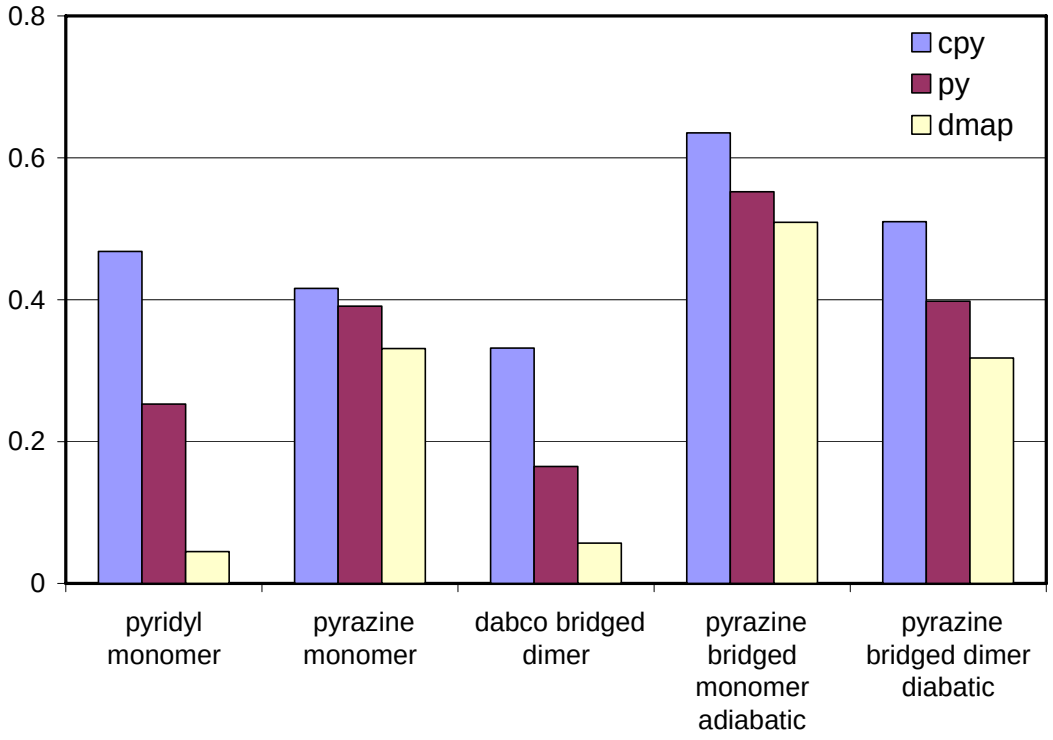

Figure 9.6. The driving forces associated with electron transfer from ^{3}ZnTPP to the pyridyl monomers, the pyrazine monomers, the dabco bridged dimers, the adiabatic wavefunctions of the pyrazine bridged dimers, and the diabatic wavefunctions of the pyrazine bridged dimers.

show good agreement with those observed for the diabatic driving forces. While there are some discrepancies between the predicted trends in k_{et} (based on driving force) and the observed trends in k_{et} (e.g.k_{et} to **2** is slower than to **8**) these only occur in cases where the differences in ΔG are small and may owe mainly to structural differences between complexes that can effect the distance of electron transfer. The rate of electron transfer is known to depend exponentially on the distance of the electron transfer[117] and so it is reasonable that the deviations in observed rate from the predicted trends could be a result of these structural differences. Thus, the trends in observed electron transfer rates strongly suggest that the electron is transferred from the triplet porphyrin to a diabatic wavefunction (or at least a wavefunction that is not fully coupled) of the pyrazine bridged dimer. The question then remains: during the back electron transfer (from the reduced ruthenium clusters to the zinc tetraphenylporphyrin radical cation), does the electron leave from an adiabatic or diabatic wavefunction? In order to address this question it is necessary to investigate the kinetics of the back electron transfer.

9.4 Conclusions

These experiments were designed with the hope that we might be able to answer the question of how an electron initially enters into a mixed valence system. This question amounts to asking if the electron is introduced into diabatic energy surfaces (after which the surfaces couple) or whether the electron enters into adiabatic energy surfaces (systems has already undergone electronic coupling prior to the addition of the electron). It is the added electron that is delocalized and, as such, it is the delocalization of the electron that provides the "driving force" for electronic mixing of the complex and for this reason it was unclear whether or not the electron entered into a diabatic or adiabatic wavefunction.

We were able to show that, for most of the ruthenium complexes presented here, the relative rate of electron transfer from ^{3}ZnTPP to the ruthenium complexes followed the trends one would expect from examination of the relative driving forces for this electron transfer. In cases were the driving forces were quite close, then it was concluded that the geometry of the complexes contribute significantly to the relative rates of electron transfer. However, the dabco bridged dimers deviated strongly from the expected trends. We offer no explanation as to why this may have occurred. It is possible that there was some error in the

making of the dabco solutions, however, the same general trends in the dabco series was also observed for the back electron transfer (not discussed here) and so it seems unlikely that this is the cause of the deviation.

Regardless of the anomalous behavior of the dabco bridged dimers, the data collected here definitely shines light onto the question originally posed. By comparing the expected driving forces for diabatic and adiabatic wavefunctions of the pyrazine bridged dimers, **1**-**3**, it was seen that the driving forces associated with the diabatic wavefunctions are in much better agreement (as opposed to the driving forces associated with the adiabatic wavefunctions) with the observed electron transfer rates. Thus, it is our conclusion that the electron enters into a diabatic wavefunction in the mixed valence systems studied here, after which the systems evolves into the adiabatic state. The timescale for this delocalization was not measured, however, it seems likely that it will depend strongly on the lifetimes of the vibrational modes that are most intimately involve in the delocalization of the electron. Future work along these lines would include measurement of the rate of back electron transfer form the $ZnTPP^{+}$ radical cation from the mixed valence ion as well as the determination of the kinetics for the evolution of the adiabatic wavefunctions.

Chapter 10: Future experiments for class II-III mixed valency

10.1 Introduction

There is one problem with completing a graduate career. For (at least in my case) the last five years I have immersed myself in the study of electron transfer. I have worried about what the term "delocalized" means. I have worried about how electrons enter into a mixed valence system and where they ultimately end up. I have also become intimately involved with the complexes that we (in the Kubiak lab) employ in this study. For five years I have laid in bed at night thinking about electron transfer and our complexes – devising ways to probe the properties of our complexes specifically and electron transfer in general. Now that I am finishing my stint in the Kubiak lab I find that I have more questions than ever before. I imagine that everyone that pursues academics finds this to be true. Indeed, this seems inevitable since the more we understand something, the more we know what to ask about it. In the case of a lifelong study, this is a blessing. In the case of graduate school it a bit of a curse. For I find that just as I have obtained a competent knowledge of my project, I am forced to leave it – and its fascinating questions – behind. Of course, this is the nature of the Ph.D. Once someone has demonstrated that he can function independently, then it is time to go. However, the pleasure of obtaining a doctorate does not fully cancel out the frustration of leaving questions unanswered.

In this last chapter then, I will discuss questions that I think are pertinent to the Kubaik group's study of electron transfer. There is neither the time nor the space to discuss all of the questions that I have accrued concerning these complexes. (This is not a reflection of any great ability on my part, but rather the immense richness of the project.) Instead, I will discuss just three areas that I feel are perhaps the most pressing or provide the most interesting diversions. So, without further introduction I will leap directly into those questions that I feel would most benefit the group at this time.

10.2 Speaking the language of mixed valency – studying the intervalence charge transfer (IVCT) band

One of the most pressing things for our lab to do is to perform a detailed study in the properties of the IVCT bands of our complexes. Up until this date study of the IVCT bands of our complexes has remained largely neglected. To some extent this neglect was warranted. The IVCT band is unable to provide any information as to the dynamics of the electron transfer[9] and the classical treatments for the IVCT band are not valid in the case of highly coupled mixed valence complexes.[11] Nevertheless, most experimentalists in the field of mixed valency do not study a system that allows for the determination of ultrafast electron transfer rates and the properties of the IVCT band remain the common language of the electron transfer community at large. As such, it behooves us to perform a detailed study into the IVCT bands of our complexes.

The first study to be done is that of solvent dependence. It is established that for Robin-Day class II (valence localized) complexes the position of the IVCT band will shift when taken in differing solvents.[7, 11, 17] This dependence arises from the fact that in class II complexes excitation of the IVCT band is accompanied by a change in dipole (as the electron moves from one redox site to the next). This change in dipole is resisted by the solvent and (in the traditional treatment) the energetic barrier this presents to electron transfer is accounted for by the dielectric solvent of the system. The end result is that the IVCT band is found to shift to higher energy as the dielectric constant of the solvent decreases. In the case of class III complexes, however, excitation the IVCT band is not accompanied by a change in dipole (the electron is delocalized) and the IVCT band shows no solvent dependence[7, 11, 17]. In the intermediate case class II-III the IVCT band also shows no solvent dependence, but the IR spectrum can provide markers for localization.[17, 32] We have already studied the IR spectrum in detail[6, 34-36, 38, 39, 44, 45, 50, 53, 96, 118, 119] and so all that remains in order to put our complexes into the same context as other mixed valence complexes is to determine the solvent dependence of the IVCT band. With this completed, we will have translated the properties of our complexes into the common language of mixed valency and, as a result, the rest of our reported results will be more easily assimilated into the mixed valence community.

The second study that should be done on the IVCT band is a temperature dependence study. We have already reported the very unusual dependence of the electron transfer rate on temperature[120] – the electron transfer rate was found to increase upon freezing of the solvent. This behavior was ascribed to the decoupling of the solvent modes from the electron transfer event and this was taken as evidence that the dynamics of the solvent and not the thermodynamics were controlling the rate of electron transfer. These finding, however, raise an interesting question; what temperature dependence would the IVCT band exhibit in these complexes? Given what we know from the temperature dependence of the electron transfer rate it seems likely that the IVCT band will show minimal temperature dependence. It is usually assumed that the IVCT band is controlled by the thermodynamics and not the dynamics of the system. Thus, the temperature dependence of the IVCT band, together with the already established temperature dependence of the electron transfer rate, will give us further insight into the relative importance of thermodynamics and kinetics in these systems. These two experiments into the properties of the IVCT band should go far towards framing our complexes in the common language of the electron transfer community.

10.3 The confirmation of the electron transfer rate for ruthenium dimers of trimers

Perhaps the most unique feature of the dimers of trinuclear clusters utilized throughout this thesis is the ability to obtain estimates for the rate of ultrafast electron transfer from steady state IR measurements. This ability has allowed us to probe how ligand substitution, tertiary ligand interactions, changes in the solvent, and the introduction of asymmetry affect the rate of electron transfer. Information concerning k_{et} has allowed us to experimentally determine how these changes affect the electronic coupling in these complexes. It is clear that the ability to consistently and accurately determine k_{et} is important to these studies. As such, I feel that the mixed valence electron transfer project would benefit by the use of other means to independently identify the rate of electron transfer in these complexes. There are three means for doing this that I feel are well suited to our complexes; 2-D IR, T_1 relaxation times as determined by NMR, and the observation of THz electromagnetic emissions from the mixed valence ion.

The technique of 2D IR has recently emerged as a promising technique for both structural and dynamic information about a chemical system. The basic principle is not entirely unlike that for 2D NMR

and one's understanding of 2D IR can benefit from consideration of a simple 2D NOESY NMR experiment (Figure 10.1).[121] The NOESY experiment involves two nuclei (**I** and **S**), which have different NMR frequencies and whose magnetic dipoles are able to exchange intensity by way of through-space couplings but unable to exchange intensity *via* scalar coupling. At the start of the experiment the magnetizations of **I** and **S** are aligned in the z-direction in the rotating frame. By the application of a 90º pulse the magnetizations of **I** and **S** can be moved into the *xy* plane where they precesses. After a time, τ_1, a second 90º pulse is applied, the effect of which is to move the *y* components of the **I** and **S** magnetizations back onto the *z* axis. A time τ_m is then allowed to pass during which the two nuclei **I** and **S** interact *via* through space coupling. Because **I** and **S** precess at different frequencies, their magnetizations will be out of phase at the time of the second 90º pulse. Therefore, **I** and **S** magnetizations will not be at their equilibrium values with respect to each other. Because of this, magnetization can be transferred between **I** and **S**. The time τ_m is held constant so that the amount of magnetization transferred between **I** and **S** depends only on the time τ_1. After the passage of τ_m, a third 90º pulse is applied to move the magnetization of nuclei **I** and **S** into the *xy* plane. The free induction decay of the system is then recorded and a double Fourier transform performed (on along ω_i and one along ω_s).

Plots of ω_1 *vs* ω_2 give two "diagonal" peaks and two "off diagonal" peaks. The off-diagonal peaks arise from the fact that nuclei **I** and **S** are frequency modulated by each other (and are also a direct result of the exchange of magnetization). Thus, in the above example, the intensity of the NMR signal for **S** is determined in part by the frequency of **I** (the same is true for the **S** nucleus). The "on diagonal" peaks are a result of the fact that after the transfer of magnetization there is still residual magnetization for each nuclei. Thus, in the above example, even after the transfer of magnetization, nuclei **I** retains some *z* magnetization and this can be observed in the free induction decay after the third 90º pulse. That is that the intensity of the NMR signal for **S** is determined, in part, by the frequency of **S** (the same is true for the **I** signal).

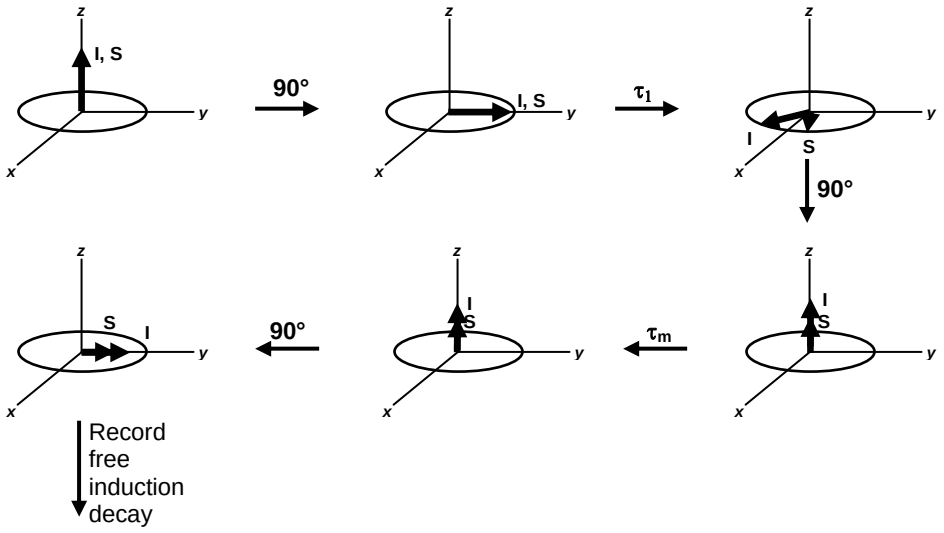

Figure 10.1 Diagram of a simple 2D NOESY NMR experiment showing the magnetization of two nuclei (I and S). In this diagram the magnetization of two nuclei are drawn as arrows in the rotating frame convention. The term "90°" indicates that a pulse of electromagnetic radiation sufficient to move the magnetization of one or both of the nuclei 90° has been applied to the system. T_1 and τ_m are the amount of time between pulses, during which the magnetization of the system is allowed to evolve.

It is now possible to consider 2D IR using NOESY as an analogy. The basic idea behind the 2D IR is the same as NOESY. That is, one uses an exchange in intensity between to peaks to generate off-diagonal peaks in the observed spectrum. The experiment involves three ultrashort IR pulses which are diagramed in Figure 10.2a.[122, 123] The first pulse creates a coherent superposition of the ground and first excited state vibrational levels (the molecular oscillations are all in phase). The coherence undergoes a free induction decay until the application of a second pulse at a time, τ, after the first pulse. This second pulse has the effect of storing the frequency and special information that arose from the first pulse and the following free induction decay. A time T_w (called the waiting time) is then allowed to pass. During this time, intensity conversion between vibrational frequencies may by way of chemical or electronic exchange may during this time (Figure 10.2b). The third pulse ends this waiting time and generates a superposition of states once again. During this time, the oscillations are not in phase as they were following the first pulse, however, after a time less than or equal to τ, the oscillations again gain coherence. When the oscillations gain coherence, then the sample has a macroscopic dipole oscillation and IR light is emitted. This emitted light, termed the echo, is then collected and a plot is made of the absorption versus emission (Figure 10.2c). The on diagonal peaks arise from vibrations that are excited at one frequency and the emit at the same frequency (this occurs in the absence of chemical or electronic exchange). If there has been chemical or electronic exchange that has led to an exchange of intensities in the IR, then the resultant graph will contain off-diagonal peaks. These peaks result from a vibration being excited at one frequency, but emitting at another. Changes to the length of T_w allow for the dynamics of the event that leads to exchange of the vibrational frequencies. Exchange of vibrational frequencies (and, hence, the chemical event) is only expected to be observed for T_w on the same timescale as the chemical or electronic exchange. Thus, by varying the length of T_w, information can be obtained about the dynamics of the chemical system.

In the case of our mixed valence dimers, the event that leads to swapping of intensities is the electron transfer between clusters. The peaks that will exchange are the two ν(CO) peaks – one at ca. 1940 cm^{-1} (corresponding to a neutral cluster) and one at ca. 1900 cm^{-1} (corresponding to a reduced cluster). By monitoring the appearance of the off diagonal peaks at a function of T_w, we will be able to determine the rate of electron exchange between the clusters in the dimers.

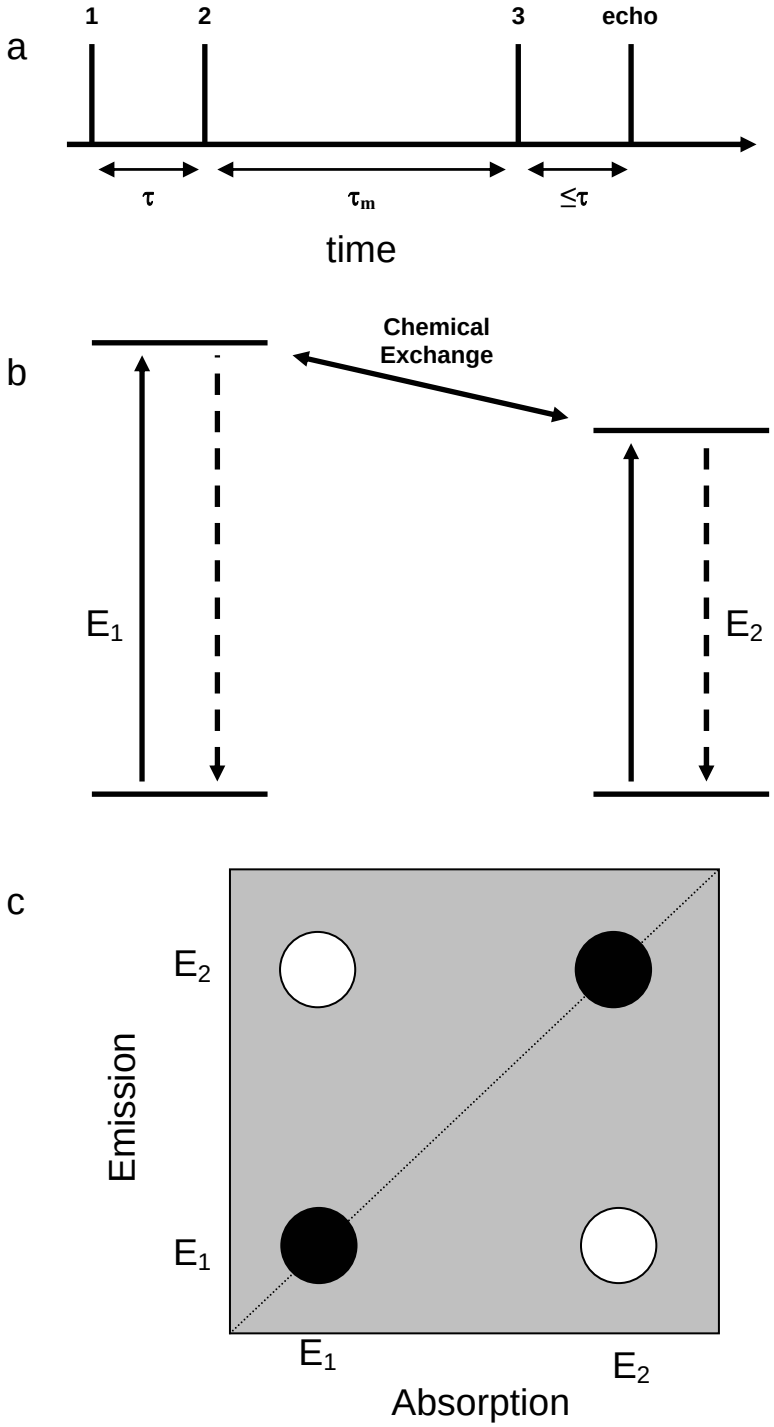

Figure 10.2. (a) The pulse sequence used in a typical 2D IR experiment. (b) Diagram of how chemical or electronic exchange can lead to the exchange the frequencies of vibrational modes. (c) Diagram of a 2D IR graph. The on-diagonal peaks result from vibrations that absorb and emit at the same frequency. The off-diagonal peaks result from vibrations that absorb and emit at different frequencies. The change in frequency is a result of chemical or electronic exchange between vibrational modes as shown in part b.

Another technique that might allow for the determination of k_{et} is the simple T_1 determination by NMR. The details of this experiment are shown in Figure 10.3. The experiment begins with the system containing a net magnetic moment (a result of the application of an external magnetic field) along the *z*-axis in the rotating frame convention (Figure 10.3 A). A 180º pulse is applied (a magnetic field is applied along the *x* axis long enough to flip the orientation of the net magnetic dipole moment so that is lies in the negative *z* direction) (Figure 10.2 B). Following this, a time, τ, is allowed to pass. During this time the magnetization begins to align itself with the external field by way of the T_1 relaxation processes. That is, the magnetization gains intensity in the positive *z* direction. The amount of positive *z* intensity regained is related to the amount of time allowed to pass. For times less than T_1, the intensity remains less than one in the *z* direction. For times greater than T_1, the intensity becomes positive in the *z* direction. When τ is equal to T_1, there is no intensity in the *z* direction (Figure 10.2 C). After the time, τ, has passed, a 90º pulse is applied, moving the magnetic dipole into the *xy* plane where it precesses about the *z* axis (Figure 10.2 D). Immediately following the 90º pulse, the free induction decay is recorded and a Fourier transform is taken to give the corresponding NMR spectrum. The intensity of the NMR signal is directly proportional to the magnitude of the magnetization. This is turn is depends on the time the system was allowed to relax, τ. If this pulse sequence is repeated for a series of times, τ, and, for each signal, a plot is made of the intensity of that NMR signal *vs* τ. The *y* intercept of this plot gives the T_1 relaxation time for the species giving rise to the signal. Thus, the T_1 experiment measures the time required for magnetic relaxation to occur. The rate of relaxation is dependent on many molecular processes. For instance, molecular rotation, chemical exchange, and gross structural changes can all influence T_1. Generally, any process that change lead to magnetic exchange with the environment or the molecule will allow for faster relaxation. In mixed valence complexes undergoing electron transfer, the electron transfer event can also function as a relaxation process. In the case of ultrafast electron transfer (picosecond lifetimes) the electron transfer is by far the fastest mechanism for relaxation and, because of this, becomes the dominant contributor to the molecules T_1. Thus, the rate of electron transfer can be obtained from determination of T_1 in the mixed valence state. Experimentally determined rates for biferrocene have already been reported using this technique.[124] The

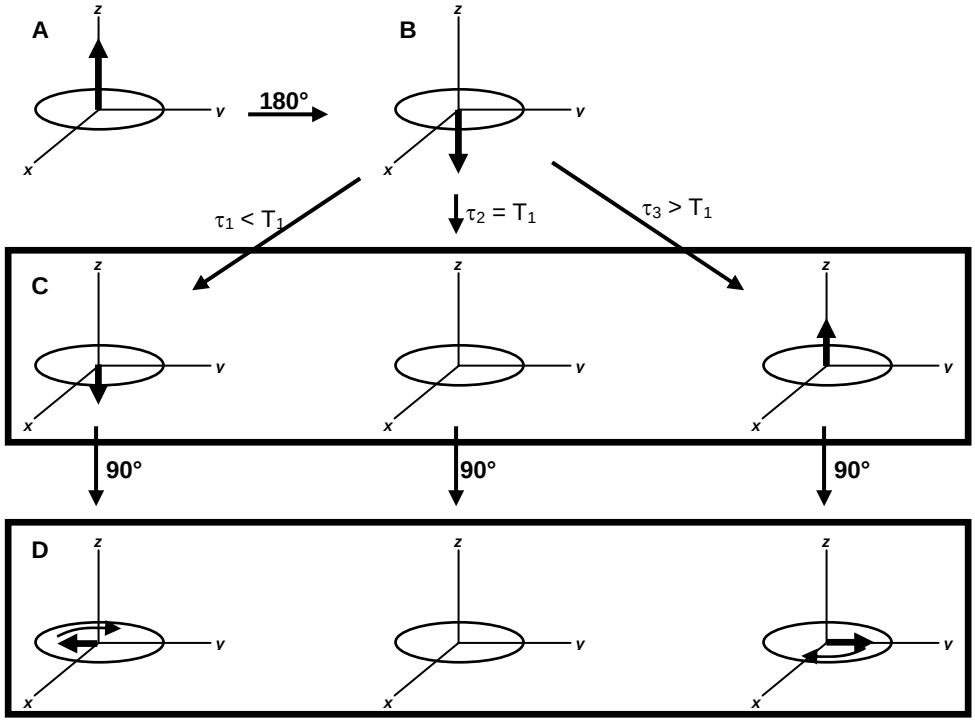

Figure 10.3. Diagram showing the magnetization of a nucleus during a typical T_1 relaxation experiment. The magnetization is represented as an arrow in the rotating frame convention. The term "90°" indicates that a pulse of electromagnetic radiation sufficient to move the magnetization of one or both of the nuclei 90° has been applied to the system. τ_1, τ_2, and τ_3 are the amount of time between pulses, during which the magnetization of the system is allowed to evolve.

ruthenium complexes present multiple nuclei appropriate for such studies (eg. pyridyl protons, the carbonyl carbon, or one of the pyrazine protons).

Another technique that could allow for the determination of the electron transfer rate in our dimers is the observation of the THz emission of out complexes in the mixed valence state. According to classical electrodynamics, oscillation of an electric field will create a corresponding electromagnetic field. The frequency of the light given off depends on the frequency of fluctuating electric field. Thus, of one was able to determine the frequency of light being emitted from a system undergoing electronic oscillations, then one would have been able to determine the frequency of the electronic oscillations. This basic idea has been used for quite some time in the semi-conductor field in order to study how electrons move in within a semiconductor.[125] In recent years this technique has been adapted for use in probing molecular electronic transitions.[125-128] All of this work has been done by Charlie Schmuttenmaer and has involved probing the light emitted by the relaxation of photo-excited dyes back to the ground state. The idea is that the excitation of the dye is accompanied by a change in dipole moment. This dipole moment then reverts back to the ground state with some characteristic lifetime. If the lifetime is on the order of picoseconds, then the frequency of the emitted light will, necessarily, be on the order of THz. Schmuttenmaer and co-workers have been able to observe the waveform emitted by such dyes as they relax to the ground state and have been able to use this information to determine the rate constant for relaxation. This same technique could be used to determine the rate of electron transfer in our mixed valence systems. Such experiments have three requirements; the electron transfer must occur on the order of picoseconds, the molecules must be in an ordered array, and the molecules must be undergoing coherent electron transfer (electron transfer in the same direction). The first of these requirements (necessary for emission in the THz regime) is met by our complexes, as is evidenced by their IR spectra in the mixed valence state.[34, 35] The second of these requirements is necessary because a random distribution of molecular orientations would result in the dipole moments canceling each other out. Orientation of the molecules could be easily accomplished by their attachment to a surface. Clusters such as those used in our dimers have already been attached to Au through thiol linkages.[129, 130] An additional benefit may be realized from the attachment of these complexes to a gold surface – the mixed valence complexes could induce an image dipole in the surface of the gold,

leading to an enhancement of the THz emission not unlike the enhancement observed for IR absorptions of molecules that are close to a metallic surface. The third requirement is necessary because a random distribution of electron transfer events in time would also lead to a cancellation of dipoles. Thus, some means would be required to synchronize the electron transfer event. This is by far the most difficult experimental requirement and will require much thought if this experiment is to work. My initial impression is that one could use asymmetric dimers and preferentially excite one of the two IVCT bands with a laser in order to accrue a non-equilibrium population of the isomers. When the laser is turned off, the system would returned to equilibrium via thermal electron transfer and the first few cycles of this process should be fairly coherent. Thus, during the return to equilibrium a THz waveform should be emitted by the sample and the period of this waveform used to obtain k_{et} for our complexes.

All in all, independent determination of k_{et} will allow us to compare multiple means for determination of k_{et}. It should also allow us to gain better insight in the physical processes of electron transfer event as well as provide us with a much firmer estimate of the electron transfer rate. Such knowledge will be extremely useful discussions of the electronic and physical properties of the dimers of trimers used in our laboratory.

10.4 Breaking the ruthenium clusters out of the electron transfer box and using them to make metal-organic boxes

During my years in the Kubiak lab I found that having a few projects going at the same time has kept me sane. When one project wasn't working I could turn to the other. One theme that has existed throughout my stint at UCSD was the making of large structures out of the trinuclear ruthenium clusters. Many structures have been proposed for making such large complexes[98] and even a few have been made.[131] Indeed, the ligand centered dendrimer discussed in chapter 8 of this thesis was a result of attempts to make large networks of these complexes. The structure of this dendrimer is representative of my early thinking concerning how to make these networks. Specifically, the networks were conceived of as built using straight or branched bridging ligands in the ancillary positions to give large networks. Ideas for bridges included pz, triazine (as used in the LCD), or phenyldiisocyanide (PDI) based ligands. The isocyanade

based ligands had the advantage that the resulting network would be overall electronically netural[99, 132, 133] (π-backbonding with the isocyanide results in the stabilization of the neutral cluster). I was, however, unable to obtain soluble complexes of the triisocianide substituted cluster. Perhaps the network could be made by mixing the solvate cluster and the diisocianide in a 1:1 mixture. I never pursued this, because I came to the conclusion that making networks by using bridging ancillary ligands was not as interesting as trying to make these networks using bridging carboxyl groups. If one were to make the clusters by using oxylate-type ligands instead of acetate, then it is conceivable that one could generate a 3-D network of clusters bridged by these dicarboxylates (Figure 10.4). Such networks would contain free ancillary positions and large intercluster cavities. Thus, it is conceivable that such a network could perform interesting chemistry. Because the clusters are well-behaved electrochemically, each cavity would contain three co-planer redox active clusters – each with an open ancillary site. My first attempt at making these networks at this was made using oxylatic acid, however, I did not obtain any promising results. The problem most likely stems from the fact that the oxylatic acid can coordinate with the ruthenium in a manner that the wrong geometry for the formation of the clusters (Figure 10.5). Thus, I next tried 1,4-Benzenedicarboxylic acid from which I obtained an insoluble green powder. Briefly, 1 equivalent of $RuCl_3 \cdot H_20$ and 1 equivalent of 1,4-Benzenedicarboxylic acid were dissolved in MeOH and the mixture was refluxed for 12 hours. The reaction mixture was then passed through a medium fritted glass filter and a green solid was obtained. The solid was insoluble in methanol, acetonitrile, THF, methylene chloride, chloroform, toluene, benzene, DMSO, and water. No further characterization was done in the complexes, though the next logical step would be to perform x-ray powder diffraction on the solid to determine if there are any repeating patterns in its 3-D structure. It seems likely that such networks could exhibit interesting chemistry and even if they do not, the theme of electron transfer reactions in large structures is one that I find fascinating and that a future student (if he was looking for an interesting side project) could pursue.

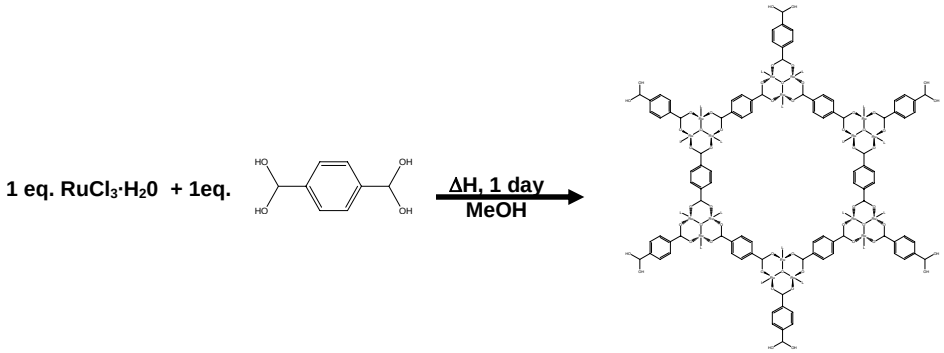

Figure 10.4. Synthetic route for the formation of supramolecular assemblies of ruthenium clusters. In this structure the dicarboxylate forms the bridge between clusters. As one goes around the structure on the right, alternating clusters are coplanar and there exists a procession of clusters immediately above and below the position of the clusters shown. Thus, one would obtain a 3D network of clusters bridged by dicarboxylates.

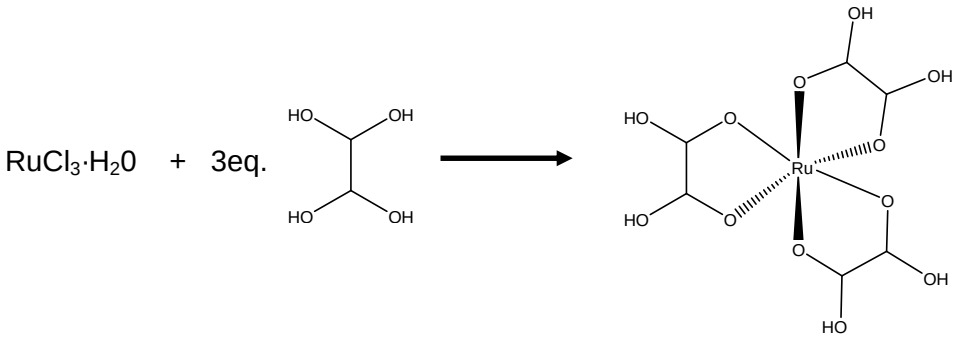

Figure 10.5. Proposed structure formed upon the reaction of ruthenium chloride hydrate with oxylic acid. In this structure the geometry of the chelating oxylates prevent the formation of the trinuclear clusters of type $Ru_3(O)(L_3)$.

10.5 Conclusions

Above, I have outlined a few of the ideas that I have had concerning these complexes over the last 9 months or so of my stay at UCSD. I am confident that the first two projects are ones that will yield important results and are ones that, should I be staying longer, I would pursue myself. These studies are of particular importance as they will allow for our complexes to be better understood by the electron transfer community at large as well as provide further details as to the electronic properties of our complexes. The last project is one that has much latent potential, but may to be merely a way of making insoluble ruthenium. It is a project that can only be advised as a means to keep a student occupied during the weeks that he must run column after column on the dimers of trimers. In the end the ruthenium electron transfer project is a rich one – a project overflowing with promise and I am sure that the students that are on it in the future will have no problem occupying themselves. To these future students I wish all the best of luck.

References

1. Libby, W. F., Theory of electron exchange reactions in aqueous solution. *Journal of Chemical Physics* **1952,** 56, 863-868.

2. *The proceedings of the 1952 meeting on electron trasfer was published in the 1952 October issue of The Journal of Chemical Physics (vol. 56).*

3. Marcus, R. A., The theory of oxidation-reduction reactions involving electron transfer. I. *Journal of Chemical Physics* **1956,** 24, 966-978.

4. Brunschwig, B.; Sutin, N., Energy surfaces, reorganization energies, and coupling elements in electron transfer. *Coordination Chemistry Reviews* **1999,** 187, 233-254.

5. Sutin, N., Theory of electron transfer reactions: insights and hindsights. *Progress in Inorganic Chemistry* **1983,** 30, 441-498.

6. Londergan, C. H.; Salsman, J. C.; Lear, B. J.; Kubiak, C. P., Observation and dynamics of "mixed-valence isomers" and a thermodynamic estimate of electronic coupling parameters. *Chemical Physics* **2006,** 324, (1), 57-62.

7. Brunschwig, B. S.; Creutz, C.; Sutin, N., Optical transitions of symmetrical mixed-valence systems in the Class II-III transition regime. *Chemical Society Reviews* **2002,** 31, (3), 168-184.

8. Hush, N. S., Intervalence-transfer absorption. II. Theoretical considerations and spectroscopic data. *Progress in Inorganic Chemistry* **1967,** 8, 391-444.

9. Turner, J. J., *Handbook of Vibrational Spectroscopy*. John Wiley and Sons Ltd.: 2002; Vol. 1, p 101-127.

10. Turner, J. J.; Poliakoff, M., Infrared-Spectroscopy from Megaseconds to Picoseconds. *Polyhedron* **1989,** 8, (13-14), 1637-1640.

11. D'Alessandro, D. M.; Keene, F. R., Current trends and future challenges in the experimental, theoretical, and computational analysis of intervalence charge transfer (IVCT) transitions. *Chemical Society Reviews* **2006,** 35, -440.

12. Bublitz, G. U.; Laidlaw, W. M.; Denning, R. G.; Boxer, S. G., Effective Charge Transfer Distances in Cyanide-Bridged Mixed-Valence Transition Metal Complexes. *Journal of the American Chemical Society* **1998,** 120, (24), 6068-6075.

13. Oh, D. H.; Boxer, S. G., Electrochromism in the near-infrared absorption spectra of bridged ruthenium mixed-valence complexes. *Journal of the American Chemical Society* **1990,** 112, (22), 8161-2.

14. Karki, L.; Hupp, J. T., Orbital Specific Charge Transfer Distances, Solvent Reorganization Energies, and Electronic Coupling Energies: Electronic Stark Effect Studies of Parallel and Orthogonal Intervalence Transfer in (NC)5OsII-CN-RuIII(NH3)5. *Journal of the American Chemical Society* **1997,** 119, (17), 4070-4073.

15. Piepho, S. B., Vibronic coupling model for the calculation of mixed-valence line shapes: a new look at the Creutz-Taube ion. *Journal of the American Chemical Society* **1990,** 112, (11), 4197-4206.

16. Piepho, S. B.; Krausz, E. R.; Schatz, P. N., Vibronic coupling model for calculation of mixed valence absorption profiles. *Journal of the American Chemical Society* **1978,** 100, (10), 2996-3005.

17. Demadis, K. D.; Hartshorn, C. M.; Meyer, T. J., The localized-to-delocalized transition in mixed-valence chemistry. *Chemical Reviews* **2001,** 101, (9), 2655-2685.

18. Marcus, R. A., Theory of charge-transfer spectra in frozen media. *Journal of Physical Chemistry* **1990,** 94, (12), 4963-4966.

19. Marcus, R. A.; Sutin, N., Electron transfers in chemistry and biology. *Biochimica et Biophysica Acta, Reviews on Bioenergetics* **1985,** 811, (3), 265-322.

20. Newton, M. D.; Sutin, N., Electron transfer reactions in condensed phases. *Annual Review of Physical Chemistry* **1984,** 35, 437-480.

21. Weaver, M. J., Dynamical solvent effects on activated electron-transfer reactions: principles, pitfalls, and progress. *Chemical Reviews* **1992,** 92, (3), 463-480.

22. Zhang, L. T.; Ko, J.; Ondrechen, M. J., Electronic structure of the Creutz-Taube ion. *Journal of the American Chemical Society* **1987,** 109, (6), 1666-1671.

23. Zhang, L. T.; Ko, J.; Ondrechen, M. J., Nonadiabatic quantum mechanical treatment of the absorption lineshape of bridged mixed-valence dimers. *Journal of Physical Chemistry* **1989,** 93, (8), 3030-3034.

24. Sutin, N., Electron transfer reactions in solution: A historical perspective. *Advances in Chemical Physics* **1999,** 106, 7-33.

25. Creutz, C.; Taube, H., A Direct Approach to Measuring the Franck-Condon Barrier to Electron Transfer between Metal Ions. *Journal of the American Chemical Society* **1969,** 91, (14), 3988-3989.

26. Robin, M. B.; Day, P., Mixed valence chemistry. A survey and classification. *Advances in Inorganic Chemistry and Radiochemistry* **1967,** 10, 247-422.

27. Ondrechen, M. J.; Ko, J.; Zhang, L. T., A model for the optical absorption spectrum of (m-pyrazine) decaamminediruthenium(5+): What hath Creutz and Taube wrought? *Journal of the American Chemical Society* **1987,** 109, (6), 1672-1676.

28. Ko, J.; Ondrechen, M. J., Line shape of the intervalence transfer band in bridged mixed-valence dimers: the delocalized case. *Journal of the American Chemical Society* **1985,** 107, (22), 6161-6167.

29. Schatz, P. N.; Piepho, S. B.; Krausz, E. R., Far infrared intervalence tunneling transitions in mixed valence systems. *Chemical Physics Letters* **1978,** 55, (3), 539-542.

30. Root, L. J.; Ondrechen, M. J., Adiabatic potentials for a bridged three-site electron-transfer system. *Chemical Physics Letters* **1982,** 93, (5), 421-424.

31. D'Alessandro, D. M.; Dinolfo, P. H.; Davies, M. S.; Hupp, J. T.; Keene, F. R., Underlying Spin-Orbit Coupling Stucture of Intervalence Charge Transfer Bands in Dinuclear Polypyridyl Complexes of Ruthenium and Osmium. *Inorganic Chemistry* **2006,** 45, 3261-3274.

32. Demadis, K. D.; Dattelbaum, D. M.; M., K. E.; J, C. J.; J., P. J.; Meyer, T. J.; S., W. P., Vibrational and structural mapping of $[Ru(bpy)_3]^{3+/2+}$ and $[Os(phen)_3]^{3+/2+}$. *Inorganica Chimica Acta* **2007,** 360, 1143.

33. Shoemaker, C. W. G., *Experiments in Physical Chemistry*. Second edition ed.; 1962.

34. Ito, T.; Hamaguchi, T.; Nagino, H.; Yamaguchi, T.; Kido, H.; Zavarine, I. S.; Richmond, T.; Washington, J.; Kubiak, C. P., Electron Transfer on the Infrared Vibrational Time Scale in the Mixed Valence State of 1,4-Pyrazine- and 4,4'-Bipyridine-Bridged Ruthenium Cluster Complexes. *Journal of the American Chemical Society* **1999,** 121, (19), 4625-4632.

35. Ito, T.; Hamaguchi, T.; Nagino, H.; Yamaguchi, T.; Washington, J.; Kubiak, C., Effects of rapid intramolecular electron transfer on vibrational spectra. *Science* **1997,** 277, (5326), 660-663.

36. Londergan, C. H.; Kubiak, C. P., Electron transfer and dynamic infrared-band coalescence: It looks like dynamic NMR spectroscopy, but a billion times faster. *Chemistry--A European Journal* **2003,** 9, (24), 5962-5969.

37. Turner, J. J.; Gordon, C. M.; Howdle, S. M., Infrared Spectral Features Due to Very Rapid Fluxional Motion: Changes in the Infrared Carbonyl Stretching Spectra of Tricarbonyl(h4-norbornadiene)iron with Temperature. *Journal of Physical Chemistry* **1995,** 99, (49), 17532-17538.

38. Londergan, C. H.; Kubiak, C. P., Vibronic Participationof the Bridging Ligand in Electron Trasfer and Delocalization: New Application of a Three-Sate Model in Pyrazine-Bridged Mixed-Valence Complexes of Trinuclear Ruthenium Clusters. *Journal of Physical Chemistry, A* **2003,** 107, 9301-9311.

39. Londergan, C. H.; Salsman, C. J.; Ronco, S.; Kubiak, C. P., Infrared Activity of Symmetric Bridging Ligand Modes in Pyrazine-Bridged Hexaruthenium Mixed-Valence Clusters. *Inorganic Chemistry* **2003,** 42, 926-928.

40. Fuerholz, U.; Buergi, H. B.; Wagner, F. E.; Stebler, A.; Ammeter, J. H.; Krausz, E.; Clark, R. J. H.; Stead, M. J.; Ludi, A., The Creutz-Taube complex revisited. *Journal of the American Chemical Society* **1984,** 106, (1), 121-123.

41. Stebler, A.; Ammeter, J. H.; Fuerholz, U.; Ludi, A., The Creutz-Taube complex revisited: a single-crystal EPR study. *Inorganic Chemistry* **1984,** 23, (18), 2764-2767.

42. Krausz, E.; Ludi, A., The Creutz-Taube complex revisited: polarized optical spectroscopy. *Inorganic Chemistry* **1985,** 24, (6), 939-943.

43. Fuerholz, U.; Joss, S.; Buergi, H. B.; Ludi, A., The Creutz-Taube complex revisited: crystallographic study of the electron-transfer series (m-pyrazine)decaamminediruthenium ([(NH3)5Ru(Pyz)Ru(NH3)5]n+ (n = 4-6)). *Inorganic Chemistry* **1985,** 24, (6), 943-948.

44. Ito, T.; Imai, N.; Yamaguchi, T.; Hamaguchi, T.; Londergan, C. H.; Kubiak, C. P., Observation and dynamics of charge transfer isomers. *Angewandte Chemie, International Edition* **2004,** 43, 1376-1381.

45. Salsman, J. C.; Kubiak, C. P.; Ito, T., Mixed Valence Isomers. *Journal of the American Chemical Society* **2005,** 127, (8), 2382-2383.

46. Toma, H. E.; Cunha, C. J.; Cipriano, C., Redox potentials of trinuclear m-oxo ruthenium acetate clusters with N-heterocyclic ligands. *Inorganica Chimica Acta* **1988,** 154, (1), 63-66.

47. Hush, N. S., *Progress in Inorganic Chemistry* **1967,** 8, 391.

48. Londergan, C. H.; Kubiak, C. P., Vibronic Participation of the Bridging Ligand in Electron Transfer and Delocalization: New Application of a Three-State Model in Pyrazine-Bridged Mixed-Valence Complexes of Trinuclear Ruthenium Clusters. *Journal of Physical Chemistry A* **2003,** 107, (44), 9301-9311.

49. Rocha, R. C.; Brown, M. G.; Londergan, C. H.; Salsman, J. C.; Kubiak, C. P.; Shreve, A. P., Intervalence-Resonant Raman Spectroscopy of Strongly Coupled Mixed-Valence Cluster Dimers of Ruthenium. *Journal of Physical Chemistry, A* **2005,** 109, (40), 9006-9012.

50. Salsman, J. C.; Ronco, S.; Londergan, C. H.; Kubiak, C. P., Tuning the Electronic Communication and Rates of Intramolecular Electron Transfer of Dimers of Trinuclear Ruthenium Clusters: Bridging and Ancillary Ligand Effects. *Inorganic Chemistry* **2006,** 45, (2), 547-554.

51. Ferretti, A.; Lami, A.; Ondrechen, M. J.; Villani, G., Role of vibronic coupling and correlation effects on the optical properties of mixed-valent and monovalent dimer compounds: the Creutz-Taube ion and its monovalent analogs. *Journal of Physical Chemistry* **1995,** 99, (26), 10484-10491.

52. Nelsen, S., "Almost Delocalized" Intervalence Compounds. *Chemistry a European Journal* **2000,** 6, (4), 581-588.

53. Londergan, C. H.; Salsman, J. C.; Ronco, S.; Dolkas, L. M.; Kubiak, C. P., Solvent Dynamical Control of Electron-Transfer Rates in Mixed-Valence Complexes Observed by Infrared Spectral Line Shape Coalescence. *Journal of the American Chemical Society* **2002,** 124, (22), 6236-6237.

54. Zavarine, I. S.; Kubiak, C. P., A Versatile Variable-Temperature. *Journal of Electroanalytical Chemistry* **2000,** in press.

55. Marcus, R. A., Theory of electrochemical and chemical electron-transfer processes. *Canadian Journal of Chemistry* **1959,** 37, 155-163.

56. Marcus, R. A.; Eyring, H., Chemical and electrochemical electron-transfer theory. *Annual Review of Physical Chemistry* **1964,** 15, 155-196.

57. McClung, R. E. D. *VibexGL: Program for the Simulation of IR Spectra of Exchanging Systems*.

58. Stephen L. Murov, I. C., Gordon L. Hug, *Handbook of Photochemistry*. Second Edition ed.; Marcel Dekker, Inc.: 1993.

59. Horng, M. L.; Gardecki, J. A.; Papazyan, A.; Maroncelli, M., Subpicosecond Measurements of Polar Solvation Dynamics: Coumarin 153 Revisited. *Journal of Physical Chemistry* **1995,** 99, (48), 17311-17337.

60. David P. Shoemaker, C. W. G., *Experiments in Physical Chemistry*. Second Edition ed.; 1962; p 490.

61. Stratt, R. M.; Maroncelli, M., Nonreactive Dynamics in Solution: The Emerging Molecular View of Solvation Dynamics and Vibrational Relaxation. *Journal of Physical Chemistry* **1996,** 100, (31), 12981-12996.

62. Stratt, R. M., The Instantaneous Normal Modes of Liquids. *Accounts of Chemical Research* **1995,** 28, (5), 201-207.

63. CambridgeSoft *CS Chem3D Ultra*, 7.0.0; CambridgeSoft: 2001.

64. Londergan, C. H.; Rocha, R. C.; Brown, M. G.; Shreve, A. P.; Kubiak, C. P., Intervalence Involvement of Bridging Ligand Vibrations in Hexaruthenium Mixed-Valence Clusters Probed by Resonance Raman Spectroscopy. *Journal of the American Chemical Society* **2003,** 125, (46), 13912-13913.

65. Kido, H.; Nagino, H.; Ito, T., Stepwise elongation of a trinuclear ruthenium unit in pyrazine-bridged linear oligomers with use of [Ru3(m3-O)(m-CH3COO)6(pyridine)(CO)(H2O)]. *Chemical Letters* **1996**, (9), 745-746.

66. Connelly, N. G.; Geiger, W. E., Chemical Redox Agents for Organometallic Chemistry. *Chemical Reviews* **1996,** 96, (2), 877-910.

67. Zavarine, I. S.; Kubiak, C. P., A versatile variable temperature thin layer reflectance spectroelectrochemical cell. *Journal of Electroanalytical Chemistry* **2001,** 495, (2), 106-109.

68. Chen, P.; Meyer, T. J., Electron Transfer in Frozen Media. *Inorganic Chemistry* **1996,** 35, (19), 5520-5524.

69. Frost, M. J.; Sharkey, P.; Smith, I. W. M., Energy and structure of the transition states in the reaction hydroxyl + carbon monoxide -> hydrogen atom + carbon dioxide. *Faraday Discussions of the Chemical Society* **1991,** 91, (Struct. Dyn. React. Transition States), 305-317.

70. Schulz, W. R.; Le Roy, D. J., Kinetics of the Reaction H + p-H_2 = o-H_2 + H. *Journal of Chemical Physics* **1965,** 42, (11), 3869-3873.

71. de Namor, A. F. D.; Cleverley, R. M.; Zapata-Ormachea, M. L., Thermodynamics of Calixarene Chemistry. *Chemical Reviews* **1998,** 98, (7), 2495-2525.

72. Baudry, R.; Kalchenko, O.; Dumazet-Bonnamour, I.; Vocanson, F.; Lamartine, R., Investigation of Host-Guest Stability Constants of Calix[n]arenes Complexes with Aromatic Molecules by RP-HPLC Method. *Journal of Chromatographic Science* **2003,** 41, (3), 157-163.

73. Gutsche, C. D., *Calixarenes*. The Royal Society of Chemistry: 1989; p 167-172.

74. Richardson, D. E.; Taube, H., Mixed-valence molecules: electronic delocalization and stabilization. *Coordination Chemistry Reviews* **1984,** 60, 107-129.

75. Badjic Jovica, D.; Nelson, A.; Cantrill Stuart, J.; Turnbull, W. B.; Stoddart, J. F., Multivalency and cooperativity in supramolecular chemistry. *Accounts of Chemical Research* **2005,** 38, (9), 723-32.

76. Grossman, R., *The art of writing reasonable organic mechanisms*. second ed.; 2002.

77. Baumann, J. A.; Wilson, S. T.; Salmon, D. J.; Hood, P. L.; Meyer, T. J., The onset of band-like properties in the ligand-bridged, trimeric cluster {[(py)2Ru3O(OAc)6(pyr)]2[Ru3O(OAc)6(CO)]}. *Journal of the American Chemical Society* **1979,** 101, (11), 2916-2920.

78. Briegleb, G., *Elektronen-Donator-Acceptor Komplexe*. Springer Verlag: Berlin, 1961.

79. Watson, J. D.; Crick, F. H., Molecular structure of nucleic acids; a structure for deoxyribose nucleic acid. *Nature* **1953,** 171, (4356), 737-8.

80. Watson, J. D.; Crick, F. H., Genetical implications of the structure of deoxyribonucleic acid. *Nature* **1953,** 171, (4361), 964-7.

81. Londergan, C. H.; Salsman, J. C.; Lear, B. J.; Kubiak, C. P., Observation and dynamics of "mixed-valence isomers" and a thermodynamic estimate of electronic coupling parameters. *Chemical Physics* **2006,** 324, (1), 57-62.

82. Allen, G. C.; Hush, N. S., Intervalence-transfer absorption. I. Qualitative evidence for intervalence-transfer absorption in inorganic systems in solution and in the solid state. *Progress in Inorganic Chemistry* **1967,** 8, 357-389.

83. Andres, R. P.; Bein, T.; Dorogi, M.; Feng, S.; Henderson, J. I.; Kubiak, C. P.; Mahoney, W.; Osifchin, R. G.; Reifenberger, R., "Coulomb staircase" at room temperature in a self-assembled molecular nanostructure. *Science* **1996,** 272, (5266), 1323-1325.

84. Stires, J. C. *e. a.*, Electronic doping of single molecules. **2007**.

85. Xu, B.; Tao, N. J., Measurement of Single-Molecule Resistance by Repeated Formation of Molecular Junctions. *Science* **2003,** 301, (5637), 1221-1223.

86. Mulliken, R. S., Overlap integrals and chemical binding. *Journal of the American Chemical Society* **1950,** 72, 4493-4503.

87. Mulliken, R. S., Structures of complexes formed by halogen molecules with aromatic and with oxygenated solvents. *Journal of the American Chemical Society* **1950,** 72, 600-8.

88. Melby, L. R.; Harder, R. J.; Hertler, W. R.; Mahler, W.; Benson, R. E.; Mochel, W. E., Substituted quinodimethans. II. Anion-radical derivatives and complexes of 7,7,8,8-tetracyanoquinodimethan. *Journal of the American Chemical Society* **1962,** 84, 3374-3387.

89. Frey, J. E.; Andrews, A. M.; Ankoviac, D. G.; Beaman, D. N.; Du Pont, L. E.; Elsner, T. E.; Lang, S. R.; Zwart, M. A. O.; Seagle, R. E.; Torreano, L. A., Charge-transfer complexes of tetracyanoethylene with cycloalkanes, alkenes, and alkynes and some of their aryl derivatives. *Journal of Organic Chemistry* **1990,** 55, (2), 606-624.

90. Mulliken, R. S., Molecular compounds and their spectra. III. The interaction of electron donors and acceptors. *Journal of Physical Chemistry* **1952,** 56, 801-22.

91. Mulliken, R. S., Molecular compounds and their spectra. II. *Journal of the American Chemical Society* **1952,** 74, 811-24.

92. Klein, M. J., Principle of detailed balance. *Physical Review* **1955,** 97, 1446-1447.

93. Steinfeld, J. I., Francisco, J. S., Hase, W. L., *Chemical kinetics and dynamics*. 2nd ed.; Prentice Hall: New Jersey, 1999.

94. Curtis, C. L.; Ritchie, J. E.; Sailor, M. J., Fabrication of conducting polymer interconnects. *Science* **1993,** 262, (5142), 2014-16.

95. Sailor, M. J.; Curtis, C. L., Conducting polymer connections for molecular devices. *Advanced Materials* **1994,** 6, (9), 688-692.

96. Salsman, J. C.; Ronco, S.; Londergan, C. H.; Kubiak, C. P., *Inorganic Chemistry* **2006**, 45, 547-554.

97. Salsman, J. C.; Kubiak, C. P.; Ito, T., Mixed valence isomers. *Journal of the American Chemical Society* **2005,** 127, 2382.

98. Toma, H. E.; Araki, K.; Alexiou, A. D. P.; Nikolaou, S.; Dovidauskas, S., Monomeric and extended oxo-centered triruthenium clusters. *Coordination Chemistry Reviews* **2001,** 219-221, 187-234.

99. Ota, K.-i.; Sasaki, H.; Matsui, T.; Hamaguchi, T.; Yamaguchi, T.; Ito, T.; Kido, H.; Kubiak, C. P., Syntheses and Properties of a Series of Oxo-Centered Triruthenium Complexes and Their Bridged Dimers with Isocyanide Ligands at Terminal and Bridging Positions. *Inorganic Chemistry* **1999,** 38, (18), 4070-4078.

100. Mruk, R.; Prehl, S.; Zentel, R., Thin films by multilayer build-up of electron transport materials. *Macromolecular Rapid Communications* **2003,** 24, (17), 1014-1018.

101. Callahan, R. W.; Brown, G. J.; Meyer, T. J., Effects of Weak Metal-Metal Interactions in Lignad-Bridged Complexes of Ruthenium. Dimeric Complexes Containing Ruthenium Ions in Different Coordination Environments. *Inorganic Chemistry* **1975,** 14, (7), 1443-1453.

102. Callahan, R. W.; Brown., G. M.; Meyer, T. J., Intervalence Transfer in Unsymmetrical, Ligand-Bridged Dimeric Complexes of Ruthenium. *Journal of the American Chemical Society* **1974,** 96, (25), 7829-7830.

103. note.

104. Baddam, S.; Bowler, B. E., Conformationally Gated Electron Transfer in Iso-1-cytochrome c: Engineering the Rate of a Conformational Switch. *Journal of the American Chemical Society* **2005,** 127, (27), 9702-9703.

105. McLendon, G.; Pardue, K.; Bak, P., Electron transfer in the cytochrome c/cytochrome b2 complex: evidence for conformational gating. *Journal of the American Chemical Society* **1987,** 109, (24), 7540-1.

106. O'Neill, M. A.; Becker, H.-C.; Wan, C.; Barton, J. K.; Zewail, A. H., Ultrafast dynamics in DNA-mediated electron transfer: Base gating and the role of temperature. *Angewandte Chemie, International Edition* **2003,** 42, (47), 5896-5900.

107. Zhou, J. S.; Kostic, N. M., Gating of photoinduced electron transfer from zinc cytochrome c and tin cytochrome c to plastocyanin. Effects of solution viscosity on rearrangement of the metalloprotein complex. *Journal of the American Chemical Society* **1993,** 115, (23), 10796-804.

108. Davis, W. B.; Ratner, M. A.; Wasielewski, M. R., Conformational Gating of Long Distance Electron Transfer through Wire-like Bridges in Donor-Bridge-Acceptor Molecules. *Journal of the American Chemical Society* **2001,** 123, (32), 7877-7886.

109. Rocha, R. C.; Toma, H. E., Proton-induced switching and control of intra-molecular electron transfer on a benzotriazole-bridged symmetric mixed-valence ruthenium complex. *Inorganic Chemistry Communications* **2001,** 4, (5), 230-236.

110. Tannai, H.; Tsuge, K.; Sasaki, Y., Switching of the Electronic Communication between Two {Ru(trpy)(bpy)} (trpy = 2,2':6',2"-Terpyridine and bpy = 2,2'-Bipyridine) Centers by Protonation on the Bridging Dimercaptothiadiazolato Ligand. *Inorganic Chemistry* **2005,** 44, (15), 5206-5208.

111. Katz, E.; Baron, R.; Willner, I., Magnetoswitchable electrochemistry gated by alkyl-chain-functionalized magnetic nanoparticles: Control of diffusional and surface-confined electrochemical processes. *Journal of the American Chemical Society* **2005,** 127, (11), 4060-4070.

112. Campbell, D. J.; Herr, B. R.; Hulteen, J. C.; Van Duyne, R. P.; Mirkin, C. A., Ion-Gated Electron Transfer in Self-Assembled Monolayer Films. *Journal of the American Chemical Society* **1996,** 118, (42), 10211-10219.

113. Walter, D. G.; Campbell, D. J.; Mirkin, C. A., Photon-Gated Electron Transfer in Two-Component Self-Assembled Monolayers. *Journal of Physical Chemistry B* **1999,** 103, (3), 402-405.

114. McCleskey, T. M.; Winkler, J. R.; Gray, H. B., Driving-force effects on the rates of bimolecular electron-transfer reactions. *Journal of the American Chemical Society* **1992,** 114, (17), 6935-7.

115. Low, D. W.; Winkler, J. R.; Gray, H. B., Photoinduced Oxidation of Microperoxidase-8: Generation of Ferryl and Cation-Radical Porphyrins. *Journal of the American Chemical Society* **1996,** 118, 117-120.

116. Itou, M.; Otake, M.; Araki, Y.; Ito, O.; Kido, H., Control of Electron Acceptor Ability with Ligands (L) in Photoinduced Electron Transfer from Zinc Porphyrin or Zinc Phthalocyanine to [Ru3(m3-O)(m-CH3COO)6L3]+. *Inorganic Chemistry* **2005,** 44, (5), 1580-1587.

117. Gray, H. B.; Winkler, J. R., Long-range electron transfer. *Proceedings of the National Academy of Sciences of the United States of America* **2005,** 102, (10), 3534-3539.

118. Londergan, C. H. Ph.D., University of California, San Diego, 2003.

119. Londergan, C. H.; Rocha, R. C.; Brown, M. G.; Shreve, A. P.; Kubiak, C. P., Intervalence Involvement of Bridging Ligand Vibrations in Hexaruthenium Mixed-Valence Clusters Probed by Resonance Raman Spectroscopy. *Journal of the American Chemical Society* **2003,** 125, (46), 13912-13913.

120. Lear, B. J.; Glover, S. G.; Londergan, C. H.; Salsman, J. C.; Kubiak, C. P., Solvent dynamical control of ultra fast ground state electron transfer: Implications for class II-III mixed valency. *Journal of the American Chemical Society* **2007,** Sumbitted.

121. Hore, P. J., *Nulcear Magnetic Resonance*. Oxford Press: Oxford, 1995; Vol. 32.

122. Zheng, J.; Kwak, K.; Fayer, M. D., Ultrafast 2D IR Vibrational Echo Spectroscopy. *Accounts of Chemical Research* **2007,** 40, 75-83.

123. Kim Yung, S.; Hochstrasser Robin, M., Comparison of linear and 2D IR spectra in the presence of fast exchange. *The Journal of Physical Chemistry. B* **2006,** 110, (17), 8531-8534.

124. Masuda, A.; Masuda, Y.; Fukuda, Y., First Evaluation of Ultrafast (Ground State) Intramolecular Electron Transfer Rate in Solution by NMR Spin-Lattice Relaxation. An Application to Mixed-Valence Biferrocene Monocation (Fe(II), Fe(III)). *Journal of Physical Chemistry A* **1997,** 101, (12), 2245-2253.

125. Schmuttenmaer Charles, A., Exploring dynamics in the far-infrared with terahertz spectroscopy. *Chemical Reviews* **2004,** 104, (4), 1759-1779.

126. Beard, M. C.; Turner, G. M.; Schmuttenmaer, C. A., Measurement of electromagnetic radiation emitted during rapid intramolecular electron transfer. *Journal of the American Chemical Society* **2000,** 122, (46), 11541-11542.

127. Beard, M. C.; Turner, G. M.; Schmuttenmaer, C. A., Measuring Intramolecular Charge Transfer via Coherent Generation of THz Radiation. *Journal of Physical Chemistry A* **2002,** 106, (6), 878-883.

128. Schmuttenmaer, C. A., A new method for measuring intramolecular charge transfer. *Science Progress* **2002,** 85, (2), 175-197.

129. Abe, M.; Michi, T.; Sato, A.; Kondo, T.; Zhou, W.; Ye, S.; Uosaki, K.; Sasaki, Y., Electrochemically controlled layer-by-layer deposition of metal-cluster molecular multilayers on gold. *Angewandte Chemie, International Edition* **2003,** 42, (25), 2912-2915.

130. Ye, S.; Zhou, W.; Abe, M.; Nishida, T.; Cui, L.; Uosaki, K.; Osawa, M.; Sasaki, Y., Electrochemical Control of CO/NO Ligand Exchange in a Triruthenium Cluster Monolayer Assembled on a Gold Electrode Surface. *Journal of the American Chemical Society* **2004,** 126, (24), 7434-7435.

131. Lear Benjamin, J.; Kubiak Clifford, P., Charge gating and electronic delocalization over a denderimeric assembly of trinuclear ruthenium clusters. *Inorganic Chemistry* **2006,** 45, (18), 7041-3.

132. Zavarine, I. S.; Kubiak, C. P.; Yamaguchi, T.; Ota, K.-i.; Matsui, T.; Ito, T., Unusual Redox State Dependent Fermi Resonances in the Infrared Spectra of Trinuclear Ruthenium Clusters with Isocyanide Ligands. *Inorganic Chemistry* **2000,** 39, (12), 2696-2698.

133. Zavarine, I. S.; Kubiak, C. P.; Yamaguchi, T.; Ota, K.; Matsui, T.; Ito, T., Unusual redox state dependent fermi resonances in the infrared spectra of trinuclear ruthenium clusters with isocyanide ligands. *Inorganic Chemistry* **2000,** 39, (12), 2696-2698.